JOINT LOADING IN INDUSTRIAL LIFTS: INFORMING MITIGATION STRATEGIES THROUGH JOINT-LEVEL BIOMECHANICS

A Dissertation
Presented to
The Academic Faculty

by

Felicia Davenport

In Partial Fulfillment
of the Requirements for the Degree
Doctor of Philosophy in the
Bioengineering Interdisciplinary Graduate Program

Georgia Institute of Technology
August 2024

JOINT LOADING IN INDUSTRIAL LIFTS: INFORMING MITIGATION STRATEGIES THROUGH JOINT-LEVEL BIOMECHANICS

Approved by:

Dr. Gregory Sawicki, Advisor
School of Mechanical Engineering & School of Biological Sciences
Georgia Institute of Technology

Dr. Karl Zelik
Department of Mechanical Engineering
Vanderbilt University

Dr. Aaron Young
School of Mechanical Engineering
Georgia Institute of Technology

Dr. Ajit Chaudhari
School of Health and Rehabilitation Sciences
Ohio State University

Dr. Omer Inan
School of Electrical & Computer Engineering
Georgia Institute of Technology

Date Approved: [July 20, 2024]

This work is dedicated to my loved ones, in the memory of my angel Maggie Mae

2015 – 2022 Forever in our hearts.

ACKNOWLEDGEMENTS

First and foremost, I give all my thanks to God who continuously gives me the strength to accomplish my wildest dreams and aspirations, and the will to smile during the peaks and valleys of this journey called life. I was blessed with the best parents, Steven and Sharon Davenport, who have been the most uplifting support system someone could ask for. I will always appreciate the sacrifices you made for me to be able to be where I am today. Thank you, Dad, for always reminding me to look out for my own health, being my sounding board, and always willing to give me a laugh. Thank you, Mom, for always being a light to my life – thank you for being so helpful while being away and whenever you're in town, your consistent prayers, and your love. I'm thankful to my Grandma Madgelene Thompson for being a constant source of joy and unconditional love – each weekend that I get to see you restores my soul. Thank you to my partner, Fidel, for taking on the adventure of traveling to a new region of the country and experiencing life with me during this journey. Together, we can handle any obstacles that academia and life may bring our way. Thank you to my beagle boy Falcon for shaking this house up for the better, and being the loyal companion that I didn't know I needed. You don't have to fill your late older sister's shoes; you have your own.

I thank all the friends that I've made over the years – my extended family – for showing me how to truly enjoy each moment in life and appreciate the art of balancing work and fun. Thank you to my mentors, especially Ms. Shaun Ashley and Laura Paige who not only provided imperative guidance in my professional journey, but cared about and ensured that my wellbeing was being maintained in the process. To my undergraduate

advisor, Dr. Mel Sabella, who helped set me on this path and still checks in on me to this day. Thank you to Dr. Greg Sawicki for giving a chance to a curious young woman, who was losing hope and her shine. Working with you has been an honor and both you and Mel have set the standard for me regarding leadership for life. I thank my PoWeR lab mates: Lindsey Trejo, Jordyn Schroeder, Ben Shafer, Jenny Leestma, Melody Modarressi, Jonathan Gosyne, Thendral Govindaraj, Laksh Kumar Punith, Amro Alshareef, Autumn Routt, Kristen Jakubowski, Pawel Golyski, and more for being the best crew to go through this trauma-bonding experience with. A huge shoutout to my fellow DOE teammates Christoph Nuesslein, Joshua Fernandez, Raymond Kim, and Ryan Casey for making our rigorous data collections and processing bouts so much more fun.

Thank you to the game of golf -- which planted the seed of interest in biomechanics – the experiences and memories, coaches, and competitors who molded my work ethic, patience, discipline. I've had to put this passion aside for a while, but back to the greens and cart paths I go – on to the next course; on to the next adventure!

TABLE OF CONTENTS

ACKNOWLEDGEMENTS iv

LIST OF TABLES viii

LIST OF FIGURES ix

LIST OF SYMBOLS AND ABBREVIATIONS xi

SUMMARY xii

CHAPTER 1. Introduction 1

CHAPTER 2. Characterize joint contact forces across industry-relevant lifting tasks and joints 9
2.1 Abstract 9
2.2 Introduction 10
2.3 Methods 13
2.3.1 Participants 13
2.3.2 Experimental Design 13
2.3.3 Data analysis 15
2.3.4 Injury risk assessment 17
2.3.5 Statistical analysis 19
2.4 Results 19
2.5 Discussion 26
2.5.1 L5/S1 28
2.5.2 Knee 31
2.5.3 Knee and L5/S1 load distribution 35
2.5.4 Limitations 36
2.6 Conclusion 37
2.7 Conflict of Interest Statement 37
2.8 Acknowledgements 37
2.9 Supplementary Figures for Chapter 2 39

CHAPTER 3. Assess the effects of exoskeletons on joint contact forces across industry- relevant lifting tasks and joints 42
3.1 Abstract 42
3.2 Introduction 43
3.3 Methods 45
3.3.1 Participants 45
3.3.2 Experimental Design 46
3.3.3 Data analysis 48
3.4 Results 54
3.4.1 Knee exo 54
3.4.2 Back exo 58

3.5 Discussion **61**
3.5.1 Knee exo 62
3.5.2 Back exo 65
3.5.3 Limitations 67
3.6 Conclusion **70**
3.7 Conflict of Interest Statement **71**
3.8 Acknowledgements **72**
3.9 Supplementary Figures for Chapter 3 **73**

CHAPTER 4. leveraging wearable sensing to estimate joint contact forces **79**
4.1 Abstract **79**
4.2 Introduction **80**
4.3 Methods **83**
4.3.1 Experimental data collections 83
4.3.2 Musculoskeletal analysis 86
4.3.3 Simulating Sensors 87
4.3.4 TCN Model 89
4.3.5 Statistical analysis 92
4.4 Results **93**
4.4.1 Joint contact force estimates – generalized tasks 93
4.4.2 Joint contact force estimates – industry-relevant tasks 95
4.5 Discussion **98**
4.5.1 Limitations 101
4.6 Conclusion **102**
4.7 Conflict of Interest Statement **103**
4.8 Acknowledgements **103**
4.9 Supplementary Figures for Chapter 4 **104**

CHAPTER 5. Conclusion **106**

REFERENCES **110**

LIST OF TABLES

Table 1	Unassisted lifting study participant demographics for Chapter 2	13
Table 2	Joint loading tolerance limits to measure injury risk for Chapters 2 and 3	19
Table 3	Effect of lifting rotation and start-to-end height on peak total joint forces in knee and lower-back (L5/S1) for Chapter 2	24
Table 4	Exo assistance lifting study participant demographics for Chapter 3	46
Table 5	Dynamic task set participant demographics for Chapter 4	85
Table 6	Dynamic dataset study participant demographics for Chapter 4	85
Table 7	Machine learning hyperparameters used for Chapter 4	89

LIST OF FIGURES

Figure 1	Experimental methods for Chapter 2	14
Figure 2	Knee and L5/S1 joint angles for Chapter 2	21
Figure 3	Knee and L5/S1 joint moments for Chapter 2	22
Figure 4	Knee and L5/S1 total joint contact forces across lifting tasks for Chapter 2	24
Figure 5	Effects of lifting postures on joint contact forces (H1) for Chapter 2	25
Figure 6	Effects of lifting ascension and descension on joint contact forces (H2) for Chapter 2	27
Figure 7	Effects of lifting below-the-waist or above-the-waist on joint contact forces (H3) for Chapter 2	29
Figure 8	Relationship between L5-S1 and knee joint contact forces across all lifting postures (H4) for Chapter 2	34
Figure 9	Supplemental Figure 1 – normalized torso and leg EMG for Chapter 2	39
Figure 10	Supplemental Figure 2 – peak joint moments for Chapter 2	40
Figure 11	Supplemental Figure 3 – integrated joint moments for Chapter 2	41
Figure 12	Experimental methods for Chapter 3	47
Figure 13	Knee kinematics, kinetics, and active knee exo assistance profiles across lifting tasks for Chapter 3	55
Figure 14	L5/S1 kinematics, kinetics, and active back exo assistance profiles across lifting tasks for Chapter 3	56
Figure 15	Knee and L5/S1 total joint contact forces across lifting tasks with exo assistance for Chapter 3	58
Figure 16	Overall effects of exoskeleton assistance on peak knee and L5/S1 total joint contact forces for Chapter 3	60
Figure 17	Overall effects of exoskeleton assistance on integrated knee and L5/S1 total joint contact forces for Chapter 3	62

Figure 18	Supplemental Figure 1 - normalized torso and leg EMG for Chapter 3	73
Figure 19	Supplemental Figure 2 - percent change in peak total joint contact forces from the use of active knee and passive back exo for Chapter 3	74
Figure 20	Supplemental Figure 3 - percent change in integrated total joint contact forces from the use of active knee and passive back exo for Chapter 3	75
Figure 21	Supplemental Figure 4 – Overall effects of exoskeleton assistance on peak and integrated joint moments at the knee and L5/S1 joint for Chapter 3	76
Figure 22	Supplemental Figure 5 – L5/S1 joint angles for Chapter 3	77
Figure 23	Supplemental Figure 6 – L5/S1 joint moments for Chapter 3	78
Figure 24	Wearable sensor locations for Chapter 4	88
Figure 25	Experimental methods for Chapter 4	91
Figure 26	TCN's performance estimating knee JCFs – R^2 for Chapter 4	92
Figure 27	TCN's performance estimating knee JCFs on grouped tasks– R^2 for Chapter 4	94
Figure 28	TCN's performance estimating knee JCFs – RMSE for Chapter 4	97
Figure 29	Normal knee JCF estimation performance and tracking utilizing real sensors for Chapter 4	98
Figure 30	Supplementary Figure 2- TCN's performance estimating knee JCFs – RMSE for Chapter 4	104
Figure 31	Supplementary Figure 3- List of tasks included in the dynamic taskset for Chapter 4	105

LIST OF SYMBOLS AND ABBREVIATIONS

EMG	Electromyography
JCF(s)	Joint contact force(s)
KW	Knee-to-waist
WK	Waist-to-knee
SW	Shoulder-to-waist
WS	Waist-to-shoulder
CEINMS	Calibrated EMG-Informed Neuromusculoskeletal Solver
RF	Rectus Femoris
VM	Vastus Medialis
VL	Vastus Lateralis
BF	Biceps Femoris
ST	Semitendinosus
LG	Lateral Gastrocnemius
ES	Erector Spinae
RA	Rectus Abdominis
LD	Latissimus Dorsi
EO	External Obliques
Exo	exoskeleton
ANOVA	Analysis of Variance
NoE	No exo
HW	HeroWear exo
KE	Knee exo

SUMMARY

Manual labor professions require workers to perform tasks which comprise their musculoskeletal integrity and expose them to heightened risks of injury from overexertion. in professions It is known that repetitive load carriage, especially during asymmetric walking, lifting, and twisting among other locomotion modes can lead to the development of tissue and joint injuries from overexertion. While it is well-documented that joint kinematics, joint kinetics, and muscle activity can be indicators of injury predisposition, we believe that internal joint loading, joint contact forces (JCFs), may provide an alternative, under-the-skin, perspective on potential biomechanical biomarkers indicative of informing about the risks of joint injuries. There is a *critical gap* in understanding the internal joint loading experienced by the joint capsule from nearby tissues (i.e. muscles, ligaments, etc.) and external factors during manual labor tasks, as well as how injury mitigation solutions such as wearable technology influence JCFs and predisposition to injury.

This dissertation explores the relationship between joint-level and muscle-level mechanics and effort and how these influences resolve into the internal joint state of JCFs across a myriad of manual labor-inspired movements and tasks. The overarching objectives were to investigate whether assistive and informative intervention strategies can help alleviate high, and potentially hazardous JCFs. In Chapter 2, we develop a framework that maps JCFs to industry-relevant lifting tasks. With the use of computational neuromusculoskeletal solvers to optimize estimates of muscle forces and JCFs, we identified a subset of work-specific movements that expose manual laborers to higher risks of injury at their lower back and knee joints. Following this work, in Chapter 3 we

investigated how the use of exoskeletons affects JCFs in the subset of injurious manual lifting tasks identified in Chapter 2. More specifically, we sought to uncover how motorized assistance from a knee exoskeleton and passive assistance from a soft, back exoskeleton influence internal lower back and knee joint loads. In Chapter 4, we leverage analyses performed in Chapters 2 and 3 to measure how wearable sensor outputs from muscles, segments, and ground reaction forces can inform users of internal joint forces during various movements as a final mitigation strategy. Using a deep learning model equipped to self-identify relevant features which map to estimates of JCFs, key findings demonstrated that muscle activations were imperative to reliable normal JCF estimation. The wearable sensors utilized in this work were not adequate inputs for shear JCF estimation; however, we did fin d that IMUs were a primary contributor to the better performing shear JCF estimates. All in all, this dissertation provides an informative lens on JCFs, a contributing factor to joint injuries, and potential effects of wearable technology on internal joint loading.

CHAPTER 1. INTRODUCTION

Overuse injuries are a persistent health concern in manual labor worksites. In 2020, about 301,890 musculoskeletal-related injuries were reported[1]. In 2021, about 70 million workdays were lost due to work-related injuries[2]. It is estimated that 33 million of those days were due to prior injuries, and it is projected that 55 million days will be lost from 2021's injuries in the future years to come[2]. Aside from the detrimental health burden these injuries have on the workers, the administrative perspective views workers developing injuries as a performance inhibitor and a financial loss. In fact, such injuries prove to be severely costly for corporations as the average amount of workers' compensation per incident is around $41,353[2]. Unfortunately, stress and strain to tissues and bone caused by overexertion remains a leading cause of injury[3] in manual material handling, manufacturing, and patient transporting professions[4]. Workers in such manual labor professions may perform repetitive, asymmetric, and physically taxing movements[5] such as twisting, pushing, or bending while handling heavy loads[6–8] which may put them at risk for acute injury when exposed to extreme peak loading or chronic overuse injury with prolonged exposure to joint and tissue loading[9,10]. Workplace musculoskeletal disorders such as low back pain and osteoarthritis in the knees can be physically and financially burdensome to members of the working class and continues to have a negative impact on society as we age[11,12]. In 2020, the Bureau of Labor Statistics (2021)[13] reported about 29,700 knee and 62,540 back injuries in the private, local, and state government sectors. **These findings ultimately support the critical need to incorporate technological interventions that**

can offload the forces experienced within the joint capsule and can reduce overall risk of injury occurrence.

To accomplish this goal, we need a metric which captures these internal joint forces at the joint capsule: joint contact forces (JCFs). JCFs inform us about internal loading at the bone as a result of forces produced by muscles, ligaments, tendons, and external loads[14]. More specifically, axial compression and shearing forces are damaging to the musculoskeletal system[15], leading to tissue weakening and strain, microdamage, or fractures to the bones[16,17] depending on the magnitude and exposure time to joint loading. However, it is difficult and surgically invasive to directly measure biological joint contact force[18]. Fortunately, advances in computational biomechanics allow us to utilize musculoskeletal modeling practices to reproduce manual lifting tasks[19,20] and estimate joint loading[21–24]. Humans lack sensory organs which detect and alert of harmful internal joint loading, so knowledge of internal joint contact forces sheds light on bone deformation and micro-damage inflicted by repetitive and prolonged mechanical loading and can serve as a metric of injury[25]. For example, knee joint contact forces are a potential metric for monitoring the onset of osteoarthritis prior to ACL injury and after reconstruction surgery due to structural changes in cartilage[1,26,27]. Also, overexertion in manual lifting tasks is considered one of the most prominent contributors to low back pain in the workplace[28–30]. **Thus, there is a need for a framework that details joint contact forces across work- specific tasks and highlights critical loading tasks in need of intervention to inform future joint loading mitigation strategies.** While manual lifting has been commonly investigated with metrics such as kinematics, kinetics, and some internal loading, few studies have investigated joint

contact forces in both the back and knee to assess the susceptibility of injury across a variety of work-specific tasks. Aim 1 (Chapter 2) addresses effects of lifting asymmetry, ascent-phase versus descent-phase, and operating height on JCFs. This work also surveys trending behavior across tasks in joint load distribution between the back and knee across the manual lifting conditions. Thus, severing as foundational work to identify how JCFs in specific tasks should be mitigated by assistive technology.

Exoskeletons are shown to be helpful at the muscle-tendon properties level[31] and at reducing user joint loading[32] and metabolic cost[31,33] during locomotion and manual labor tasks. These findings have influenced the slow adoption of such devices in workplaces where manual labor tasks that involve twisting and lifting high loads are associated with high worker injury rates[34]. Both active and passive commercial exoskeletons are designed to offset joint loading by providing assistive torque either in parallel or perpendicular to the body. Such assistance reduces user muscle forces and activations[35,36]. Previous research has proposed that joint kinematics, joint kinetics, and muscle activity can indicate injury predisposition; however, few studies have investigated how exoskeletons affect internal joint loading in manual labor tasks. Further, the impact of exoskeletons on joint contact forces is largely unknown due to the inability to measure in vivo and the complex musculoskeletal modeling tools required for estimation. Aim 2 (Chapter 3) will address these gaps by modeling the assistive torques as applied forces to the body and investigate how wearable devices affect internal joint loading in work-specific lifting tasks. This will provide insight on the benefits of exoskeletons or lack thereof for mitigating overexertion injuries. Results could influence the adoption of exoskeletons into the workplace and begin

discussions on whether the cost of exoskeletons compare to the cost of workers compensation. This work can also inform the design of exoskeletons and controllers to mitigate hazardous joint loading by helping people move or teach them how best to move.

Wearable sensors are useful in measuring biomechanical states and providing insight into other relevant metrics. More specifically, IMUs, EMG, and force sensors are highlighted for their ability to monitor musculoskeletal health, risks, and overall user performance for the intention of refinement[37]. For example, IMUs, could be a key proponent to addressing injury risk by prescribing user-independent stretching regimen's needed before a daily workload[38], providing preventative biofeedback[37], monitoring the ratio between acute and chronic workload[39]. Historically, in response to growing concerns of unsafe working conditions, companies became privy to the need for reform to working conditions and procedures[40]. Since then, companies have gone on to incorporate strategic health and risk assessments[41] and training, screenings to ensure workers meet task requirements, required personal protective equipment (PPE), and hire qualified ergonomists to enforce Occupational Safety and Health Administration (OSHA) restrictions to keep the workplace safe[42]. This initiated thorough documentation of workplace conditions and employee performance, delegation of ergonomic teams to improve workplace conditions, and developing training protocols for employees to be aware of injury risks and ways to mitigate these risks[43]. Manual labor personnel may also be encouraged to wear insufficient bracing to alleviate pain and prevent injury. Despite these measures, laborers are still getting hurt. Therefore, there is a need to leverage the capabilities of wearable sensing to truly combat the remaining prevalence of injuries within the workplace.

Machine learning has shown promising performance in measuring biological parameters that were once complicated and time-intensive to compute. A growing trend to use wearable sensors such as pressure insoles and/or inertial measurement units (IMUs) to estimate joint moments[44], internal bone forces[45], and even injury risks[46,47] is paving a way to probe the relationship between injury mitigation and internal joint contact forces. However, there still is a considerable amount we do not know regarding the most robust and widely applicable model to achieve such goals. Aim 3 (Chapter 4) will address these gaps by creating assistive technology through a deep learning model, the temporal convolutional network (TCN) that can help estimate joint contact forces. Through using subject-dependent data which has already been heavily processed via musculoskeletal modeling pipelines and using these outputs (JCFs) as ground truth for the TCN, we are able to train a model with data enriched with variability that would support the model's capability to personalize JCFs estimations across diverse populations[48]. This advantage hereby opens the possibilities of utilizing simulated wearable sensor data, real sensor data in the future, to estimate JCFs in the future. This work could inform the establishment of biofeedback systems to deliver real-time sensory information regarding joint contact forces during working tasks[49], assist clinicians with diagnoses without the need for expensive imaging equipment, inform implementation joint contact force estimation models into device controllers to provide preventative assistance against high loading in a given task.

The long-term goal of this dissertation is to address the intersectionality of the aforementioned efforts as a means mitigate potentially hazardous JCFs across tasks commonly encountered in a daily workload of a manual labor employee. To accomplish

this, there are three primary aims to this dissertation: 1) to characterize and identify how lifting weights from different heights and degrees of twisting influence JCFs at the L5/S1 and knee joints, 2) to measure how an active knee exo and passive back exo influence internal joint loading, and 3) determine how a minimized wearable sensor system-informed machine learning intervention can support JCF estimations at the knee joint. The original research outlined in these aims are expanded upon across 3 chapters.

To obtain these goals, my objective is to evaluate joint contact forces at the knee and lower back during industry-relevant lifting conditions with (1) no exoskeleton, (2) an active knee exoskeleton, and (3) a passive back exoskeleton and to estimate joint contact forces using machine learning techniques. My central hypotheses are that (1) exoskeletons will reduce internal joint contact forces and (2) wearable device-inspired machine learning will effectively estimate joint contact forces during manual lifting tasks. Furthermore, the strain of muscle forces on the joints will indirectly lower net joint contact forces by reducing compressive contact forces; thus, lowering injury risk. The use of wearable sensors (e.g., inertial measurement units (IMUs), EMG, etc.) will provide useful kinematic and kinetic data to train a machine learning model to map to joint contact forces.

Chapter 2, which is a submitted manuscript in the Journal of Applied Biomechanics, illustrates a framework that relates JCFs in a lower back joint (L5/S1) and knee joint to an assortment of symmetric and asymmetric manual lifting tasks. This work identifies a subset of work-specific movements that exposes workers to higher joint loads, and potentially higher risks of injury. This chapter also highlights the distribution of internal joint loads

between the lower back and knees during these tasks which could inform ergonomists, clinicians, and engineers on whether the back and/or knee require supplemental assistance and in which tasks to provide the support.

Chapter 3 contains work I intend to submit to IEEE Transactions on Medical Robotics and Bionics. This study addresses the second aim of incorporating wearable devices, exoskeletons, in the manual lifting conditions that elicited higher JCFs at the lower back joint (L5/S1) and knee joint in Chapter 2. With the knowledge of how exos can offload muscle-level and external joint-level factors, we sought to understand if and how the use of exos will decrease JCFs as the joint they are prescribed to (i.e., knee device assisting knee joint loading and back device assisting lower back spinal loading). This aim also explores how and if exos may indirectly reduce JCFs of the unassisted joint (i.e., back device assisting knee joint loading and knee device assisting lower back spinal loading. This work will support existing literature that exhausts the benefits of using wearable devices at the whole-body, muscle, and joint levels by shining a light on their impact on mechanical bone loading and its relation to injury mitigation. Also, this aim can inform the implementation of work-inspired exoskeletons to increase safety in manual labor professions.

Chapter 4, which comprises of work I intend to submit to the IEEE Transactions on Biomedical Engineering or Annals of Biomedical Engineering, probes a different injury prevention strategy: looking to deep learning to support JCF estimations without the use of neuromusculoskeletal modeling. With knowledge of the utility of wearable sensors

such as IMUs, EMG, and pressure insoles to inform us of other biomechanical metrics, our goal was to find out the most minimalistic combination of sensor types needed to support the TCN's capability to reliably estimate normal and shear JCFs. The structure of the model utilized in this aim's analyses supports the generalizability of JCF estimations across a broad array of dynamic, and manual labor-inspired tasks. This work shows promise to a trajectory of JCF estimative research to provide users with instructional feedback on mechanical modifications to influence and, hopefully, lower JCFs. This approach also serves as a cost-effective tool that can inform rehabilitative strategies.

Altogether, the studies outlined in this dissertation will positively contribute to existing literature by: 1) surveying and characterizing the effects repetitious twisting and bending during manual lifting on JCFs, 2) establishing a cost-benefit of incorporating exoskeletons on the classified joint loading "hot spot" movements of manual lifting conditions, and 3) assessing the ability of a minimal wearable sensor set to provide reliable estimates of internal joint forces. It is my hope that this dissertation will inspire further advancement in joint injury intervention strategies and experimentations to alleviate the occurrences of loading induced injuries not only in the workplace, but also in various environments. Additionally, this work can potentially influence wearable device design to best suit user needs and ergonomic practices in the workplace to further prevent injuries.

CHAPTER 2. CHARACTERIZE JOINT CONTACT FORCES ACROSS INDUSTRY-RELEVANT LIFTING TASKS AND JOINTS

The first work of my dissertation examines how various manual lifting postures influence internal joint loading in the lower back and knees. This work has been submitted to the Journal of Applied Biomechanics titled "EMG-informed estimates of joint contact forces within the lower-back and knee joints during a diverse set of industry-relevant manual lifting tasks". At this time, this article's status is pending after having responded to reviewer's feedback. That article is outlined in this chapter.

2.1 Abstract

Repetitive manual labor tasks involving twisting, bending, and lifting commonly lead to lower back and knee injuries in the workplace. To identify tasks with high injury risk, we recruited N=9 participants to perform industry-relevant, two-handed lifts with an 11 kg weight. These included symmetrical/asymmetrical, ascending/descending lifts that varied in start-to-end heights (knee-to-waist and waist-to-shoulder). We used a data-driven musculoskeletal model that combined force and motion data with a muscle activation-informed solver (OpenSim, CEINMS) to estimate 3D internal joint contact forces (JCFs) in the lower-back (L5/S1) and knee. Symmetrical lifting resulted in larger peak JCFs than asymmetrical lifting in both the L5/S1 (+20.2% normal ($p < 0.01$), +20.3% shear ($p = 0.001$), +20.6% total ($p < 0.01$)) and the knee (+39.2% shear ($p = 0.001$)) and there were

no differences in peak JCFs between ascending vs. descending motions. Below-the-waist lifting generated significantly greater JCFs in the L5/S1 and knee than above-the-waist lifts ($p < 0.01$). We found a positive correlation between knee and L5/S1 peak total JCFs ($R^2 = 0.60$, $p < 0.01$) across the task space, suggesting motor coordination that favors sharing of load distribution across the trunk and legs during lifting.

2.2 Introduction

Workplace musculoskeletal disorders such as low back pain and osteoarthritis in the knees can be physically and financially burdensome to members of the working class and will continue to have a negative impact on society as they age[11,12]. One of the leading causes of workplace injuries is overexertion in tasks such as manual materials handling (MMH), manufacturing, and patient transport[4]. Workers in manual labor professions may perform repetitive, asymmetric, and physically taxing movements[5] such as twisting, pushing, or bending while handling heavy loads[6–8] - putting them at risk for acute injury when exposed to extreme peak loading or chronic overuse injury with prolonged exposure to joint and tissue loading[50]. Common approaches to characterize and mitigate injury risk in manual lifting have relied on metrics derived from measures of joint kinematics and kinetics. Factors such as varying the mass of a lifted object[51–54], the size of a lifted object[55], lifting speed[52], lifting technique[55,56], stance width and foot position[55,57], lowering versus lifting[58,59], and symmetry versus asymmetry (turning)[28,52,53,56,58,60]. In sum, external loads

on the limb-joints during MMH tasks have been well characterized and helped provide best practices to guide lifting techniques that can help avoid injuries.

Characterizing internal loads on underlying musculoskeletal structures may provide a more direct assessment of injury risk than external measures based on inverse dynamics. Indeed, joint contact forces (JCFs), a potential biomarker for the onset of osteoarthritis prior to ACL injury and after reconstruction surgery due to structural changes in cartilage[1,26,27], could reveal key underlying changes in cartilage and bone health. Joint contact forces quantify the internal loading at bone-to-bone interfaces necessary to support the forces produced by surrounding muscles, ligaments, tendons that are necessary to counter external loads[14]. Despite their potential utility, JCFs are impossible to measure non-invasively in humans, with only a few examples of direct *in vivo* measurements of JCFs[61,62]. Furthermore, mechanical analyses that attempt to map net external forces and moments to internal joint loads are not straightforward and require estimates of how antagonistic muscle forces are coordinated[63]. Fortunately, advances in computational biomechanics make it possible to utilize musculoskeletal modeling practices to reproduce MMH tasks in simulation[19,20] and estimate JCFs[21–24,64]. EMG-informed solvers can reduce errors in JCF estimation from purely simulated muscle activation inputs by accounting for muscle co-activation[65,66], which is a critical piece of the puzzle given that muscle action typically accounts for well over half the joint contact load [67,68]. These advanced computational tools make it possible to move 'outside-in' and evaluate tissue level mechanics in the context of highly dynamic movements – enabling monitoring of a new set of 'local' biomarkers that could offer more precise injury prevention measures.

The purpose of this study was to extend limb-joint analyses and establish a framework to examine how external loads resolve as three-dimensional JCFs *inside limb-joints* during MMH tasks. To bridge this gap, we designed a comprehensive study protocol comprised of a diverse set of lifting tasks spanning a range of start-end heights and across a range of lift symmetries. In these conditions we collected full body motion data using high speed motion capture, external ground reaction forces and electromyography from a carefully selected set of muscles around the back and knee. We paired these experimental data with state-of-the-art computational modeling, simulation, and optimization techniques to evaluate lower-back (L5/S1) and knee joint loads during lifts that varied starting and ending heights and lift symmetry, providing insight into potential 'hot spots' for injury over a wide range of possible lifting situations. We hypothesized that asymmetrical[69,70], ascending[52], below the waist lifts[53,71] would induce the highest JCFs at both the L5/S1 and knee (H1-3). We expected JCFs at the knee and L5/S1 joints would be proportional to each other[51,52,71–73], independent of the lifting task (H4) – reflecting a motor control strategy to avoid overloading the L5/S1 or knee by distributing loads across the limb-joints. Studying the effects of MMH tasks on multi-joint internal joint loading will enable a comprehensive mapping from task space to injury risk during industry-relevant lifting tasks. In doing so, we hope to provide a greater awareness of the susceptibility to eventual tissue and bone-damaging injuries in the workplace that can be used as a prophylactic tool to avoid prolonged exposure to critical loading in the workplace.

2.3 Methods

2.3.1 Participants

This study was approved by the Georgia Institute of Technology Institutional Review Board and all participants provided signed consent to the study prior to collection. We enrolled nine participants (7 male, 2 female; weight: 80.7 ± 15.0 kg; height: 178.7 ± 11.1 cm; age: 25.1 ± 2.9 years). Participants were excluded if they had a history of debilitating injuries from neurological, musculoskeletal, or cardiovascular conditions that prohibited them from successfully performing the manual labor tasks in this study.

Table 1 – Unassisted lifting study participant demographics. Standard deviation = SD.

Participant	Gender	Age (years)	Height (cm)	Weight (kg)
1	F	24	165.4	67.0
2	M	24	181.3	90.9
3	M	23	165.3	60.4
4	M	24	188.4	86.9
5	M	29	185.5	102.5
6	M	26	174.0	73.03
7	F	25	181.0	64.30
8	M	30	190.0	85.5
9	M	21	197.3	95.9
Mean ± SD	7M / 2F	25.1 ± 2.8	180.9 ± 10.9	80.7 ± 15.0

2.3.2 Experimental Design

All participants performed 24 different lifts with varied lift start-end heights and degrees of twisting (Figure 1). Start-end height combinations included knee-to-waist (KW), waist-

to-knee (WK), shoulder-to-waist (SW), and waist-to-shoulder (WS). Symmetric lifting had 0° of twisting, while asymmetric lifting could be with 90° or 180° of twisting, with turns centered around a neutral posture (i.e., 180° lifts started and ended at ±90° from neutral). Across conditions, participants lifted a 25 lb. (11.34 kg) dumbbell at their preferred lifting speed to fixed shelf positions at knee (17.8 cm (7 in)), waist (72.4 cm (28.5 in)), or shoulder (133.5 cm (52.5 in) height.

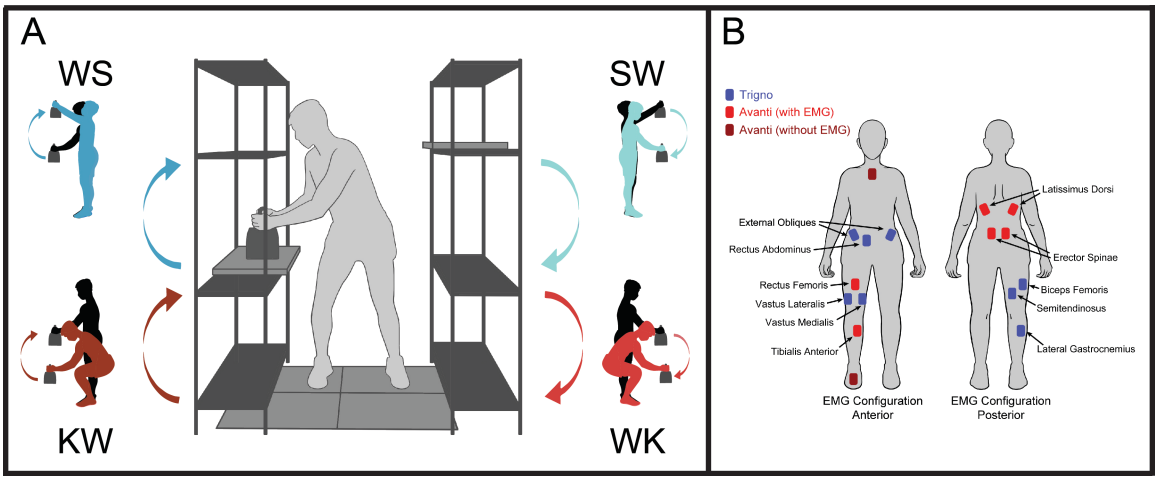

Figure 1 - (A) Manual lifting conditions visualized by starting shelf height and target shelf position of the weight. During 0° (symmetric) lifts, a single shelf was oriented directly in front of participants and weight was lifted to-and-from various heights. For both 90° and 180° (asymmetric) lifting, tasks were performed starting from both sides of the body: left-starting lifts (clockwise rotation) and right-starting lifts (counterclockwise rotation). In 90° lifts, shelves were offset 45° from neutral. In 180° lifts, two shelves were placed on opposite sides of the participants. The top, blue arrows represent above-the-waist lifting conditions: shoulder-to-waist (SW) in light blue and waist-to-shoulder (WS) in dark blue. The bottom, red arrows represent below-the-waist lifting conditions: knee-to-waist (KW) in dark red and waist-to-knee (WK) in light red. (B) Placement of surface EMG sensors. Muscles were selected to capture activity from muscle groups salient to the targeted joints under study: lower back (L5/S1) and knee. Anterior and posterior muscle groups were collected for the torso and legs, but only the right leg was instrumented with sensors.

Participants wore a full-body reflective marker set to record segment positions (Vicon, Oxford, UK, 100Hz). We collected data from fourteen surface electromyography (EMG) sensors (Delsys, Natick, Massachusetts, USA, 2000 Hz). EMG sensors were placed on the right leg muscles (tibialis anterior, lateral gastrocnemius, rectus femoris, vastus medialis, vastus lateralis, bicep femoris, and semitendinosus) and bilaterally on the torso muscles (erector spinae, latissimus dorsi, external obliques, and right-only rectus abdominis) (Figure 1B). Maximum voluntary contractions (MVCs) were performed by each participant preceding the protocol to collect the maximum muscle activations for normalization[74,75]. We used SENIAM to inform sensor placement and MVC collection[76]. We collected ground reaction forces under each foot and each shelf (Bertec, Columbus, OH, USA, 2000 Hz).

2.3.3 Data analysis

2.3.3.1 Data processing

Raw EMG signals were bandpass filtered (20-400 Hz, 2nd order Butterworth), full-wave rectified, lowpass filtered (6 Hz, 5th -order Butterworth), and half-wave rectified to create positively signed envelopes. Finally, the EMG signals were normalized using the peak MVC value across three MVC trials. We used the rate of change of ground reaction force from force plates on the shelves with a threshold value of 0.10 N/s to detect the start-end position of the dumbbell and define the initiation-termination time of each lift.

2.3.3.2 Musculoskeletal analysis

We implemented two OpenSim 4.0 (SimTK, Stanford, CA, USA)[22] models to simulate experimental lifting trials: Full Body Running (FBR) model[77] for knee-joint analyses and Lifting Full Body (LFB) model[21] for L5/S1-joint analyses. The FBR model contains 12 segments with 92 trunk and lower-limb musculotendon actuators, while the LFB model contains 30 segments with 238 torso musculotendon actuators. The FBR and LFB models have a high resolution of knee and back muscles, respectively, providing representative muscle activations and forces from muscles which we collected EMG. To accurately simulate our unique lifting conditions, we modified the range-of-motion constraints of joints within the arms, torso, pelvis, and legs to allot freedom for the model skeleton to match the participants' movements. Additionally, to account for the external load contributions of the 25 lb. weight to internal musculoskeletal states, we added half the dumbbell mass to each hand using OpenSim *WeldJoint*.

Next, we fitted the two OpenSim models to participant-specific anthropometry taken from captured static pose data using the Scaling Tool. We used the Inverse Kinematics Tool to calculate joint angles. OpenSim's Inverse Dynamics Tool computed joint kinetics for each participant incorporating the effects of external loads. We used the Muscle Analysis Tool to solve for musculotendon unit (MTU) lengths and muscle moment arms.

Then, we used the Calibrated EMG-Informed Neuromusculoskeletal Modeling Toolbox (CEINMS)[78] to perform optimization (i.e., simulated annealing) and reduce error in joint and muscle-level property estimations. First, the CEINMS Hybrid mode optimized

muscle activity over those muscles without experimental data inputs. Then, we used both the experimental and simulated muscle excitation signals, musculotendon lengths, and muscle moments to calibrate the model by reducing the error between estimated and experimental joint moments. The following objective function weighting parameters were inspired by those utilized in similar analyses by Molinaro et al.[28] to balance muscle activations and torque tracking performance: torque tracking (α) = 10,000, muscle excitation minimization (β) = 10, and EMG tracking (γ) = 1,000[28].

Finally, we used the OpenSim Joint Reaction Analysis Tool, taking CEINMS simulated output, to calculate the JCFs. From-time series data, we computed peak and integrated values using custom MATLAB scripts. We divided JCFs into normal, shear, and total components. We calculated shear and total JCFs using the Euclidean norm of the anterior-posterior and mediolateral shear forces and the Euclidean norm of the normal and shear forces, respectively. We normalized JCFs by the product of participant mass and acceleration of gravity to minimize the effects of performance variance across participants. To avoid duplication of data in asymmetrical lifting conditions (90° and 180° turns), we compared the forces in clockwise (left-starting) and counterclockwise (right-starting) directed lifts and analyzed/presented the trial with the maximum JCF (i.e. the 'worst case'). We reported right-knee JCFs, from the leg instrumented with EMG sensors.

2.3.4 Injury risk assessment

To better understand how the JCFs produced in performing this study's manual lifting tasks related to injury risk in the lower back and the knee, we compared the JCFs to

injurious joint loading values found in literature. In the lower back, joint loading (moments and internal forces) has been used as a determinant of low back pain risk[79]. A study by Anderson showed that compressive forces of at least 3400 N[79,80] can lead to an increased risk of developing low back pain by 40%[80]. The National Institute for Occupational Safety and Health (NIOSH) went on to recommend this value as a biomechanical criterion in their revised lifting equation[81], which computes an individual's estimated lifting capacity and tasks which expose them to hazardous joint loading. Shear forces of at least 1000 N[79,82–84] are also believed to contribute to increased risk of low back pain[79]. In the knees, similar metrics of joint loading (moments and internal forces) can be indicative of knee pain or disorders such as osteoarthritis[85]. Studies have observed the extreme limits of knee joint loading during blunt trauma experiments which can lead to cartilage degeneration and bone fractures[86]. Haut found that the average contact force of 8500 N led to bone fracturing at the patella or femoral condyles[87]. Kajzer et al. (1999) explained that peak shear forces of 2400 N at the knee lead to ACL-related ligament damage during lateral impact experiments[88]. In order to relate these values to JCFs in our data, we normalized the injury risk threshold peak forces by the average participant weight in Chapter 3 (70 kg multiplied by 9.81 m/s^2). The resulting values used for injury risk assessment are found in Table 2.

Table 2 – Injurious joint loading thresholds for peak and cumulative (integrated) JCFs (x BW).

	Joint	Normal JCF	Shear JCF	Total JCF
Peak Loading	L5/S1	4.9	1.4	5.1
	Knee	12.2	3.5	12.7
Cumulative Loading	L5/S1	489.0	143.6	509.0
	Knee	1220.8	344.7	1269.0

2.3.5 Statistical analysis

We employed a two-way repeated measures Analysis of Variance (ANOVA) to test for significance of lift symmetry, direction, and start-to-end height on each component of the JCFs (H1-3). Subsequently, we performed a *post hoc* Bonferroni pairwise multivariate comparison test to determine statistical significance of differences in JCFs across lifting conditions with the threshold for significance set at $\alpha = 0.05$ (Minitab - Penn State University, State College, PA). We used a linear regression model to compute correlation coefficients between the L5/S1 and knee JCFs (MATLAB) (H4).

2.4 Results

Participants used different postures across lift conditions. Joint kinematics indicate asymmetric lifts had greater L5/S1 flexion (sagittal plane), lateral bending (frontal plane), and axial rotation (transverse plane) than symmetric lifts. Peak right knee flexion (sagittal plane) was less in asymmetric lifts than symmetric lifts across conditions (Figure 2). In addition, participants used different kinetic strategies[25] to perform lifting tasks (Figure 3).

The peak (Figure 10) and integrated (Figure 11) flexion moments about the L5/S1 and right knee joints were smaller in asymmetric lifts (90°,180°) compared to symmetric lifts (0°). The peak (Figure 10) and integrated (Figure 11) lateral bending and axial rotation moments about the L5/S1 joint were greater in asymmetric lifts than symmetric lifts.

Muscle activations are an important variable in determining muscle forces, the primary contributor to JCFs[25,67]. Across lifting conditions (Figure 9), the external obliques (EO), vastus medialis (VM), biceps femoris (BF), and semitendinosus (ST) all had greater peak normalized muscle activations (EMG) in asymmetric (90°,180°) versus symmetric lifts (0°). In contrast, the erector spinae (ES), rectus femoris (RF) and lateral gastrocnemius (LG), all had greater peak normalized EMG in symmetric (0°) versus asymmetric lifts (90°,180°). Latissimus dorsi (LD) and rectus abdominis (RA) muscles had negligible differences in their normalized EMG across lifts.

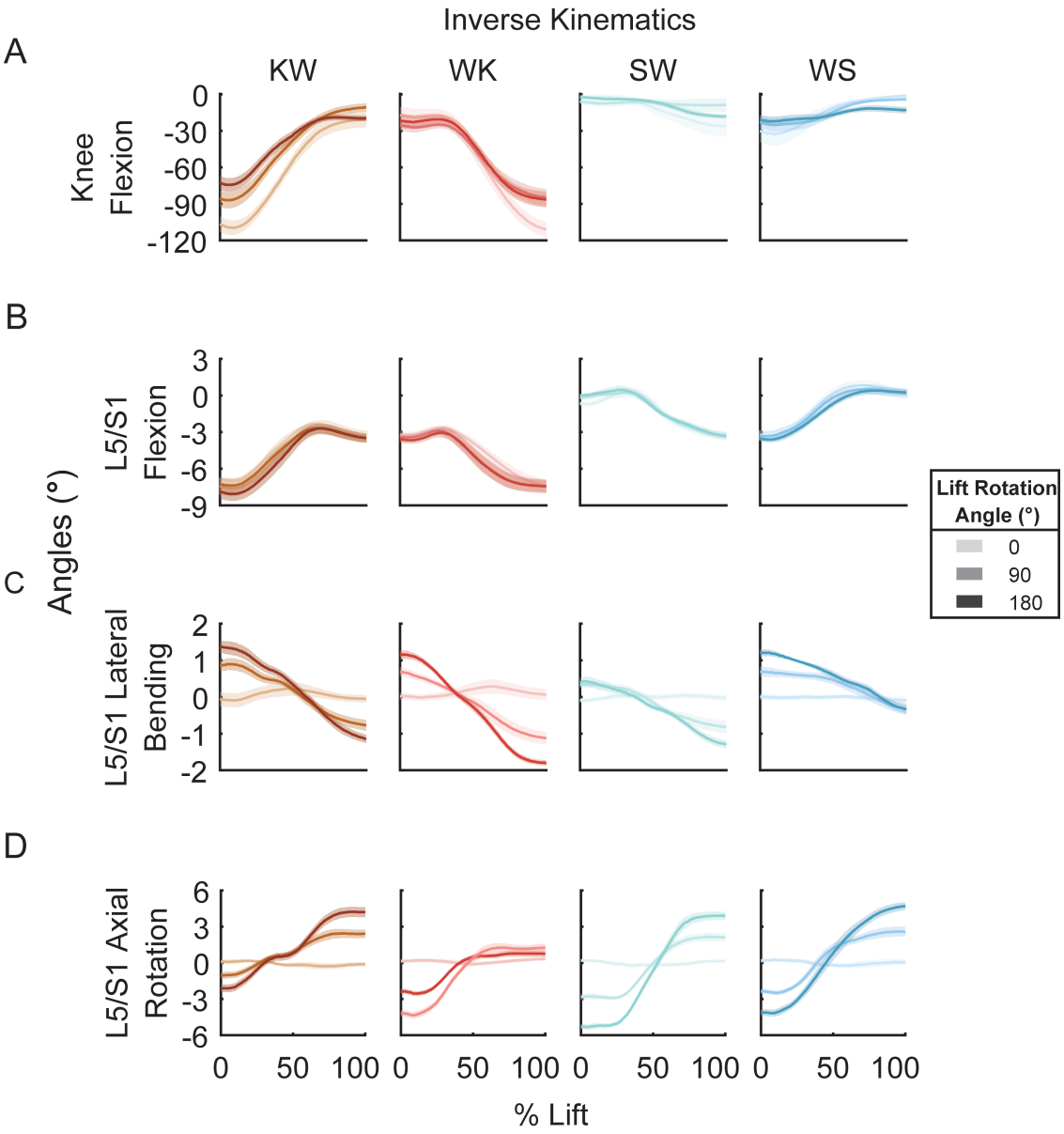

Figure 2 - The across-participant averaged time series of knee and L5/S1 kinematics of knee flexion (A), L5/S1 flexion (B), lateral bending (C), and axial rotation (D) during knee-to-waist (KW), waist-to-knee (WK), shoulder-to-waist (SW), waist-to-shoulder (WS) lifting conditions. The color opacity of each data line increases with the degree turn of lift: from 0° (lightest) to 180° (darkest). The haze surrounding each average represents the standard error of the mean. Positive joint angles for the L5/S1 and knee flexion components resulted in negative values with positive values representing extension. Axial rotation and lateral bending components of the L5/S1 joint were positive counterclockwise and to the right, respectively. Asymmetric lift (90° and 180°) results shown for inverse kinematics are reported from the right starting side, while all knee data is from the right, instrumented leg.

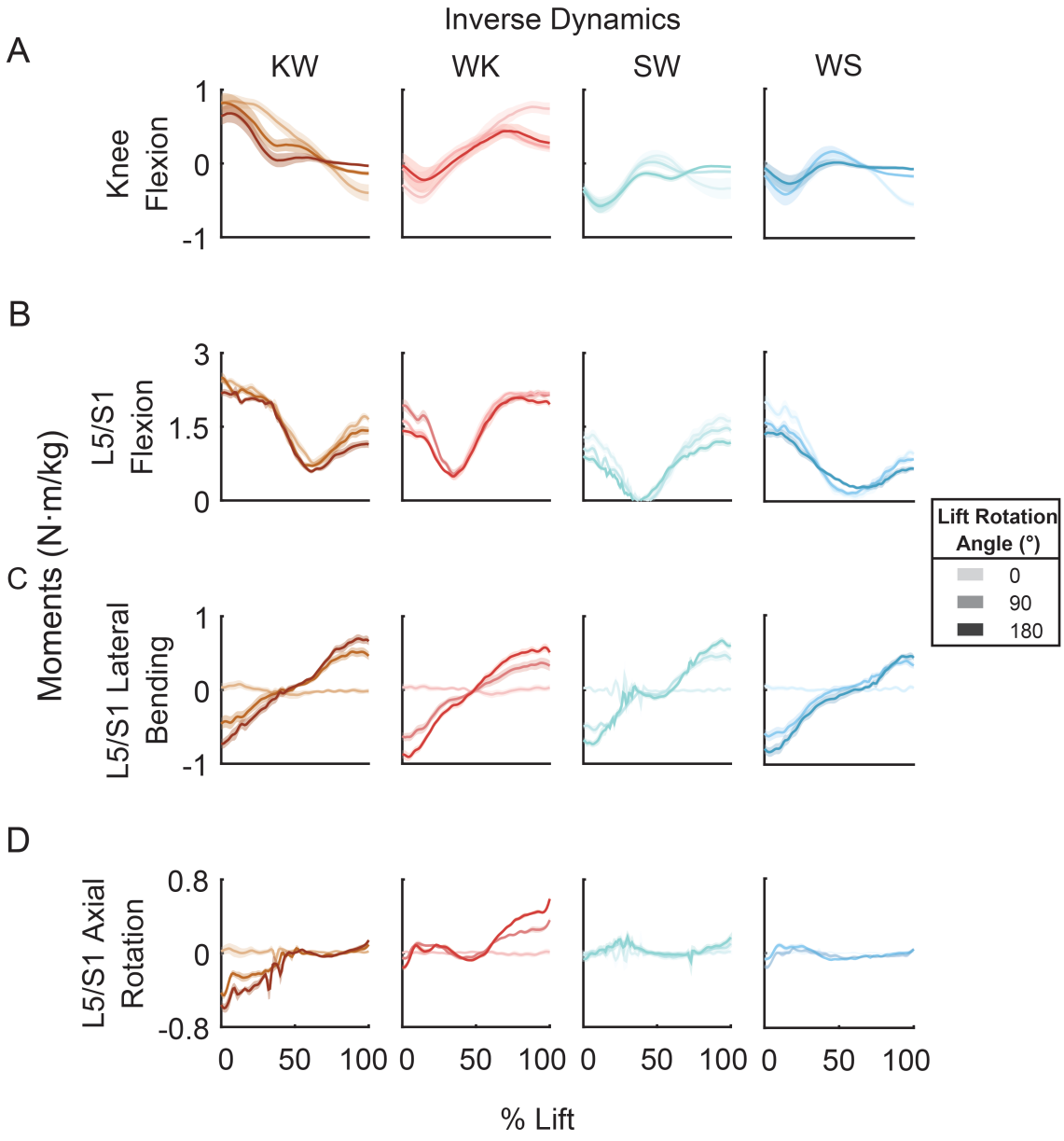

Figure 3 - The across-participant averaged time series of L5/S1 and knee kinetics of knee flexion (A), L5/S1 flexion (B), lateral bending (C), and axial rotation (D) during knee-to-waist (KW), waist-to-knee (WK), shoulder-to-waist (SW), waist-to-shoulder (WS) lifting conditions. The color opacity of each data line increases with degree turn of lift: from 0° (lightest) to 180° (darkest). The haze surrounding each

average represents the standard error of the mean. A comparative analysis was performed across each asymmetric lift (90° and 180°) condition to select data from the starting side (right or left) that resulted in greater (worse) joint moments. Knee joint moments were reported from the right, instrumented leg. Positive joint moments for the L5/S1 and knee flexion components represented greater joint flexion. Axial rotation and lateral bending components of the L5/S1 joint were positive moving away from the starting side.

In the L5/S1 joint, asymmetric lifts (90°/180°) resulted in lower normal, shear, and total JCFs when compared to symmetric lifts (Figure 4A). Peak normal forces were 7.2% ($p = 0.046$) and 20.2% ($p < 0.01$) lower in asymmetric lifts at 90° and 180° versus symmetric lifts (0°), respectively. Peak shear forces were 20.3% ($p = 0.001$) and 14.3% ($p = 0.032$) lower for 90° and 180° lifts versus symmetric lifts (0°). Peak total forces were 7.3% ($p = 0.032$) and 20.6% ($p < 0.01$) lower for 90° and 180° lifts versus symmetric lifts (0°) (Figure 5A, Table 3). Peak normal, shear, and total JCFs were not different in ascending (KW/WS) versus descending (WK/SW) lifts in the L5/S1 joint (Figure 6A). Peak normal, shear, and total JCFs were 21.0%, 49.3%, and 23.3% higher in below-the-waist (KW/WK) than above-the-waist (SW/WS) conditions ($p < 0.01$) in the L5/S1 joint (Figure 7A).

Table 3 - Effect of Lifting Rotation and Start-to-End Height on Knee and Lower-back (L5/S1) Peak Total Joint Contact Forces (x BW)

Knee				
Rotation (°)	**Start-to-End Heights**			
	KW	**WK**	**SW**	**WS**
0°	6.71 ± 2.10	7.81 ± 3.53	5.67 ± 1.34	5.16 ± 1.22
90°	7.82 ± 2.28	8.09 ± 3.16	6.04 ± 1.70	5.54 ± 1.44
180°	6.93 ± 2.22	7.49 ± 3.04	4.02 ± 1.03	4.08 ± 1.03
Lower-back (L5/S1)				
Rotation (°)	**Start-to-End Heights**			
	KW	**WK**	**SW**	**WS**
0°	10.86 ± 3.49	10.01 ± 3.40	8.55 ± 2.95	8.36 ± 2.71
90°	10.04 ± 2.53	9.71 ± 2.62	7.81 ± 2.00	7.45 ± 1.52
180°	9.29 ± 2.68	8.28 ± 2.38	6.16 ± 1.92	6.28 ± 1.57

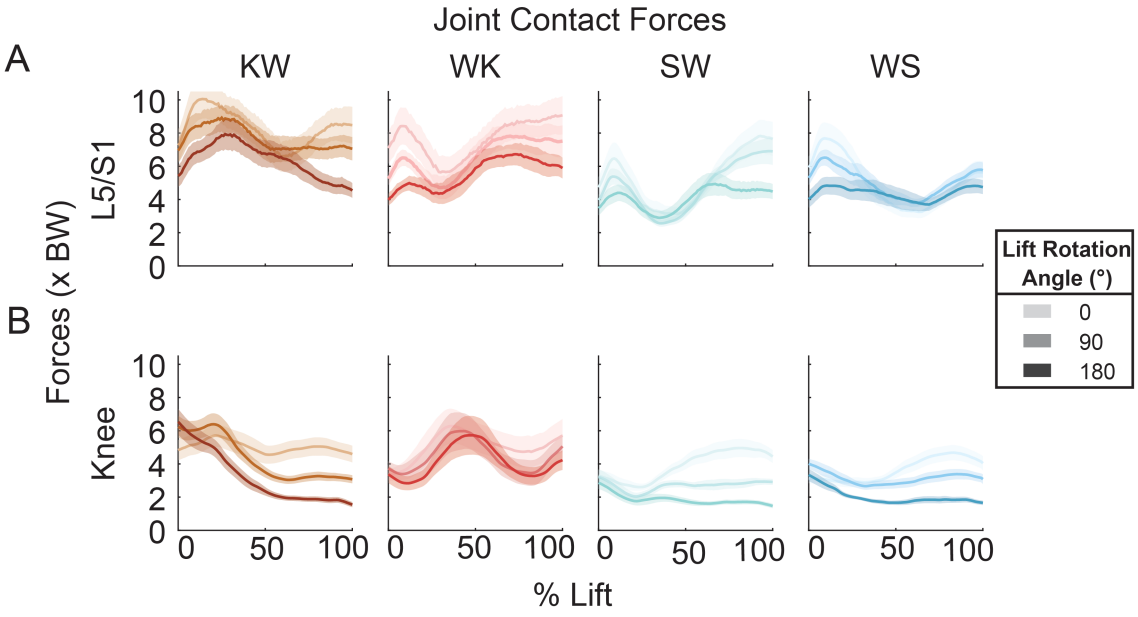

Figure 4 -- The across-participant average time series for total JCFs in the L%/S1 joint (A) and knee (B). The four panels illustrate JCFs from each of the independent lifting conditions: knee-to-waist (KW), waist-to-knee (WK), shoulder-to-waist SW), and waist-to-shoulder (WS).The color opacity of each data line increases with

degree of turn: from 0° (lightest) to 180° (darkest). The haze surrounding each line represents the standard error of the mean.

In the right knee, 180° asymmetric lifts resulted in lower normal, shear, and total JCFs when compared to 0° and 90° lifts (Figure 4B). Peak normal forces were 17.5% lower ($p < 0.01$), peak shear forces were 39.2% lower ($p < 0.01$). Peak total forces were 18.1% lower ($p < 0.01$) in 180° versus 90° lifts (Figure 5B, Table 3). Peak shear forces in the knee were 42.1% greater in descension versus ascension lifting tasks ($p < 0.01$) (Figure 6B). At the knee, peak normal, shear, and total JCFs were 29.6%, 72.8%, and 32.0% higher in below-the-waist versus above-the-waist lifts ($p < 0.01$) (Figure 7B).

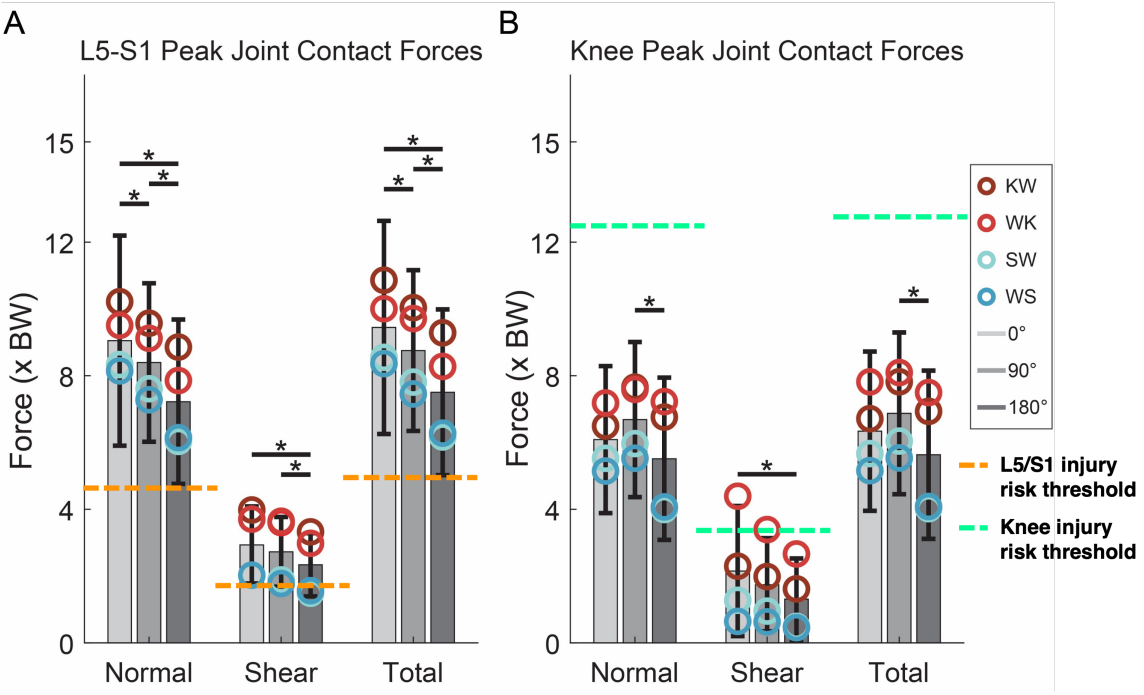

Figure 5 - The across-participant averaged peak normal, shear, and total JCFs in the (A) L5/S1 joint and (B) knee as explored in the first hypothesis (H1). The bars represent the JCF value averaged across the four lift conditions (KW, WK, SW, and

WS) for each of the three lift degrees (0°, 90°, and 180°) in gray. Independent values for each lift condition are labeled as circles in the corresponding color (KW – red, WK – pink, SW – dark blue, WS – light blue). Injury risk thresholds for the L5/S1 joint (estimated from [79,80,83,84,88]) and knee joint (estimated from [86–88]) are represented by orange and green dashed horizontal lines, respectively (see Table 2). Significantly different groups are denoted with an asterisk. Statistical significance across all conditions concluded when α = 0.05.

There was a positive linear correlation ($R^2 = 0.60$, $p < 0.01$) between L5/S1 and knee and JCFs. That is, larger knee contact forces were associated with larger L5/S1 contact and vice versa (Figure 8).

2.5 Discussion

The purpose of this study was to go beyond limb-joint analyses and establish a framework to examine how external loads resolve as three-dimensional JCFs *inside limb-joints* during MMH tasks. Specifically, to gain insight into potential for injury risk from exposure to acute peak loading during repetitive, asymmetric, and physically taxing movements[5], we characterized both lower back (L5/S1) and knee joint loads in occupational MMH lifting tasks across four different starting positions and three degrees of twisting (Figure 1). We hypothesized that asymmetrical (H1), ascending (H2), below the waist (H3) lifts would induce the highest JCFs at both the back and knee. Surprisingly, our data did not support H1 and H2 as asymmetric (180 lifts had *lower* peak normal, shear, and total JCFs than 0 and 90 lifts (Figures 4, 5) and lifting descension (WK/SW) tasks had *higher* peak shear JCFs only at the knee compared to ascension (KW/WS) tasks (Figures 4, 6). In support of H3 and H4, we found that below-the-waist lifting tasks (KW/WK) had

higher JCFs than above-the-waist (SW/WS) lifting tasks for both joints (Figure 7) and the knee and L5/S1 peak total JCFs had a positive linear correlation across the task space (Figure 8).

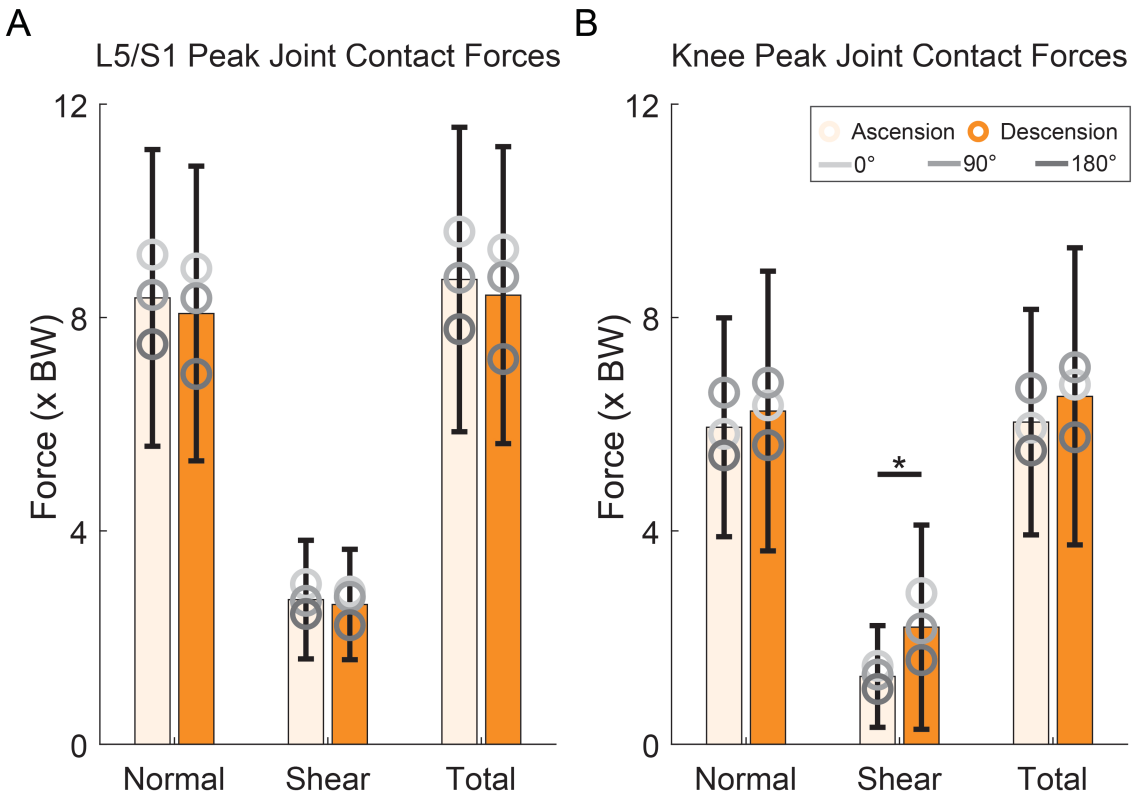

Figure 6 - The across-participant averaged peak normal, shear, and total JCFs in the L5/S1 joint (A) and knee (B) as explored in the second hypothesis (H2). The bars represent the JCF value averaged across the three lift degrees (0°, 90°, and 180°) for both the ascension (KW, WS) and descension (WK, SW) lifting tasks in orange. Independent values for each lift degree are labeled as circles in the corresponding

color. Significantly different groups are denoted with an asterisk. Statistical significance across all conditions concluded when $\alpha = 0.05$.

2.5.1 L5/S1

We anticipated asymmetrical lifting would generate more injurious JCFs than symmetrical lifting (H1) in the L5/S1 joint due to elevated shear forces caused by a shift in segmental centers of mass and increased external loading from the hands holding a weighted object[53]. However, our results suggest that *symmetric* lifting actually induced *higher* peak normal, shear, and total JCFs than *asymmetric* lifting across conditions (Figure 4, Figure 5A). Instances of greater lumbar flexion (Figure 2) aligned with increases in peak JCFs (Figure 4) – a postural shift that causes increased external loading and concomitant increases in muscle activations to stabilize the body, resulting in higher JCFs. Indeed, peak muscle activations, primarily from the erector spinae (ES), and peak L5/S1 joint moments in the sagittal plane were both greater in symmetric lifting than asymmetric lifting (Figures 10, 11). In addition to these findings, we believe local peak JCFs are likely caused by large moment arms created through constraints within the execution of each lifting task. Participants in the study were constrained to place one foot on each force plate, configuring symmetric lifts side-by-side and asymmetric lifts diagonally adjacent. These stance configurations likely affected how they transported the weight from the initial to terminal shelf position. In 0° lifts, shelf placements caused participants to stand further away and extend the weight further from their center of mass. Thus, creating a larger moment arm

about the L5/S1 joint, larger external moments about the lower back, and ultimately higher compressive and shear forces in the joint. In contrast, the asymmetric lifts (90°,180°) did not present shelf obstructions, and participants could hold the weight closer to their torso throughout the lift. This technique yielded smaller moment arms between load and L5/S1 joint and resulted in lower compressive and shear forces in the joint[55].

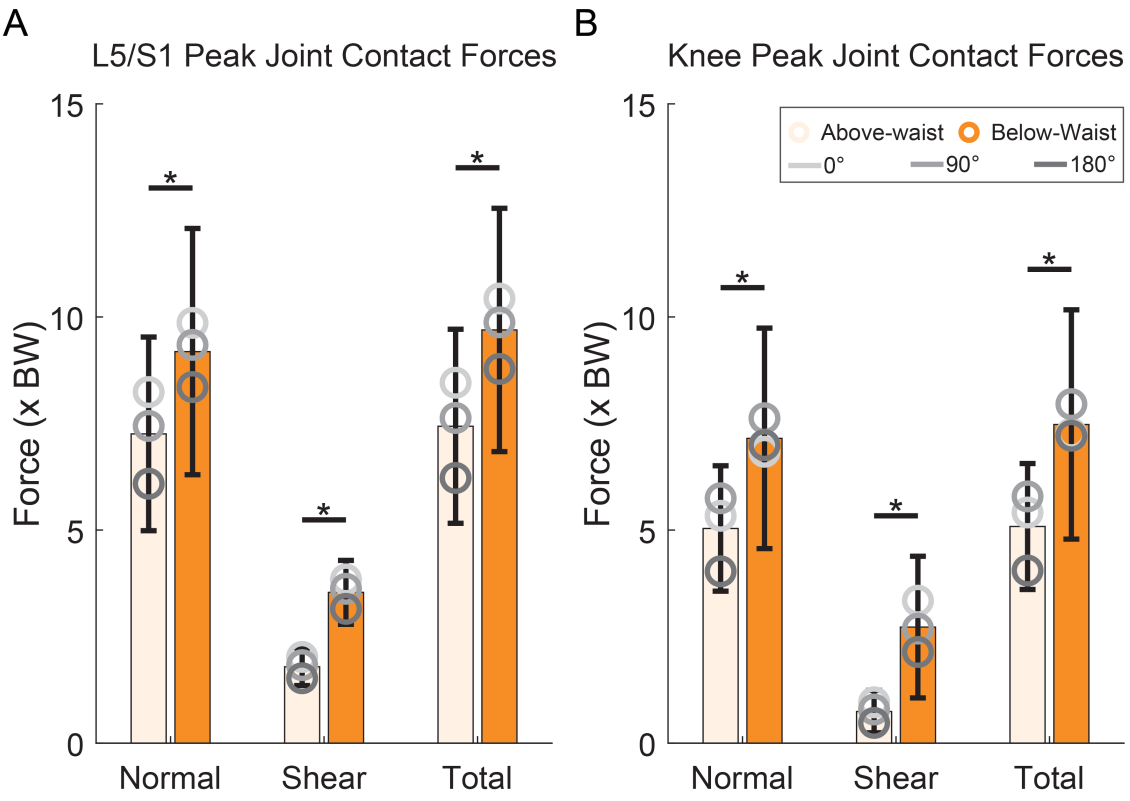

Figure 7 - The across-participant averaged peak normal, shear, and total JCFs in the L5/S1 joint (A) and knee (B) as explored in the third hypothesis (H3). The bars represent the JCF value averaged across the three lift degrees (0°, 90°, and 180°) for both the below-waist (KW, WK) and above-waist (SW, WS) lifting tasks in orange. Independent values for each lift degree are labeled as circles in the corresponding

color. Significantly different groups are denoted with an asterisk. Statistical significance across all conditions concluded when $\alpha = 0.05$.

We predicted that ascending lifts would induce greater contact forces at the L5/S1 joint than descending lifts (H2) because we assumed the lumbar extension moment generated to counteract gravitational and inertial forces, both from the participant and the added mass being lifted, would be higher during ascending lifts[52] (i.e., accelerating upward against gravity would be more demanding). However, we found no significant differences in joint loading when comparing ascension vs. descension (Figure 6A). We found no significant difference in lifting durations between ascension (2.78 s) and descension (2.76 s). The weight lifted was likely did not influence the rate of the lifts in our study or cause inertial effects as large as reported in other studies where participants lifted up to 40 kg[52,56].

We expected that below-the-waist lifting conditions (KW and WK) would cause higher JCFs than above-the-waist (SW and WS) lifting at the L5/S1 joint (H3) due to greater flexion in the trunk, knees, and hips[71]. In flexed postures, higher external moments are needed to compensate for poor mechanical advantage against body weight, shifts in centers of mass across segments[53], and the load of the weighted object in participants' outstretched hands. Our results supported this rationale with below-waist lifts showing higher peak and integrated L5/S1 external moments (Figures 10, 11) to go along with higher peak JCFs (Figures 4 and 7A). This confirms the intuition that lifts with higher degrees of trunk flexion places people in a vulnerable and weaker posture[89] that leads to higher shear forces[60] and increased injury risk.

Our data support that normal, shear, and total JCFs at the L5/S1 joint exceeded the literature-supported tolerance thresholds[79–83] (Figure 5, Table 2). This suggests that similar lifting tasks performed by manual labor workers could lead to an increased risk of developing musculoskeletal disorders such as low back pain[81]. Therefore, we would recommend decreased frequency of performing such tasks, introducing effective breaks, or assistive mitigation strategies[90] to offset the joint loads to be below threshold values.

2.5.2 Knee

We expected that adding asymmetrical twisting to a given lift would induce axial moments about the joint[91] and increase shear forces in the knee leading to higher JCFs when compared to symmetrical lifting (H2). Contrary to our expectation, asymmetry in a lift had little effect on knee joint loading. We propose two potential explanations: (1) the constrained foot placements altered participants' squatting stance width and/or (2) the nonintuitive mechanics of the quadriceps in deep knee flexion. Escamilla et al.[57] found that knee (tibiofemoral) compressive forces were 16% greater in wider stances than narrow stances. Following this line of reasoning, we saw that on average, participants had wider stances and greater contact forces in 90° asymmetrical lifts (Figure 5B) compared to the 0° and 180° lifts. On the other hand, according to Nisell and Ekholm[92], a "wrapping effect" results from the contraction of the quadriceps muscle pulling the patellar tendon posteriorly towards the femur (i.e., intercondylar fossa) in very deep flexion which can act to alleviate knee joint loading by providing an additional contact point for force distribution and transfer[93]. In addition, literature suggests that peak knee compressive joint forces occur

around 90° knee flexion in squatting[93–95]. This further supports our contention that the biomechanical technique that participants used when lifting symmetrically resulted in deeper knee flexion and incited the indirect benefits of the wrapping effect to reduce peak contact forces.

During squat descension the knee extensor moment acts to control deceleration to levels below that induced by gravitational forces. In theory, this external mechanical demand should be less than that in ascent, when the extension moment must first overcome gravitational forces before it can accelerate the limbs – and as a result we expected JCFs to be lower in descent vs. ascent (H2). Surprisingly, we found little difference in JCFs between ascending and descending lifts at the knee. *Only* shear forces showed differences, with statistically greater contact forces appearing in descension versus ascension (Figure 6B), potentially due to the inertial effects of the added mass being lifted. These results agree with the findings of Dahlkvist et al.[96] who also observed similarities in knee joint forces between squats in descent and ascent. De Looze et al.[58] explain that similar muscle activity in ascent and descent lead to loading similarities but suggest that descending tasks are more predisposed to injury occurrence due to muscle lengthening during loading. Similarly, Van Rossom et al.[97], found that medial knee (tibiofemoral) peak and average shear forces are greater in stair descent than in stair ascent which further solidifies the idea that the momentum of deceleration leads to greater JCFs. Taken together, we interpret these studies to suggest that lifting may be safer than lowering heavy weight if the goal is to reduce joint loading on the knees.

Our results support our hypothesis that below-the-waist lifting (KW and WK) would generate higher contact forces than above-the-waist (SW and WS) lifting for knee (H3) (Figure 7B). Delisle, Gagnon, and Desjardins[98] found that minor knee flexion alleviates some stress from the L5/S1 joint in lifting. Indeed, we observed that above-the-waist lifting conditions in this study were performed with only slight knee flexion compared to below-the-waist lifts. In a nearly upright posture, activations and forces of the quadriceps (knee extensors), hamstrings, and gastrocnemius (knee flexor) are known to be relatively quiescent [96], yielding smaller knee JCFs than in below-the-waist lifting.

Our data support that normal and total JCFs at the knee joint are below the literature-supported tolerance thresholds[86–88] (Figure 5, Table 2). However, KW lifts cause shear knee JCFs to exceed the tolerance threshold (Figure 5, Table 2). This suggests that KW lifting tasks performed by manual labor workers could lead to an increased risk of developing degenerative musculoskeletal disorders such as osteoarthritis[85]. Consequently, we would recommend decreased frequency of task performance or intervention tools[90] which offload knee shearing forces to be below threshold values.

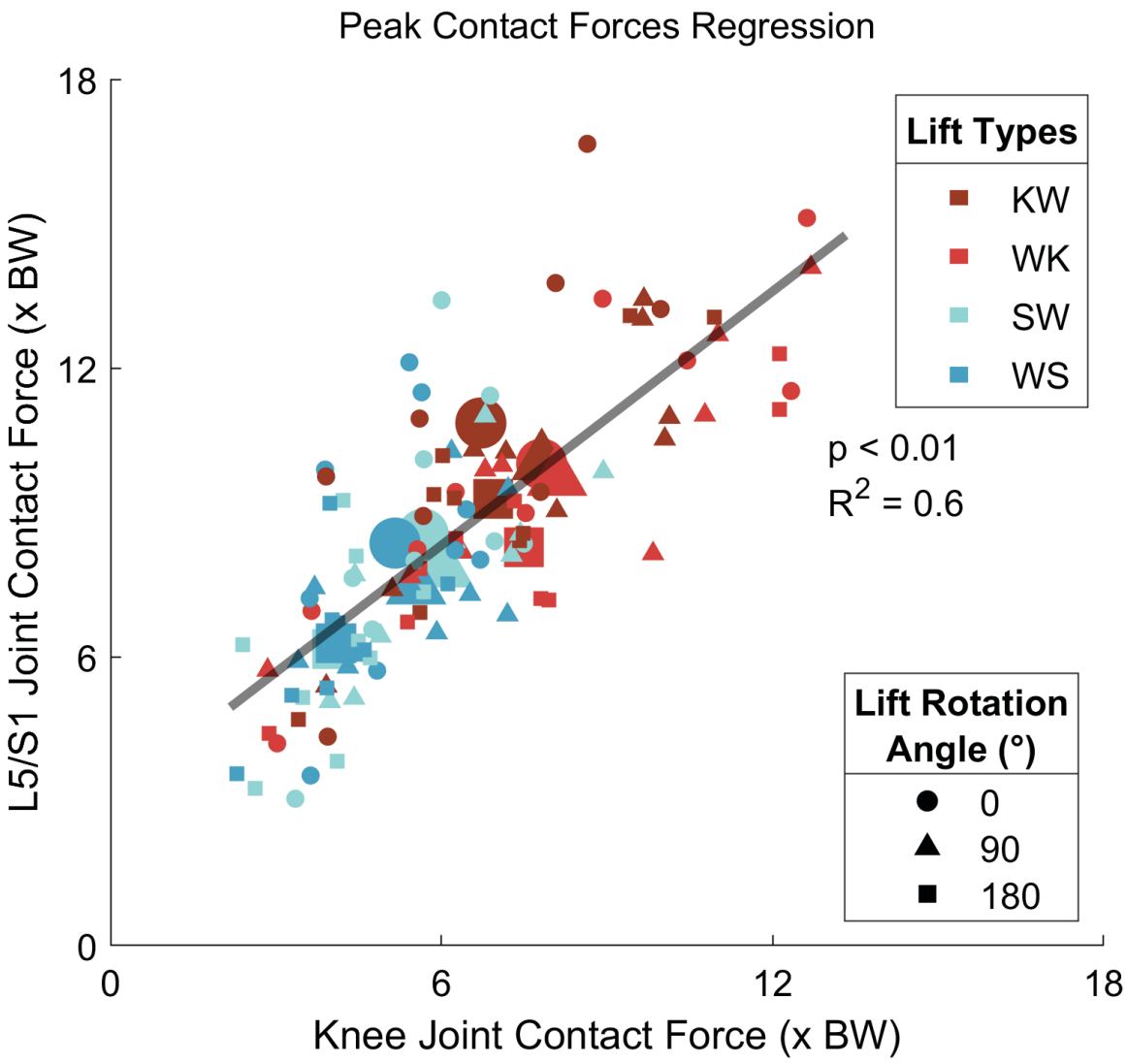

Figure 8 - Linear regression comparing peak total (net) contact forces between the L5/S1 and knee joints as explored in the fourth hypothesis (H4). All lift conditions (KW, WK, SW, WS) and degrees of turn (0°, 90°, 180°) combinations for all nine participants are included in the regression analysis. Each participant's corresponding datapoints are represented by the smaller shapes, while the larger shapes represent across-participant averages for the conditions.

2.5.3 Knee and L5/S1 load distribution

In this study, we allowed participants to lift without a pre-defined technique to assess the effect of natural repetitive lifting on internal joint loading and participants seemed to prefer movements that traded-off loads in lower-back and knee. We found that, across all lifting tasks, peak JCFs between the L5/S1 and knee joints scaled linearly (Figure 8) perhaps reflecting a motor control principle to limit peak loading at any one joint. Studies have confirmed that posture is an important factor[52,71] which can influence load distribution across the body or off-loading away from a joint[91] in lifting tasks. Lifting techniques, such as stoop (backlift) versus squat (leg lifting)[56,58,89,99–101], induce postural constraints that can bias applied external loads and joint moments[91]. For example, studies have shown that lifting form is user-specific and is dependent on the starting height of the movement, but also the trunk, knees, and hips become more kinematically coordinated in below-waist lifting; hence why often the preferred lifting technique is a blend between stooping and squatting[51,72]. Along these lines, Splittstoesser et al.[102] conducted a lifting study while kneeling, fixing the role of the knee joint. Interestingly, they found that without contributions from the knee to perform the lift, moving loads to positions above the waist led to greater compressive forces in the back. Thus, highlighting the potential importance of coordinating lower-limb joints to reduce loading in the lower back[71]. Indeed, Bejjani et al.[73] concluded that both the back and the knees must bend about 60° and 90°, respectively, to reduce the average force distributed between both joints; thus posing the question if individuals might naturally opt for lifting postures which produce lower average JCFs.

2.5.4 Limitations

There are several limitations which could have affected our experimental outcomes. We controlled the weight being lifted (11.34 kg), lifting conditions (starting-ending positions and degree of turn), and foot placement; however, the rate of lifting, consistency in reach distance from shelf, and stance width are all factors which were loosely regulated and may have contributed to variance in our results. We collected EMG from 14 muscles across the torso and legs, limiting CEINMS to simulate most muscle activity. Knee JCF results were focused on the right, EMG-instrumented leg, but we expect similar forces on the left knee. Also, the lack of female representation in this study restricted us from investigating the effects of sex on JCFs.

Lastly, utilizing discrete tolerance thresholds to relate the JCFs shown in this study to injury risk does not capture as many nuances of the task which largely affect the joint loading risks. Evaluation tools such as the revised NIOSH lifting equation[81,103] take into account critical features[104] like vertical and horizontal distance of the lifting weight (moment arms) and the asymmetrical lifting angle to better characterize the lifting capacity of a person for that task and if a task is potentially harmful to their lower back. We would recommend utilizing a more complex injury risk equation or assessment tool to compare its ability to measure and identify hazardous JCFs.

2.6 Conclusion

This study investigated how JCFs in the knee and lower-back (L5/S1) vary during manual lifting tasks. We found highest JCFs in symmetric (i.e., load straight in front of the body), below the waist lifting tasks. Taken together, our results suggest that asymmetric lifting can *actually reduce* JCFs in the lower back and knee when compared to moving loads straight in front of the body. Interventions to reduce JCFs during heavy lifting should emphasize transporting weight above the waist or close to the body, while encouraging postures that minimize trunk and knee flexion (i.e., small external moment arms). Therefore, asymmetrical twisting and lifting may not be as hazardous to joint loading. Lastly, we found that JCFs were proportionally distributed across knee and lower back joints, suggesting that preferred lifting techniques might be selected to balance JCFs across joints and avoid local overloading – a motor control principle indicating a trade-off that might be leveraged by assistive technology applied at one joint (e.g., back) to protect another (e.g., knee).

2.7 Conflict of Interest Statement

There is no conflict of interest reported by the authors.

2.8 Acknowledgements

This work was supported by Sandia National Laboratories, a multi-mission laboratory managed and operated by the National Technology and Engineering Solutions of Sandia LLC, a wholly owned subsidiary of Honeywell International Inc. for the U.S.

Department of Energy's National Nuclear Security Administration under contract DE-NA0003525. This paper describes objective technical results and analysis. Any subjective views or opinions that might be expressed in the paper do not necessarily represent the views of the U.S. Department of Energy or the United States Government. We would like to formally thank Jason Wheeler for his instrumental involvement in the development of this study. We would also like to show our appreciation to all the participants of this study.

2.9 Supplementary Figures for Chapter 2

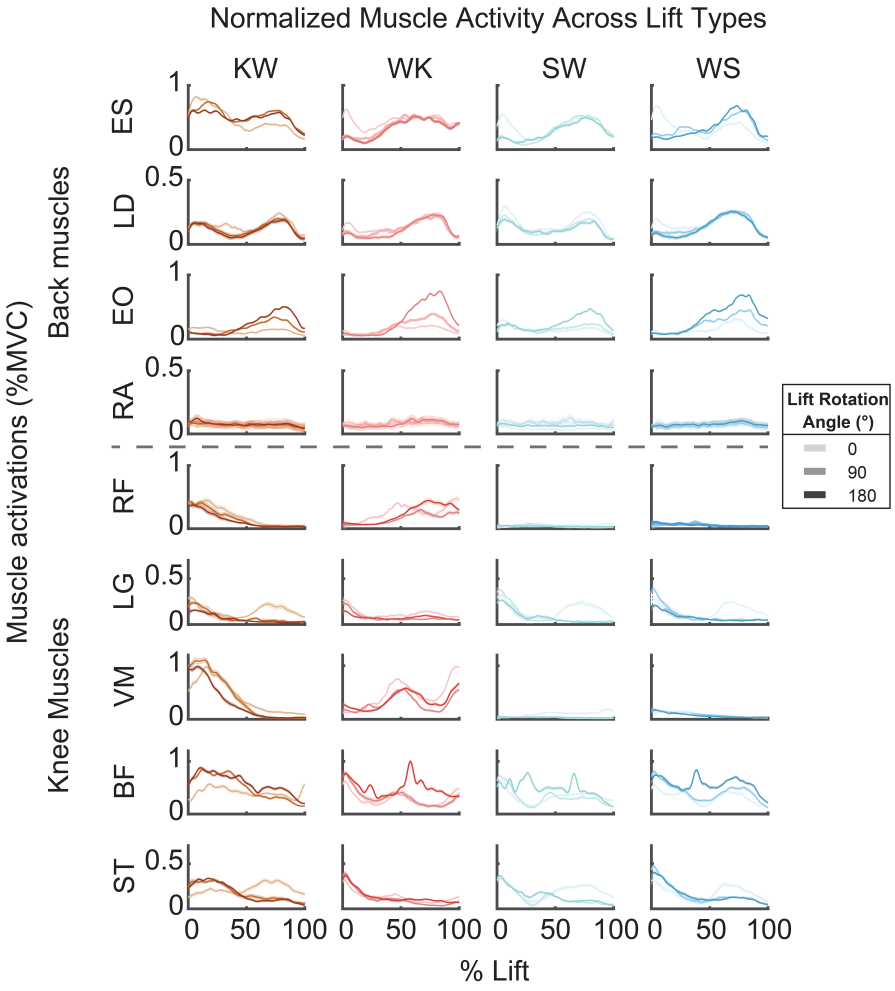

Figure 9 - The across-participant averaged time series of normalized muscle activity in relevant muscles to the back (ES- right erector spinae, LD – right latissimus dorsi, EO – right external oblique, RA – right rectus abdominis) and the knee (RF – right rectus femoris, LG – right lateral gastrocnemius, VM – right vastus medialis, BF – right biceps femoris, ST – right semitendinosus) during knee-to-waist (KW), waist-to-knee (WK), shoulder-to-waist (SW), waist-to-shoulder (WS) lifting conditions. The color opacity of each data line increases with degree turn of lift: from 0° (lightest) to 180° (darkest). For ease in visualization, the left counterparts of back-relevant muscles were excluded, as well as tibialis anterior for the knee.

Experimentally collected EMG data is reported as the average and the standard error of the mean of the adjusted EMG signals reconfigured via CEINMS are illustrated by the surrounding haze to confirm that the corresponding muscle forces from activations used to compute joint contact forces remain consistent to those that are experimentally collected.

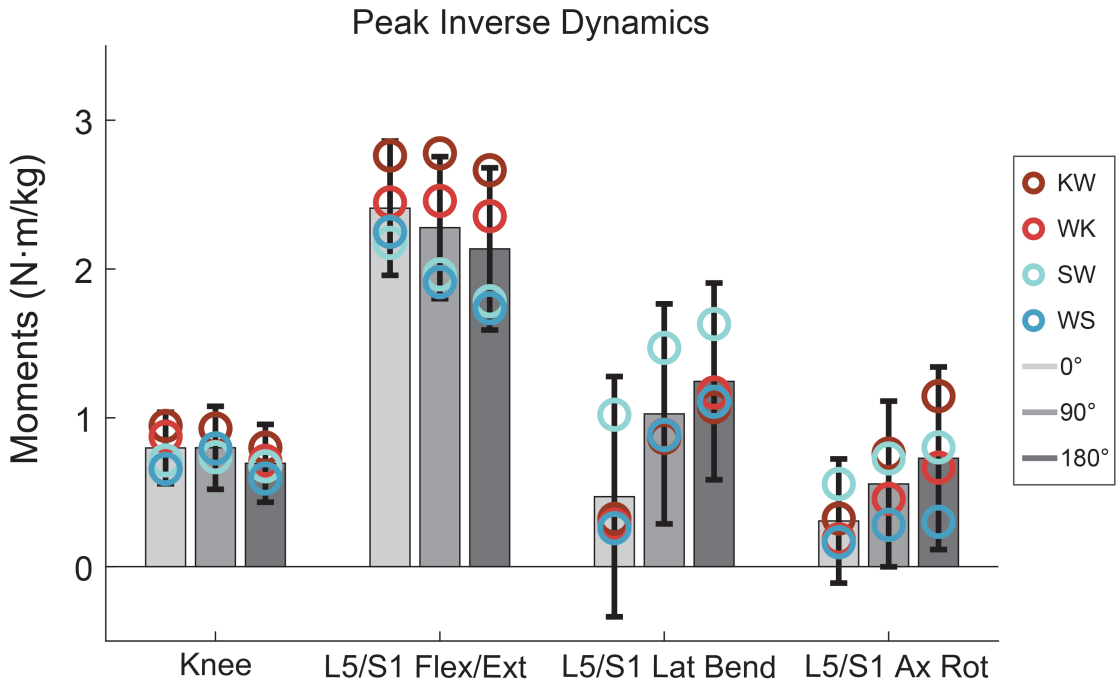

Figure 10 - The across-participant averaged peak normal, shear, and total joint moments in the knee and L5/S1 joint as explored in the first hypothesis (H1). Gray bars represent the joint moments averaged across the four lift conditions (KW, WK, SW, and WS) for each of the three lift symmetries (0° =light gray, 90°, and 180°= dark gray). Independent values for each lift condition are labeled as circles in the corresponding color (KW – red, WK – pink, SW – dark blue, WS – light blue). Significantly different groups are denoted with an asterisk. Statistical significance across all conditions concluded when $\alpha = 0.05$.

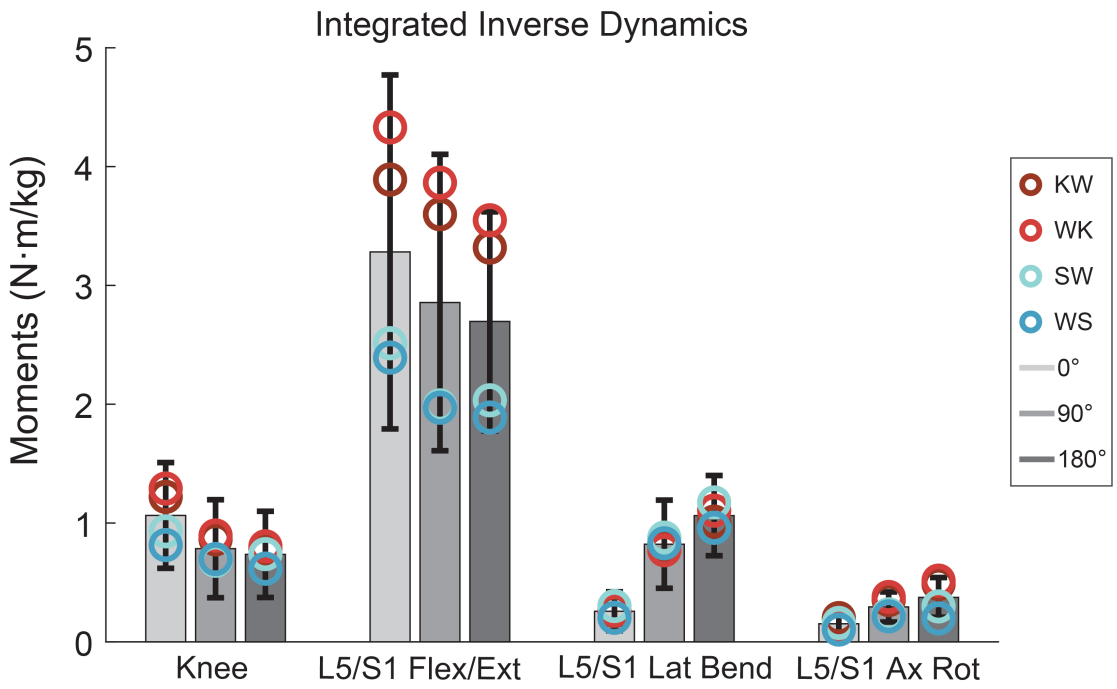

Figure 11 - The across-participant averaged integrated normal, shear, and total joint moments in the knee and L5/S1 joint as explored in the first hypothesis (H1). The bars represent the joint moments averaged across the four lift conditions (KW, WK, SW, and WS) for each of the three lift degrees (0°, 90°, and 180°) in gray. Independent values for each lift condition are labeled as circles in the corresponding color (KW – red, WK – pink, SW – dark blue, WS – light blue). Significantly different groups are denoted with an asterisk. Statistical significance across all conditions concluded when $\alpha = 0.05$.

CHAPTER 3. ASSESS THE EFFECTS OF EXOSKELETONS ON JOINT CONTACT FORCES ACROSS INDUSTRY- RELEVANT LIFTING TASKS AND JOINTS

The second work of my dissertation examines the effect of an active knee exo and a passive back exo on internal joint loading in the lower back and knees during manual lifting. This work is currently undergoing internal review and we intend to submit to IEEE Transactions on Medical Robotics and Bionics and is tentatively titled "Offsetting The Load: Can Exoskeletons Mitigate Injury Risk During Industrial Lifting Tasks?". The manuscript is outlined in the following chapter.

3.1 Abstract

Due to the prevalence of repetitive lifting, twisting, and bending tasks in the workplace, interventions are needed to reduce the occurrence of musculoskeletal injuries. Exoskeletons could be that solution, but we have yet to understand how they could reduce injury risk resulting from hazardous internal joint loading. To quantify exoskeletons' influence on joint loading, we recruited N=10 participants to perform two-handed manual lifting of an 11 kg weight while donning (active knee and passive back (HeroWear)) and doffing an exoskeleton. The lifting captured combinations of asymmetrical/asymmetrical, lifting and lowering between knee and waist height. We implemented musculoskeletal modeling (OpenSim, CEINMS) to integrate kinematics and kinetics with EMG-informed muscle force approximations to estimate knee and lower-back joint contact forces (JCFs). We found that the HeroWear reduced peak shear JCFs at the L5/S1 joint by 17.4% ($p <$

0.03). The active knee exoskeleton reduced peak normal and total JCFs in the knee by 12.1% ($p < 0.018$) and 11.2% ($p = 0.03$). The exoskeletons also reduced JCFs in the non-targeted joint of assistance: the HeroWear reduced total JCFs in the knee by 6.1%, and the knee exoskeleton lowered L5/S1 shear JCFs by 6.6%. Thus, suggesting the utility of the HeroWear and knee exoskeleton at directly and indirectly relieving tissue overexertion in the lower-back and knee and reducing the risk of injury in manual lifting.

3.2 Introduction

The prevalence of musculoskeletal disorders continues to persist in the workplace, imposing both physical and financial burdens on laborers[11,12]. The repetitious bending, twisting, and lifting[5–8] inherent in manual labor professions, such as loaded carriage by patient transporters[4], leave workers susceptible to excessive joint and tissue loading[50] and overall overexertion - the leading cause of musculoskeletal disorders[3] such as low back pain or knee osteoarthritis. Biomechanical analyses have shown how various factors such as lifted mass[51–53], lowering versus ascending[58,59], and lifting symmetry[28,52,53,56,58,60] influence movement (kinematics) and external contributions of joint loading to provide insight on musculoskeletal injuries. However, characterizing the *internal* forces articulating across bone-on-bone junctions offers a more direct reference point for musculoskeletal injury risk assessment. Joint contact forces (JCFs), the bone-to-bone forces required to support forces elicited from muscles, ligaments, tendons, and external loads[25]. Technological advancements in computational tools[19,20,22,65] allow us to estimate muscle forces and JCFs without utilizing invasive practices[21–24,64,105,106]. There exists a need for promising intervention technology to reduce the effects of hazardous external

loads on JCFs, and consequently the occurrence of musculoskeletal disorders, in manual labor tasks.

Wearable robotic devices are a promising solution to offload the harmful effects of external loading on internal *limb-joint* forces during manual labor. More specifically, the use of exoskeletons has lowered whole-body energy expenditure (metabolics)[31,33,107,108], muscle activations[35,108], and joint moments[32,108] during walking and manual labor tasks. Since muscle forces more often the dominant contributor to JCFs[67], the ability of exoskeletons to reduce muscle activations and forces[108–110] is promising to also offload JCFs[110–112]. Exoskeletons, however, can be developed to be very task dependent, limiting their applications and overall usability. Multi-joint assistive devices could be the solution[111,113] as they can simultaneously directly assist more areas, but also strategic design of single-joint devices could have residual benefits to neighboring joints and tissues[111]. Additionally, as more exoskeleton designs and studies are focusing on improving muscle fatigue[110,114], task performance[114], and comfortability[114,115] – work conditions often plagued by overexertion and poor device design – they prove to be a more viable intervention strategy for mitigating workplace injuries.

The intent of this research is to advance analytical practices on internal *limb-joint* forces and assess the influence of exoskeleton assistance on lower-back and knee three-dimensional JCFs during manual lifting tasks. There is a limited understanding on whether positive effects observed from exoskeletons usage may be harmful or beneficial to the loads experienced within the joint capsule, and consequently, how this may affect injury risks. To address this, wearable devices need to be properly characterized to better represent their assistance's contributions to JCFs. To emulate a controlled experience of manual laborers, we designed an experimental protocol consisting of manual lifting tasks varying in

symmetry and lifting/lowering, each performed with exoskeletons donned (passive lower-back device, active knee device) and doffed (no device). By leveraging musculoskeletal modeling and optimization tools[65,105] which utilized motion capture, electrography, force plates (external forces), and torque/force outputs from the exoskeletons as inputs, we evaluated the effects of exoskeletons on knee and lower-back (L5/S1) JCFs. Previous research has shown that lower-back exoskeletons reduce compressive loading in the lumbar spine[109,112]; therefore, we hypothesized that the passive lower-back exoskeleton would reduce JCFs in the low back (L5/S1 joint) during industry-relevant lifting and the active knee exoskeleton (KE) would lower JCFs in the knee (H1). Furthermore, we also hypothesized that the either devices' assistance will lower the JCFs of the non-targeted joint, meaning the KE will reduce L5/S1 JCFs and the HW will decrease knee JCFs during manual lifting (H2). The results will shed light on the inherent advantages or disadvantages of assistive devices for manual lifting tasks and inform future designs and implementations of industry-directed wearable devices to target offloading critical joint loads during manual labor.

3.3 Methods

3.3.1 Participants

Ten healthy participants (Table 4) enrolled in this study, who did not exhibit or have a history of any debilitating neurological, musculoskeletal, or cardiovascular conditions which prevent the successful completion of manual labor tasks. The Georgia Institute of Technology Institutional Review Board approved of this research study, and we obtained signed consent from all participants prior to data collection.

Table 4 – Exo assistance study participant demographics. Standard deviation = SD.

Participant	Gender	Age (years)	Height (cm)	Weight (kg)
1	M	25	169.3	79.55
2	M	22	174.1	78.15
3	F	26	177.75	90.95
4	M	25	173	78.05
5	M	24	171.85	70.75
6	M	22	177.8	62.95
7	M	24	164.6	61.05
8	F	30	159.6	62.15
9	M	21	169.85	70.35
10	M	19	173.8	52.5
Mean ± SD	8M / 2F	23.8 ± 2.9	171.2 ± 5.4	70.6 ± 10.7

3.3.2 Experimental Design

3.3.2.1 Experimental lifting tasks

Participants completed 12 lifting configurations of lift start-end heights, degrees of twisting, and exoskeleton usage. Lifts were initiated from knee height (knee-to-waist (KW)) or waist height (waist-to-knee (WK)), while degrees of twisting included 0° (symmetric), or facing forward, and 90° (asymmetric) turns (Figure 12A). Asymmetric lifts began on either the right or left side with 90° rotations towards neutral (facing forward). The order of exoskeletons usage was randomized, as well as the order of performed tasks within each exoskeleton condition. All lifts were performed at the participants' preferred lifting speed while holding a 25 lb. (11.34 kg) dumbbell at their preferred lifting speed to fixed shelf positions at knee (17.8 cm (7 in)) and waist (72.4 cm (28.5 in)) height.

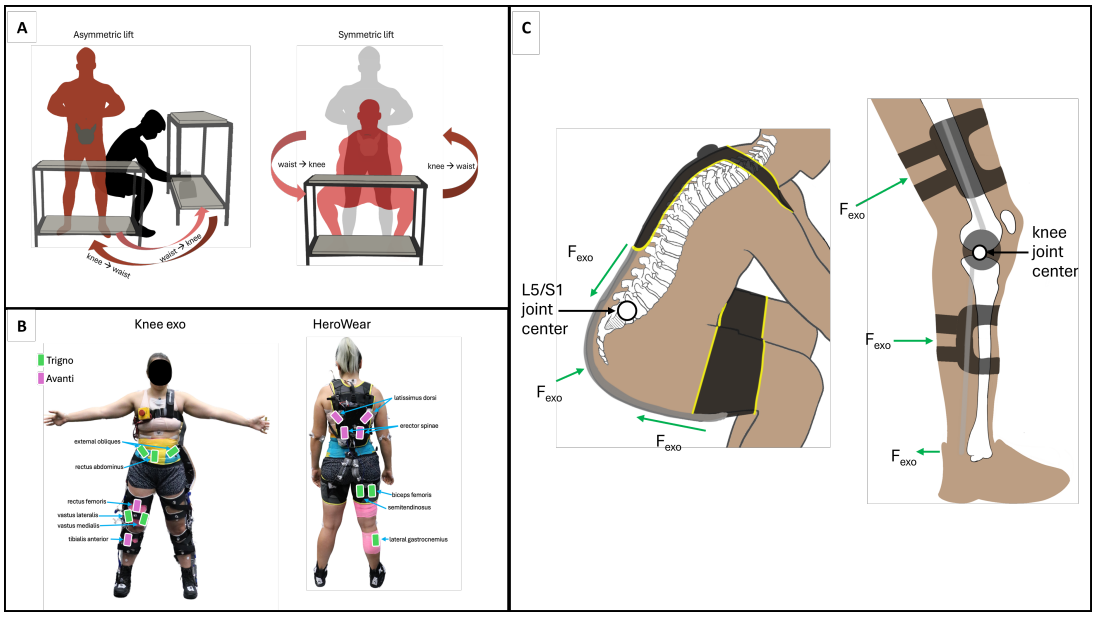

Figure 12 - (A) Visualization of asymmetric -- 90° (left) and symmetric -- 0° (right) lifting conditions with starting and target shelf height configurations between the knee and waist. Duplicates of asymmetric lifting were performed by starting from both sides of the body to capture clockwise rotations (left initial side) and counterclockwise rotation (right initial side). Shelves were offset 45° from participants' neutral stance to perform 90° lifts. The dark maroon arrows represent knee-to-waist (KW) lifts and pink arrows represent waist-to-knee (WK) lifts. (B) EMG sensor placements of muscles whose activity has influence on this study's targeted joints: the knee and lower back (L5/S1). Sensors were placed anteriorly and posteriorly on the torso and right leg. Also shown are the exoskeleton devices utilized: active knee (left) and HeroWear (right). (C) Representation of device assistance modeled as force vectors acting along the body in sagittal plane. The force vectors were modeled as bilateral vectors, so that there was a total of six from the active knee exo and six from the passive back exo.

3.3.2.2 Data collection

We instrumented participants with full-body reflective marker sets to track body segment orientations (Vicon, Oxford, UK, 100Hz) and recorded muscle activity from fourteen surface electromyography (EMG) sensors (Delsys, Natick, Massachusetts, USA, 2000 Hz). EMG sensor placements, informed by SENIAM[76], included the right leg (rectus

femoris, vastus medialis, vastus lateralis, bicep femoris, semitendinosus, tibialis anterior, and lateral gastrocnemius) and the trunk, bilaterally (erector spinae, latissimus dorsi, external obliques, and right-only rectus abdominis). (Figure 12B). We obtained ground reaction forces under both feet and forces from the dumbbell on the shelves (Bertec, Columbus, OH, USA, 2000 Hz).

3.3.3 Data analysis

3.3.3.1 Data processing

Raw EMG signals were processed using a bandpass filter (20-400 Hz, 2nd order Butterworth), full-wave rectification, a low-pass filter (6 Hz, 5th-order Butterworth), and a final half-wave rectification to ensure positive muscle activations. We performed a sweep across all tasks to find which lifting condition caused the most of the muscles recorded to experience peak activations (90° knee-to-waist) and averaged across 5 maximum values for each muscle to serve as our maximum voluntary contraction value. We then normalized EMG signals to these averaged peak activation values. We used the rate of change of ground reaction force with a threshold value of 0.10 N/s to detect the start-end position of the dumbbell and define the initiation-termination time of each lift.

3.3.3.2 Musculoskeletal analysis

We recruited two musculoskeletal models equipped to account for the involvement of arms to simulate the experimental lifting motions totally using OpenSim v4.0 (SimTK, Stanford, CA, USA). The Full Body Running model includes 92 musculotendon actuators distributed within the trunk and lower extremities, providing a high resolution of muscles about the knee joint. The Lifting Full Body model includes 238 musculotendon actuators

distributed within the trunk, providing a high resolution of muscles spanning the back and spine. To better track the participants' motion, we modified the ranges of motion constraints for joints in the arms, torso, pelvis, and legs. To account for the dumbbell's inertial contributions, we havened its mass and applied it to each hand using OpenSim *WeldJoint*.

To compute joint angles, moments, and contact forces, we followed the computational methodology outlined by Davenport et al.[105] with the exception the execution of Inverse Dynamics. We expressed the exoskeleton assistance as external forces prior to running the Inverse Dynamics Tool. Refer below to section 3.3.3.5 for details on this process.

We computed all data and extracted features highlighted in the results using custom MATLAB scripts. We split JCFs into normal, shear, and total components. Shear JCFs are the Euclidean norm of the anterior-posterior and mediolateral shear forces. Total JCFs are the Euclidean norm of the normal and shear forces. JCFs are normalized to the product of mass and acceleration of gravity (times body weight). To condense our dataset for analysis and visualization, we compared joint moments and contact forces for 90° asymmetrical lifting by averaging across the clockwise and counterclockwise-directed performance of the same task (e.g., 90° waist-to-knee, starting right versus starting left). Thus, permitting our analyses to report representative outcomes for variations in natural lifting techniques.

3.3.3.3 Injury risk assessment

Similar to Chapter 2, we leveraged joint loading tolerance values found in literature to assess the effectiveness of the exos in reducing injury risk in the lower back and knee. In the lower back, the compressive force of 3400 N[79,80] and the shear force of 1000 N[79,82–

[84], which have shown relevance to increased risk of developing low back pain[79], were used as L5/S1 JCF tolerance criterion. In the knees, the compressive force of 8500 N[87] and the shear force of 2400 N[88] were used as knee JCF tolerance criterion. To assess the exos' affect on injury risk in cumulative loading, we integrated these tolerance criteria values over a full lift cycle. In order to relate these values to JCFs in our data, we normalized the injury risk threshold peak and integrated forces by the average participant weight in (70 kg multiplied by 9.81 m/s^2). The resulting values used for injury risk assessment are found in Table 2.

3.3.3.4 Statistical analysis

We performed one-way repeated measures ANOVA to test for the significance of using no exo, an active knee exo, and a passive back exo on normal, shear, and total JCFs at the knee and L5/S1 joint (H1-H2). To do this, we utilized a Mixed Effects Model with participants as random factors, exo conditions as fixed factors, and the continuous response variables were the desired JCF component. A *post hoc* Bonferroni pairwise multivariate comparison test evaluated the statistical significance between the resulting knee and back JCFs averaged across all lifting conditions from exo usage with the threshold for significance set at $\alpha = 0.05$ (Minitab - Penn State University, State College, PA).

3.3.3.5 Exoskeleton selection

Previous findings by Davenport et al.[105] highlight the need for intervention strategies at the knee and lower back to reduce JCFs and resulting injuries; thus, informing

our selection of knee and back exoskeletons. The knee exoskeleton (KE) was locally constructed in Georgia Institute of Technology's Exoskeleton and Prosthetic Intelligent Controls Lab[90,116]. This device was rigidly anchored to the user's shoe, with Velcro straps fastening the thigh and shank interfaces to their respective segments (Figure 12C), with the motor aligned in parallel with the knee joints, providing an extension torque that dampened the lowering phase of a lift and a spring-like assist during the ascending phase of a lift. The KE weighed 4.8 kg and actively provided bilateral assistance up to 17 N-m torque, and 9 N-m continuously. Complete details on its impedance controller design are outlined in work by Nuesslein et al.[90] We chose the HeroWear Apex exosuit (HeroWear Apex, HeroWear, USA) as our back exoskeleton. The HeroWear (HW) device is a commercially available comprised of soft, breathable trunk and thigh interfaces linked by two elastic bands and weights 1.9 kg. When the HW is engaged, the elastic bands stretch about the users' backside during trunk flexion to provide assistance passively. We instrumented a uniaxial load cell (2000 Hz) in series to the elastic bands to record the summed band force synchronously with motion data.

3.3.3.6 Modeling of exoskeletons

Standard procedure in biomechanics analyses with exoskeletons is to subtract the device's torque contribution from the total moment calculated from inverse dynamics to get biological joint moments. JCFs are sensitive to the moment arms that forces are applied with respect to the joint; hence why large muscle forces close to the joints dominate the intersegmental forces which arise from external loading[25,67]. For these reasons, we exercised caution in the modeling of assistance from the KE and HW as external point forces in OpenSim.

For the KE, we modeled the assistive torque as six posterior force vectors in the thigh, shank, and foot, bilaterally (Figure 12C). We utilized the measured torque (200 Hz) output variable measured by the actuators to capture the true assistance each user experienced during the lifting tasks due to user resistance (Figure 13B). The measured torque was processed with a bandpass filter (5-20 Hz, 4th-order Butterworth). We used positions of reflective markers on the thigh, shank, foot, and bony landmarks to compute moment arms about the knee joint and construct a plane for each segment about which we oriented each force vector using linear algebra. We made the assumption that the torque is applied purely to the thigh segments (Equation 3), but there is a coupled dynamic between the shank and foot due to the device's foot/ankle attachment point producing residual torques. Next, we generated systems of equations for the sum of forces, $\sum$F(x, y, z) (Equation 2), and torques,$\sum\tau$(x, y, z) (Equation 1), about the thigh, shank, and foot, with the thigh force and torque terms being known (Equation 4). We constrained these equations to remain balanced to match the kinematics performed. Using Gaussian elimination, we solved the unknown thigh and foot/ankle forces and torques in each linear equation. Assuming a uniform distribution of force on each segment's exoskeleton interface, we calculated the average position of the thigh, shank, and foot markers to define the location of the point force.

$$\sum\vec{\tau} = \vec{\tau}_{exo} + \vec{\tau}_{foot} + \vec{\tau}_{shank} = \vec{r} \times \vec{F} \quad (1)$$

$$\sum\vec{F} = \vec{F}_{thigh} + \vec{F}_{foot} + \vec{F}_{shank} = m\vec{a} \quad (2)$$

$$\vec{\tau}_{exo} = \vec{\tau}_{thigh} = \frac{\vec{r}_{thigh}}{|\vec{r}_{thigh}|} \times \vec{F}_{thigh} \quad (3)$$

$$\vec{\tau}_{thigh} + \vec{r}_{foot} \times (\vec{F}_{thigh} + \vec{F}_{shank}) + \vec{r}_{shank} \times \vec{F}_{shank} = 0 \quad (4)$$

Lastly, due to the KE providing an extension torque, we determined the direction of the thigh and shank force vectors to point anteriorly but were subject to fluctuation due to the computed values from the measured torque. The force vector at the foot/ankle was defined as a residual force to balance the exo's contribution and was determined to face posteriorly but was subject to change due to the measured torque values.

For the HW, we modeled the assistive torque as six posterior force vectors on the trunk, pelvis, and thigh, bilaterally (Figure 12C). The single load cell was aligned in series with the elastic bands, requiring the divvying of forces per band. Through tension testing, we found the linear with stiffness of each band to be 1.67 N/mm. We used the positions of reflective markers placed along the elastic bands, as well as the origin and insertion of the bands on the HW's trunk and thigh interfaces, respectively, which showed the individual displacement of the bands. With an optimization algorithm using the filtered load cell data as the resultant force between both bands as the target and each band's slack length as variables, we resolved for their individual force contributions (Figure 14B). Assuming uniform tension in concentrated areas of the band, we applied the vectors as point forces pulling away from the trunk and thighs and pushing towards the pelvis.

For both devices, we appended each point force's three-dimensional components of force, position, and torque to the external loads file containing ground reaction forces prior to running the Inverse Dynamics Tool.

3.4 Results

3.4.1 Knee exo

Participants were able to maintain similar lifting postures and sagittal plane knee kinematics across symmetric and asymmetric conditions while using the KE compared to NoE (Figure 13A). Noticeable differences in knee angle patterns between exo usage conditions arise during periods of greater knee flexion (i.e., first 50% of KW lifts, last 50% of WK lifts). On average, commanded and/or measured torque output higher magnitudes of assistance from the KE during greater knee flexion (Figure 13B). However, the magnitude of assistive torque provided to each user (measured) was much lesser than that of what was commanded – hereby alluding to user resistance to the device. Consequently, the biological knee moments computed after incorporating the measured KE assistive torques as external point forces show an increase across all tasks with respect to the NoE condition (Figure 13C). Peak and integrated JCFs were increased with the use of the KE (Figure 21). Interestingly, the total (exo + biological) knee moments show that when the users were assisted with a torque closer to the commanded torque value, the net external moments using the KE are reduced from the NoE moments (Figure 13D). Otherwise, the KE did not provide an assistive torque which could offload the biological moment contribution.

The KE did substantially alter L5/S1 flexion/extension angles from the NoE joint angles during the lifting conditions (Figure 14A). On average, the KE caused users to extend their lower back more (Figure 14A) across tasks, decreased L5/S1 lateral bending

(Figure 22B) across tasks, and decreased L5/S1 axial rotation (Figure 22C) during symmetric lifting tasks. The KE had minimal effect on biological flexion moments at the L5/S1 joint (Figure 14C), but reduced lateral bending (Figure 23B) and axial rotation moments (Figure 23C).

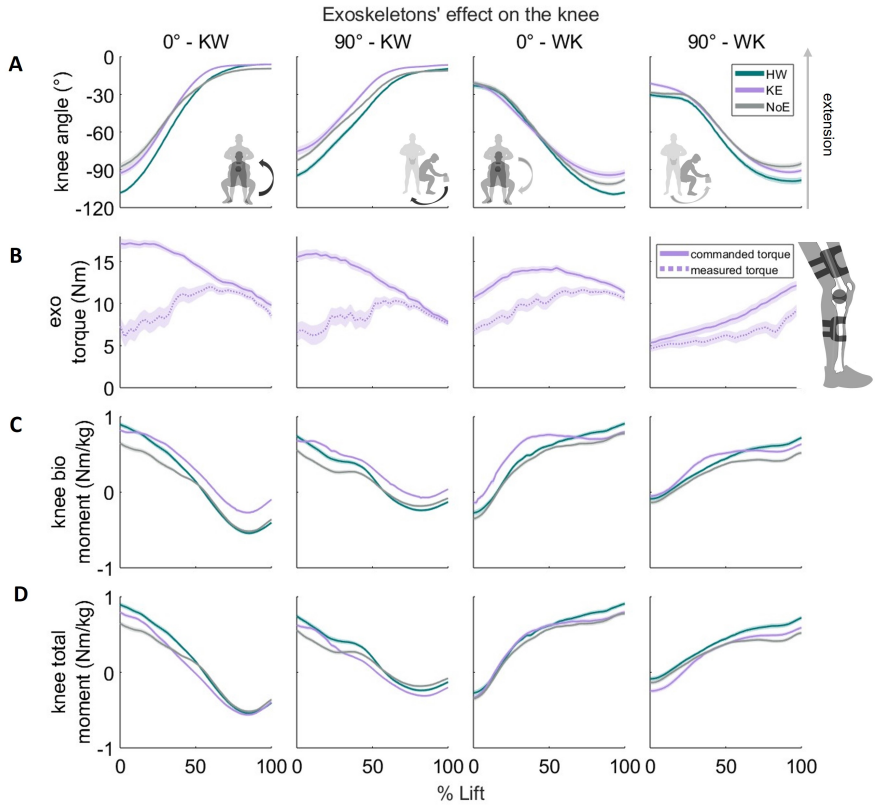

Figure 13 - The across-participant averaged time series of knee kinematics of knee flexion (A), commanded and measured torque from the active knee exoskeleton (KE) (B), biological knee flexion moments (C), and total knee flexion moments (D) during symmetric and asymmetric knee-to-waist (KW) and waist-to-knee (WK) lifting conditions. Conditions of exoskeleton usage are illustrated as no exoskeleton (NoE – black), passive HeroWear exoskeleton (HW – blue), and active knee exoskeleton (KE – red). Standard error of the mean is represented by haze surrounding about the average. Kinematics are reported from the right starting side of asymmetric conditions. The right and left starting sides asymmetric (90°) lifting conditions were averaged for knee flexion moments. Positive knee angles indicate knee extension, and positive moments represent flexion moments.

Muscle activations are an important factor contributing to muscle forces and consequently JCFs; therefore, it is crucial to understand how muscles may function differently with exoskeleton usage and how these resolve into JCFs. Wearing the KE during lifting led to reductions in EMG of rectus femoris (RA), lateral gastrocnemius (LG), vastus medialis (VM), semitendinosus (ST), and biceps femoris (BF) during symmetric (0°) and asymmetric (90°) lifting (Figure 18B). The KE greatly reduced rectus abdominis (RA) activations across tasks and minimally changed other back and torso-related muscles

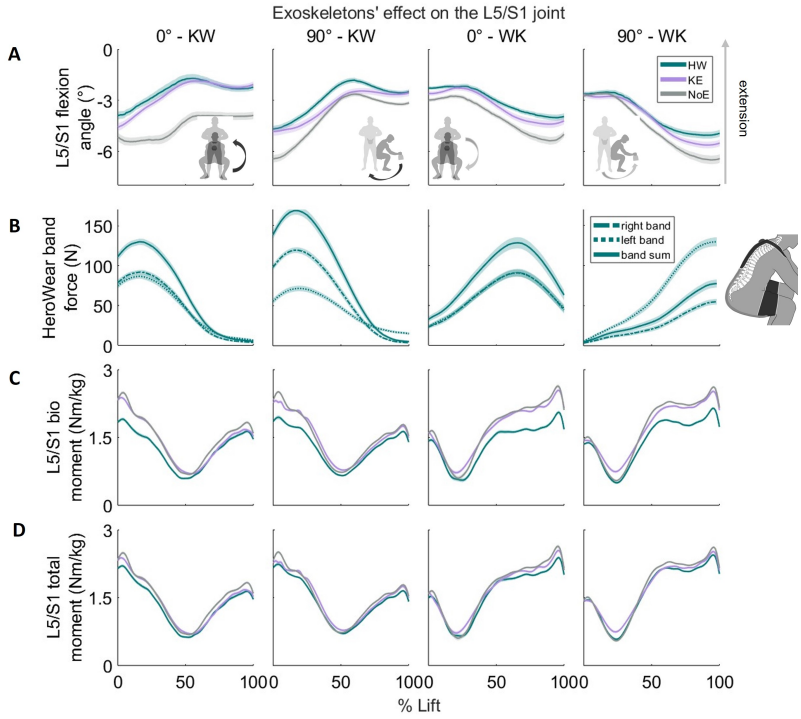

Figure 14 - The across-participant averaged time series of L5/S1 flexion (A), force output (N) of uniaxial load cell and individual elastic band contributions from HeroWear (HW) passive exoskeleton (B), biological L5/S1 flexion moments (C), and total L5/S1 flexion moments (D) during symmetric and asymmetric knee-to-waist (KW) and waist-to-knee (WK) lifting conditions. Conditions of exoskeleton usage are illustrated as no exoskeleton (NoE – gray), passive HeroWear exoskeleton (HW – blue), and active knee exoskeleton (KE – purple). Standard error of the mean is represented by haze surrounding about the average. Asymmetric lifting conditions using the right starting side were represented in the 90°-KW and -WK kinematic outputs. The right and left starting sides asymmetric (90°) lifting conditions were averaged for L5/S1 moments. Positive L5/S1 angles represented back extension.

such as the external obliques (EO), erector spinae (ES), and latissimus dorsi (LD) (Figure 18A).

Workers performing manual lifting are often tasked to lift heavy objects and materials unexpectedly. To measure this, we sought to examine peak JCFs. In exploring the effects of active exoskeletons on JCFs, we found that the KE reduced total JCFs across all lifting conditions (Figure 15B) in the knee joint. The KE caused reductions of 12.1% (p = 0.018) in normal and 11.2% (p = 0.03) total peak JCFs in the knee compared to NoE (Figure 16A). It is also important to consider how exoskeletons could modify JCFs when exposed to heavy loads over time. To measure this, we examined integrated JCFs. The KE significantly reduced normal (p = 0.023), shear (p = 0.038), and total (p = 0.019) integrated knee JCFs by 12.6%, 23.7%, and 13.3%, respectively (Figure 17A).

Interestingly, the KE incited higher JCFs at the L5/S1 joint during asymmetric KW and WK lifts (Figure 15A) throughout the task duration. The KE did not statistically affect peak JCFs in the L5/S1 joint (Figure 16B). The KE did not significantly reduce integrated L5/S1 joint JCFs but did lower L5/S1 shear JCFs by 5.8% (Figure 17B).

To readdress the relationship between lower back and knee joint loading introduced in sections 2.4 and 2.5.3 (Figure 8), we turn to the grouped percent changes in total back and knee peak JCFs while using the KE with respect to the NoE condition (Figure 19B). The KE was not successful in reducing both the L5/S1 and knee JCFs simultaneously when considering peak joint loading or cumulative (integrated) joint loading.

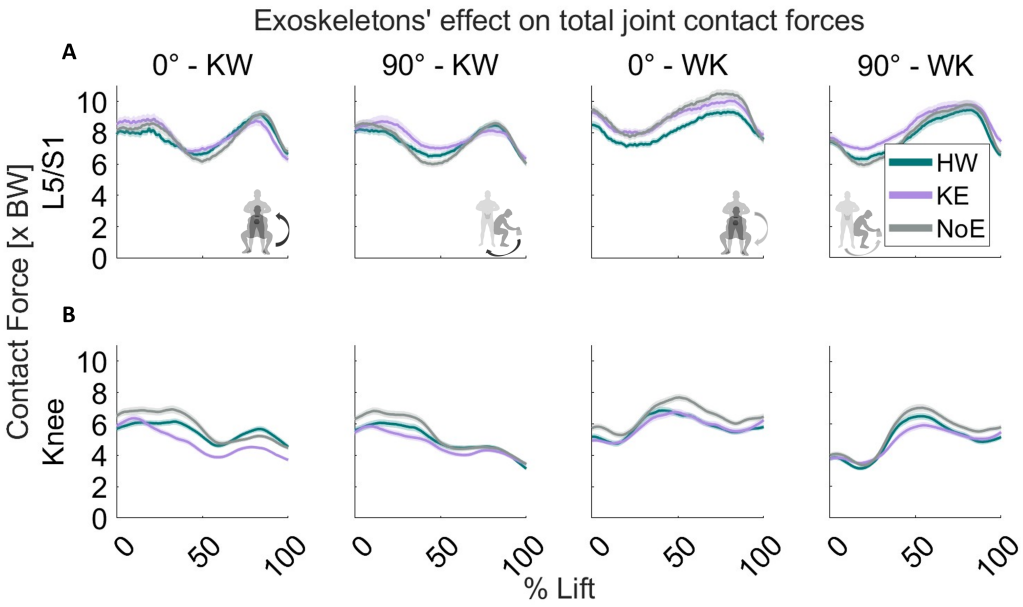

Figure 15 - The time series across-participant average for total JCFs at the L5/S1 joint (A) and knee (B). Conditions of exoskeleton usage are illustrated as no exoskeleton (NoE – black), passive HeroWear exoskeleton (HW – blue), and active knee exoskeleton (KE – purple). Shown are symmetric (0°) and asymmetric (90°) lifts with knee-to-waist (KW) and waist-to-knee (WK) starting height configurations. The right and left starting sides asymmetric (90°) lifting conditions were averaged for JCFs. Standard error of the mean is represented by haze surrounding about the average.

3.4.2 Back exo

Pivoting to assess the effects of passive exoskeletons on JCFs, the HeroWear device permits wearers to perform the instructed lifts with modified lifting mechanics to those without an exo (Figure 14A), with increasingly noticeable variations in L5/S1 joint angles during periods where the elastic bands are providing more assistance (Figure 14B). The increased L5/S1 extension shows that HW constrains participants to remain more upright when performing lifting and lowering tasks. The HW also causes reduced lateral bending (Figure 22B) and axial rotation (Figure 22C) joint angles across lifting conditions compared to the no exo condition. The flexion, lateral bending, and axial rotation moments

at the L5/S1 joint were reduced across all lifting tasks (Figure 14B. Figure 23), especially during periods within the lifting duration where the HW elastic band assistance was higher. More specifically, the HW reduced peak and integrated L5/S1 flexion and axial rotation moments, while increasing peak and integrated lateral bending moments (Figure 21).

The HW did cause the knee joint angles to maintain a more flexed posture compared to NoE across lifting tasks (Figure 13A). When the knees are more flexed, the HW causes the biological and total knee moments to be higher across tasks; on the other hand, these moments show negligible differences from NoE across lifting conditions (Figure 13 C,D). On average, the HW increased peak and integrated biological knee moments (Figure 21).

Wearing the HW during lifting led to reductions in muscle activations of torso muscles such as the erector spinae (ES), latissimus dorsi (LD), external obliques (EO), and rectus abdominis (RA) during symmetric (0°) and asymmetric (90°) lifting (Figure 18A).The use of the HW led to increase in muscle activations in the rectus femoris (RF) and vastus medialis (VM), and reductions in the biceps femoris (BF) across all conditions (Figure 18B).

The lowering of L5/S1 joint moments and activations of neighboring muscles funneled into the result that the HW reduced L5/S1 JCFs (Figure 15A). Modeling unexpectedly peak loads manual labor employees could be exposed to, we found that the HW lowered peak shear JCFs at the L5/S1 joint by 17.4% ($p < 0.027$). To address exposure to prolonged loading, integrated L5/S1 JCFs also showed reductions in shear forces by 21.1% ($p < 0.003$). The HW also caused normal and total knee JCFs to be 7.0% and 6.1% less than without an exo. The HW decreased integrated normal and total JCFs in the knee by 9.1% and 7.8%.

It is apparent that the HW benefits the loading relationship between lower back and knee joint (sections 2.4 and 2.5.3 (Figure 8)). Percent changes in JCFs in the total back and knee peak JCFs while using the HW device with respect to the NoE condition (Figure 19A) show mutual reductions in loading. Similarly, the HW proved to decrease total back and knee integrated JCFs. Therefore, the HW was ultimately successful in reducing both the L5/S1 and knee JCFs simultaneously, although not with significance, when considering peak loading and cumulative (integrated) loading.

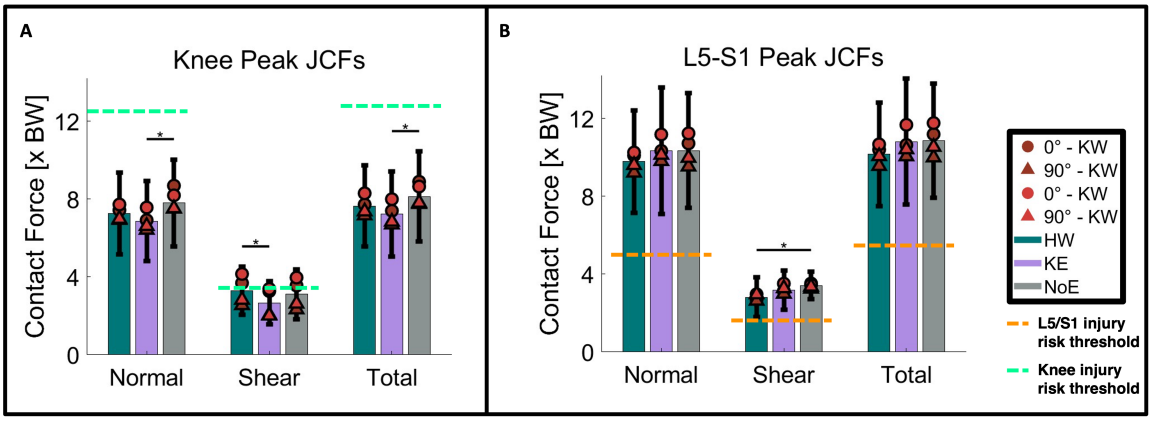

Figure 16 – Group-averaged peak normal, shear, and total JCFs in the knee (A) and L5/S1 (B) joint as explored in the hypotheses (H1 and H2). Conditions of exoskeleton usage are illustrated as no exoskeleton (NoE – gray), passive HeroWear exoskeleton (HW – blue), and active knee exoskeleton (KE – purple) bars for all force components. Each bar is the average JCF across the lifting and starting height configurations (KW and WK) and lifting degrees of turn (0°, 90°). Across-participant averages of independent start-end height and degree of lift condition are identified by shape and color: 0° KW – maroon circle, 0° WK – pink circle, 90° KW – maroon triangle, 90° WK – pink triangle. Injury risk thresholds for the L5/S1 joint (estimated from [79,80,83,84,88]) and knee joint (estimated from [86–88]) are represented by orange and green dashed horizontal lines, respectively (see Table 2). Significantly different groups are denoted with an asterisk. Statistical significance across all conditions concluded when $\alpha = 0.05$.

3.5 Discussion

In this study, we sought to evaluate how assistance from an active knee and passive back exoskeleton device influenced three-dimensional JCFs *inside limb-joints* during manual lifting tasks. More precisely, we designed an experiment to challenge the effectiveness of wearable devices at mitigating the higher L5/S1 and knee JCFs found in symmetric (0°) and asymmetric (90°) below-the-waist lifting conditions identified in Section 2.5.3 (Figure 8)[105]. We performed analyses which accounted for the motorized and elastic support from each device to assess how the assistance influences short-term and prolonged exposures to joint loading. We hypothesized that the passive lower-back exoskeleton (HW) would reduce JCFs in the low back (L5/S1 joint) and the active knee exoskeleton (KE) would decrease knee JCFs during industry-relevant lifting (H1). Additionally, we were interested in how each device would influence loading of the unprescribed joint. Therefore, we hypothesized that the HW would lower knee JCFs and the KE would reduce JCFs at the L5/S1 joint during manual lifting (H2). We accepted H1 as our data show that HW was successful at decreasing peak and integrated shear L5/S1 JCFs (Figures 16B, 17B) and the KE lowered peak and integrated normal and total JCFs (Figures 16A, 17A). On the other hand, our data demonstrates that neither device could *significantly* reduce the JCFs of an unprescribed joint, therefore we reject H2.

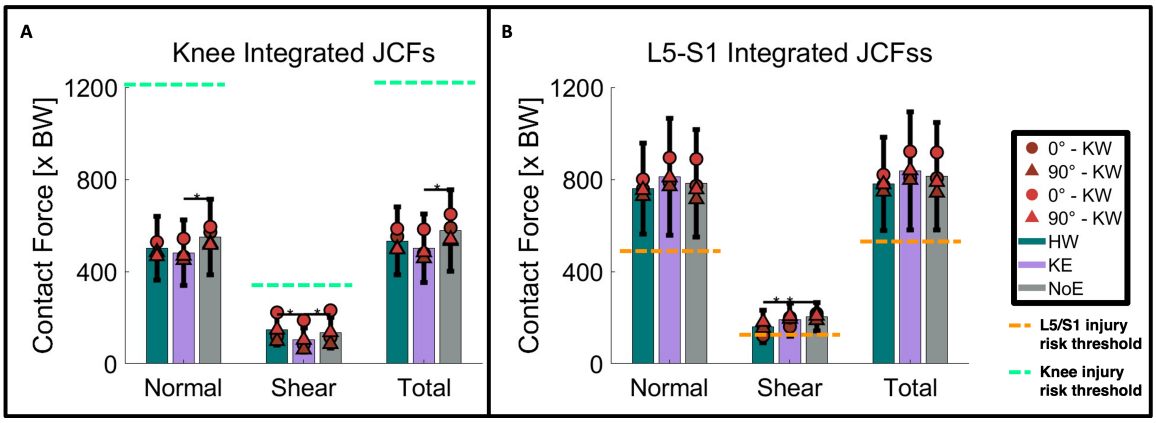

Figure 17 – Group-averaged integrated normal, shear, and total JCFs in the knee (A) and L5/S1 (B) joint as explored in the hypotheses (H1 and H2). Conditions of exoskeleton usage are illustrated as no exoskeleton (NoE – gray), passive HeroWear exoskeleton (HW – blue), and active knee exoskeleton (KE – purple) bars for all force components. Each bar is the average JCF across the lifting and starting height configurations (KW and WK) and lifting degrees of turn (0°, 90°). Across-participant averages of independent start-end height and degree of lift condition are identified by shape and color: 0° KW – red circle, 0° WK – pink circle, 90° KW – red triangle, 90° WK – pink triangle. Injury risk thresholds for the L5/S1 joint (estimated from [79,80,83,84,88]) and knee joint (estimated from [86–88]) are represented by orange and green dashed horizontal lines, respectively (see Table 2). Significantly different groups are denoted with an asterisk. Statistical significance across all conditions concluded when $\alpha = 0.05$.

3.5.1 Knee exo

We anticipated that the KE would reduce knee JCFs across all tasks (H1). The method we used to apply the assistive motor torques as force vectors acting on the thigh, shank, and foot segments contributed mostly shear forces about the knee joint (Figure 12C). We believed that the resolution of these shear forces would not cause harm to the joint but lead to the reduction in compression and total knee JCFs, similar to the effect exemplified in the relationship between knee torque, biological knee moments, and the resulting total

knee moment (Figure 13B-D). We found this demonstrated across all tasks on average (Figures 16A, 17A). The KE was successful at reducing peak and integrated total knee JCFs in symmetric, knee-to-waist (KW) lifting (Figures 19B, 20B) – the condition identified as the "hot spot" for joint loading in Chapter 2 (Figure 8) – but also in all other conditions.

Arriving to the result that the KE reduces knee JCFs (H1) sheds light on interesting takeaways in some of the factors responsible. Hondzinski et al. (2018)[117] showed that an active lower-body exo that spanned the hip and knee joints did not alter knee kinematics in order to be effective as an assistive or augmentative tool[117]. Our data showed a similar trend in minor deviations of knee kinematics (i.e., less flexed during lifts) with the use of an active KE (Figure 13A) with respect to without one (NoE). Net external joint forces (moments) also are a commonly utilized metric in assessing general trends in joint loading, especially in observing the effectiveness of wearable technology[111]. A literature search by Koch and Font-Llagunes (2021)[118] showed that lower-limb exosuits have the capability of reducing knee adduction moments[17,118]. In response to the measured KE torque (Figure 13B), the biological knee moments increased compared to NoE knee moments (Figure 13C) which was an unintuitive result. We know that the total joint moment is the sum of the exo torque and the biological joint moment, which remains the case in this context. However, we believe the difference is derived from the knee biologically providing a flexion moment, whereas the KE is providing an extension torque, leading to some cancellation shown in the total knee moments (Figure 13). Through traditional practices of subtracting exo torques from total joint moments, we would only demonstrate the sum of

two positive, non-negating components. Thus, further supporting the need for more rigorous implementation and modeling of exo assistance. The KE also reduced muscle activations in knee flexors and extensors (Figure 18) across lifting tasks which indirectly led to reductions in muscle forces. The complex combination of all these features led to the reduction of JCFs in the knee joint, ultimately highlighting that joint moments do not always tell the whole story of injurious joint loading.

We also expected that the KE would reduce lower spine (L5/S1) JCFs (H2). This hypothesis was rejected as the KE led to no significant changes in either peak nor integrated JCFs at the L5/S1 joint (Figures 16B,17B). Although not statistically significant, relative to the other tasks, the KE does reduce peak and integrated L5/S1 JCFs in symmetric KW lifts. We believe these reductions in JCFs may have stemmed from posture modifications in the lower back (less flexed) during these lifts while wearing the KE (Figure 14A). The use of the KE did not strongly influence biological and total L5/S1 moments, with the exception of increasing peak and integrated moments (Figure 21). Additionally, muscle activations of back/torso muscles were largely unaffected, except for rectus abdominis experiencing reductions in activations (Figure 18) across conditions. Hondzinksi et al. (2018) warned of the hazardous consequences when knee kinematics are largely unchanged such as higher resulting internal and external loading on the spine, affecting tissues and normal and compressive JCFs[117]. It is possible that the L5/S1 joint angles resulting from using the KE increased risk of injury in the lower back.

In totality we would recommend the KE to target JCF loading at the knee for mitigating peak and cumulative (integrated) loading. On average, the KE does not harm peak joint loading at the L5/S1 joint, but over time, it does cause increases in integrated total L5/S1 JCFs. Additionally, our data also support that normal, shear, and total JCFs at the knee joint are below the literature-supported tolerance thresholds[86–88] (Figure 5, Table 2) without the KE, and are further reduced with the KE (Figures 16A, Figures 17A), but this is not true at the L5/S1 joint (Figures 16B, Figures 17B). This suggests that KE is an effective tool for mitigating hazardous joint loads when targeting a single joint (the knee) or for acute use if seeking to offload multiple joints during manual lifting.

3.5.2 Back exo

We anticipated that the HW would reduce lower spine (L5/S1) joint loading (H1). The method we used to apply the assistive loads as force vectors from the elastic bands acting on the posterior side of the torso, pelvis, and thigh segments contributed mostly compressive forces about the L5/S1 joint (Figure 12C). We believed that this would contribute to an increase in joint compression forces – not to cause detriment to the joint—but would overall lead to the reduction in shear and total knee JCFs. We accept this hypothesis as we did see reductions in shear peak and integrated L5/S1 JCFs as a result of HW usage, simply not enough to reduce the total JCF.

We believe that changes in kinematics, kinetics, and muscle activations led to the result that the HW reduced shear JCFs in the L5/S1 joint (H1). Goršič et al. (2021)[119]

performed a study using the HW and showed its ability to reduce the range of motion of flexion and extension of the back[119], which supports our data (Figure 14A), but we also saw this results in lateral bending and axial rotation (Figure 22). Passive back exos have also been shown to reduce L5/S1 joint moments[120], which our data shows throughout each lift (Figures 14C, 21). Use of passive back exos, like the HW, provide a considerable amount of support in their ability to reduce muscle activations[119,121,122]. In our experiment, the HW was also effective at offloading muscle-level effort in torso/back flexors and extensors in the lifting tasks performed in our study (Figure 18). The reductions in lumbosacral range of motion, biological joint moments, and surrounding muscle activations from wearing the HW all led to significantly less JCFs in L5/S1 joint than without the use of the HW (NoE) (Figures 15-17).

We also expected that the HW would reduce knee JCFs (H2). Studies have shown that the use of a back exoskeleton altered knee kinematics (hyper-extension)[112] and reductions in knee flexor muscle activity[123]. Thus, inspiring the expectation that exoskeletons may indirectly affect joint contact forces of the unassisted joint. However, we reject this hypothesis as we did not find any statistically significant changes in knee JCFs with the use of the HW. However, we did find promising reductions in peak and cumulative normal and shear JCFs in the knee (Figures 13,14). Conversely, the HW did cause some increase in peak and integrated knee moments (Figure 21), potentially due to the tension force from the elastic bands pulling on the exosuit's thigh cuffs. Wearing the HW also caused users to flex their knees more than without an exo (NoE) across all lifts (Figure 14A), potentially due to participants being more comfortable in this flexed-knee posture

given the exo's assistance. The extension moment produced by the HW's elastic band assistance[122] led to offloading in knee extensor muscle activations but increases in knee flexor muscles (Figure 18). Potentially, if the HW were able to provide an assistance which decreases peak and integrated knee moments and knee flexor muscle activity, the reductions in knee JCFs could be significant to redefine its utility to a multi-joint exosuit.

All in all, we would recommend the HW to target JCF loading at the lower back for peak and cumulative loading mitigation. Considering the HW does not harm either joint with its usage in either joint loading context, we would also support its use to anecdotally reduce JCFs in the knees as well. Additionally, our data show that normal, shear, and total JCFs at the L5/S1 joint exceeded the literature-supported tolerance thresholds[79–83] (Figure 5, Table 2) in peak and cumulative loading with and without the use of the HW (Figures 16B, 17B). The HW slightly reduces knee JCFs to be further away from reaching the joint loading capacity (Figures 16A, 17A). These results shed light on the HW's potential utility to offload neighboring joints during manual labor tasks, but also introduces that more assistance is needed to reduce L5/S1 JCFs below the injury risk threshold.

3.5.3 Limitations

There are a few limitations to this study worth mentioning which could have implications on the aforementioned outcomes. Participants were allowed to perform each lift with natural mechanics, but we controlled the weight being lifted (11.34 kg), lifting conditions (starting-ending positions and degree of turn), and foot placement. Variation in their lifting rate or foot stance, may have contributed to variance in our results. We

leveraged the neuromusculoskeletal solved CEINMS to simulate deep muscles and those we could not experimentally collect. Knee JCF results were focused on the right, EMG-instrumented leg, but we expect similar forces on the left knee. Additionally, the lack of female representation in this study restricted us from investigating the effects of gender on JCFs.

Another limitation could be from how users were fit to the exos. The knee exo is a rigid device designed to be fastened to thigh and shank segments with Velcro and an additional interface was adhered to the lateral side of their shoes near the ankle with screws. The motors were intended to be aligned in parallel with the knee joint centers; however, misalignment from human error is possible. Misalignment could be represented in the results in various ways, especially at the level of controller output. While the knee exo's controller was designed to provide an extension torque about the knee, this felt like a damping torque on the lift descent (squat) and a spring torque on lift ascent. Controller validation pilots showed that the torque response predominantly scaled with the speed of the lift instead of the steepness of squat. The stiffness-damping parameter combination (k = 4.6 Nm/rad, b = 2.8 Nm/rad/s) was selected because it showed the least muscle activation across each pilot participant (Nuesslein et al., 2024). Prior to experimentation, this provided confidence that the exoskeleton assistance should be helpful for many participants. However, when comparing the commanded torque and measured torque from the knee device, we saw large discrepancies indicating resistivity to the device from users. We believe this stemmed from the minor misalignment or even lack of device adaptation, despite scheduling participants to train in each device on a separate day prior to

biomechanics data collections. The back exoskeleton (HeroWear) has an online sizing calculator which accepts sex, chest and thigh circumference, and the diagonal length of the back to best fit the vest, thigh cuffs, and elastic bands to each individual user. The participants were also trained in a separate session prior to collecting biomechanics data to increase habituation and effectiveness of exoskeletons[124]. These employed methods of tailoring to each user can ensure a robust, personalized assistance which can prove more beneficial to joint loading than a singular standard setting for all users. However, when presetting the posture at which the elastic bands should begin assisting with the clutch, there is slight room for human error.

Another limitation could be the devices selected for this study. There are many commercial exoskeletons to utilize for the proposed project which have useful applications for the studied manual lifting tasks[32,125]. The knee exoskeleton was developed in our lab for previous studies[116,126,127], and showed promising reductions in joint contact forces[126]. This reason combined with its accessibility motivated its use in these protocols. The HeroWear was a cost-effective[119], commercial device that was available to acquire for testing. However, it is possible that users would have performed these tasks with lower JCFs in the lower back and knees with devices capable of providing more assistance. Further testing on stronger devices would be needed to address this.

Lastly, similar to Chapter 2 findings, the use of discrete tolerance thresholds to quantify injury risk from the JCFs elicited in each lifting task does not take into account important aspects (i.e., vertical distance traveled by carried weighted object) that largely

affect the joint loading risks[104]. We would suggest implementing a more in-depth injury risk equation[81,103] or assessment tool to compare its ability to identify hazardous JCFs in manual lifting.

3.6 Conclusion

This study investigated how exoskeleton assistance affects JCFs in the knee and lower-back (L5/S1) during a symmetric and asymmetric manual lifting tasks. We found highest JCFs in symmetric (i.e., load straight in front of the body), below the waist lifting tasks. Taken together, our results suggest that asymmetric lifting can *actually reduce* JCFs in the lower back and knee when compared to moving loads straight in front of the body. Interventions to reduce JCFs during heavy lifting should emphasize transporting weight above the waist or close to the body, while encouraging postures that minimize trunk and knee flexion (i.e., small external moment arms). Therefore, asymmetrical twisting and lifting may not be as hazardous to joint loading. Lastly, we found that JCFs were proportionally distributed across knee and lower back joints, suggesting that preferred lifting techniques might be selected to balance JCFs across joints and avoid local overloading – a motor control principle indicating a trade-off that might be leveraged by assistive technology applied at one joint (e.g., back) to protect another (e.g., knee).

The intent of this research is to advance analytical practices on internal *limb-joint* forces and assess the influence of exoskeleton assistance on lower-back and knee three-dimensional JCFs during manual lifting tasks. There is a limited understanding on whether positive effects observed from exoskeletons usage may be harmful or beneficial to the loads

experienced within the joint capsule, and consequently, how this may affect injury risks. To address this, wearable devices need to be properly characterized to better represent their assistance's contributions to JCFs. To emulate a controlled experience of manual laborers, we designed an experimental protocol consisting of manual lifting tasks varying in symmetry and lifting/lowering, each performed with exoskeletons donned (passive lower-back device, active knee device) and doffed (no device). By leveraging musculoskeletal modeling and optimization tools[65,105] which utilized motion capture, electrography, force plates (external forces), and torque/force outputs from the exoskeletons as inputs, we evaluated the effects of exoskeletons on knee and lower-back (L5/S1) JCFs. Previous research has shown that lower-back exoskeletons reduce compressive loading in the lumbar spine[109,112]; therefore, we hypothesized that the passive lower-back exoskeleton would reduce JCFs in the low back (L5/S1 joint) during industry-relevant lifting and the active knee exoskeleton (KE) would lower JCFs in the knee (H1). Furthermore, we also hypothesized that the either devices' assistance will lower the JCFs of the non-targeted joint, meaning the KE will reduce L5/S1 JCFs and the HW will decrease knee JCFs during manual lifting (H2). The results will shed light on the inherent advantages or disadvantages of assistive devices for manual lifting tasks and inform future designs and implementations of industry-directed wearable devices to target offloading critical joint loads during manual labor.

3.7 Conflict of Interest Statement

There is no conflict of interest reported by the authors.

3.8 Acknowledgements

This work was supported by Sandia National Laboratories, a multi-mission laboratory managed and operated by the National Technology and Engineering Solutions of Sandia LLC, a wholly owned subsidiary of Honeywell International Inc. for the U.S. Department of Energy's National Nuclear Security Administration under contract DE-NA0003525. This paper describes objective technical results and analysis. Any subjective views or opinions that might be expressed in the paper do not necessarily represent the views of the U.S. Department of Energy or the United States Government. We would like to formally thank Jason Wheeler for his instrumental involvement in the development of this study. We would also like to show our appreciation to all the participants of this study.

3.9 Supplementary Figures for Chapter 3

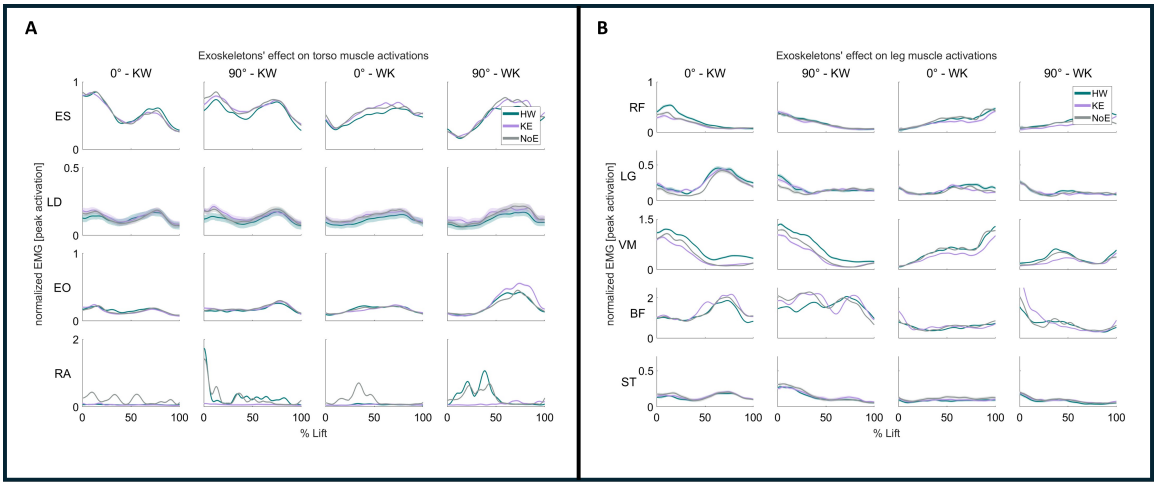

Figure 18 - The across-participant averaged time series of EMG from muscles in the torso and right leg. The muscles are as follows: erector spinae (ES) (A), latissimus dorsi (LD), external obliques (EO), right rectus abdominis (RA), rectus femoris (RF), lateral gastrocnemius (LG), vastus medialis (VM), biceps femoris (BF), semitendinosus (ST). Averaged muscle activity from muscles recorded with a right-left pairing (see Figure 1B) are shown across the conditions. Conditions of exoskeleton usage are illustrated as no exoskeleton (NoE – black), passive HeroWear exoskeleton (HW – blue), and active knee exoskeleton (KE – red). Shown are symmetric (0°) and asymmetric (90°) lifts with knee-to-waist (KW) and waist-to-knee (WK) starting height configurations. The right and left starting sides asymmetric (90°) lifting conditions were averaged for EMG. Standard error of the mean is represented by haze surrounding about the average.

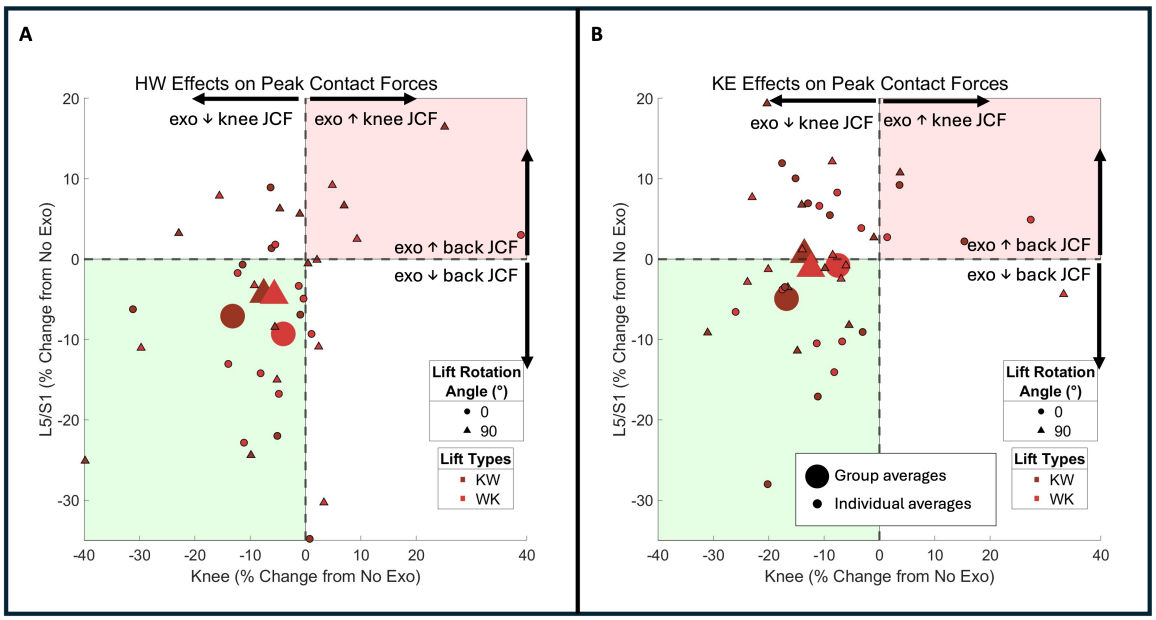

Figure 19 - Percent change of peak total L5/S1 and knee JCFs while donning the active knee device (KE) with respect to no exoskeleton use. The red zone of the quadrant signifies hazardous loading for both the knee and lower-back and is least preferable. Meanwhile, the bottom left green zone indicates the exoskeleton reduced internal joint loading for the lower-back and knee. The white quadrant regions illustrate that the exoskeleton only reduced joint loading on the knee *or* the lower-back. Circles represent symmetric (0°) lifts, and triangles represent asymmetric lifts (90°). Dark, maroon-colored shapes represent knee-to-waist lifts, and pink-colored shapes represent waist-to-knee lifts. Larger shapes represent group averages and smaller shapes are participant-average datapoints.

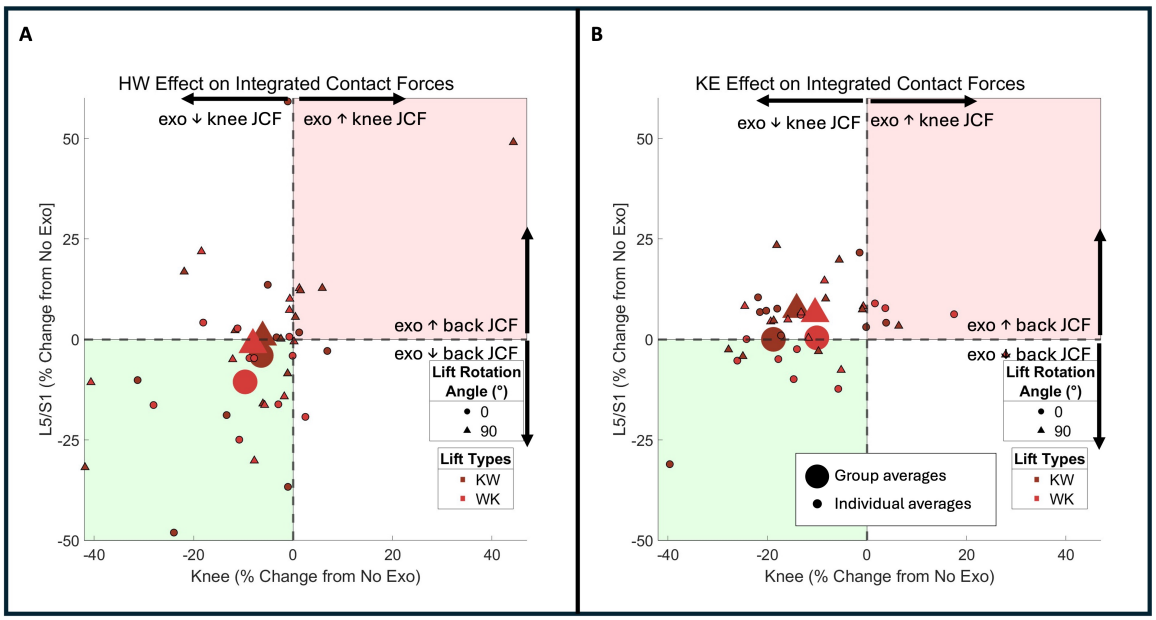

Figure 20 - Percent change of integrated total L5/S1 and knee JCFs while donning the (A) HeroWear (HW) and (B) the active knee exo with respect to no exo use. The red zone of the quadrant signifies hazardous loading for both the knee and lower-back and is least preferable. Meanwhile, the bottom left green zone indicates that the exoskeleton reduced JCFs for the lower-back and knee. The white quadrant regions illustrate that the exoskeleton only reduced joint loading on the knee *or* the lower-back. Circles represent symmetric (0°) lifts, and triangles represent asymmetric lifts (90°). Dark, maroon-colored shapes represent knee-to-waist lifts, and pink-colored shapes represent waist-to-knee lifts. Larger shapes represent group averages and smaller shapes are participant-average datapoints.

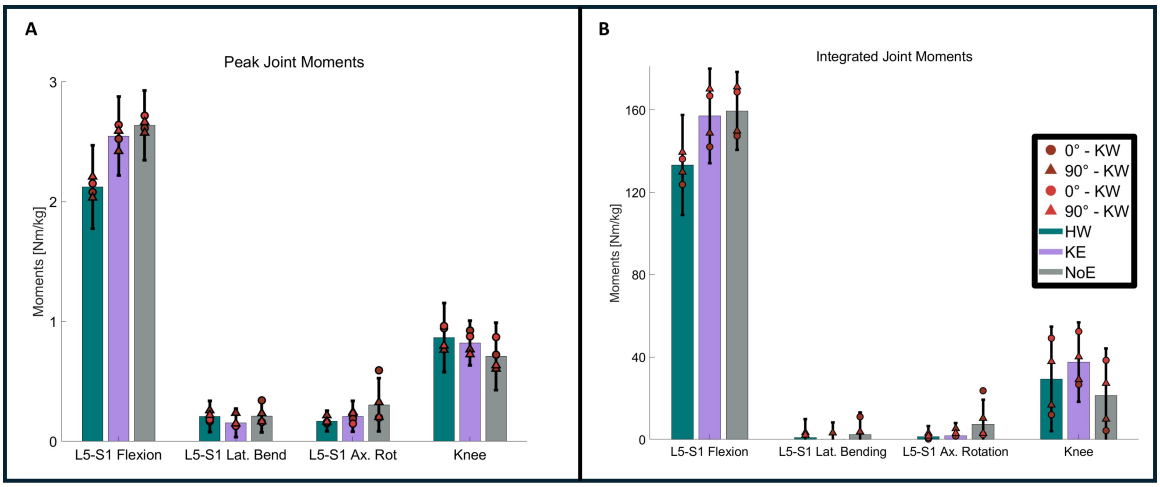

Figure 21 - Group averaged peak (A) and integrated (B) joint moments in L5/S1 flexion, L5/S1 flexion, L5/S1 flexion, and knee flexion as explored in the hypotheses (H1 and H2). Conditions of exoskeleton usage are illustrated as no exoskeleton (NoE – gray), passive HeroWear exoskeleton (HW – blue), and active knee exoskeleton (KE – purple) bars for all force components. Each bar is the average JCF across the lifting and starting height configurations (KW and WK) and lifting degrees of turn (0°, 90°). Across-participant averages of independent start-end height and degree of lift condition are identified by shape and color: 0° KW – maroon circle, 0° WK pink circle, 90° KW – red triangle, 90° WK – pink triangle.

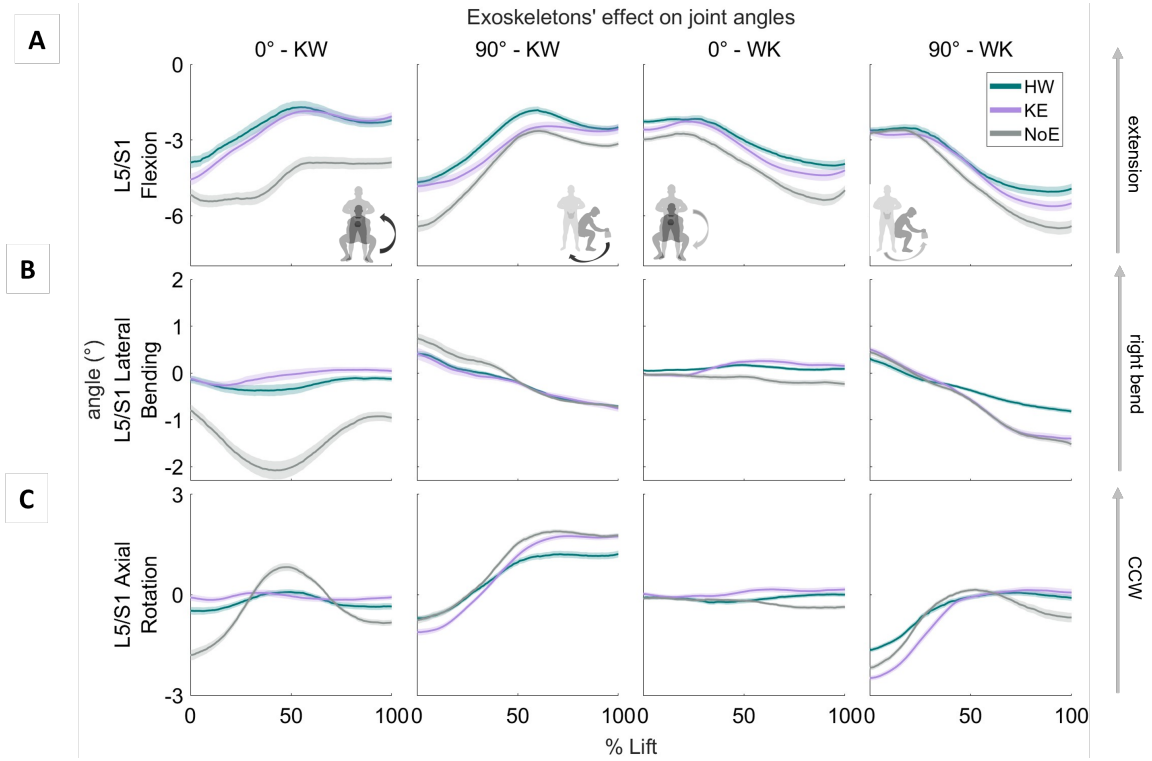

Figure 22 - The group averaged joint angles of L5/S1 flexion (A), L5/S1 lateral bending (B), and L5/S1 axal rotation (C) during symmetric and asymmetric knee-to-waist (KW) and waist-to-knee (WK) lifting conditions. Conditions of exoskeleton usage are illustrated as no exoskeleton (NoE – gray), passive HeroWear exoskeleton (HW – blue), and active knee exoskeleton (KE – purple). Standard error of the mean is represented by haze surrounding about the average. Positive angles indicate extension in L5/S1 flexion, bending toward the right in lateral bending, and counterclockwise (CCW) rotation in axial rotation.

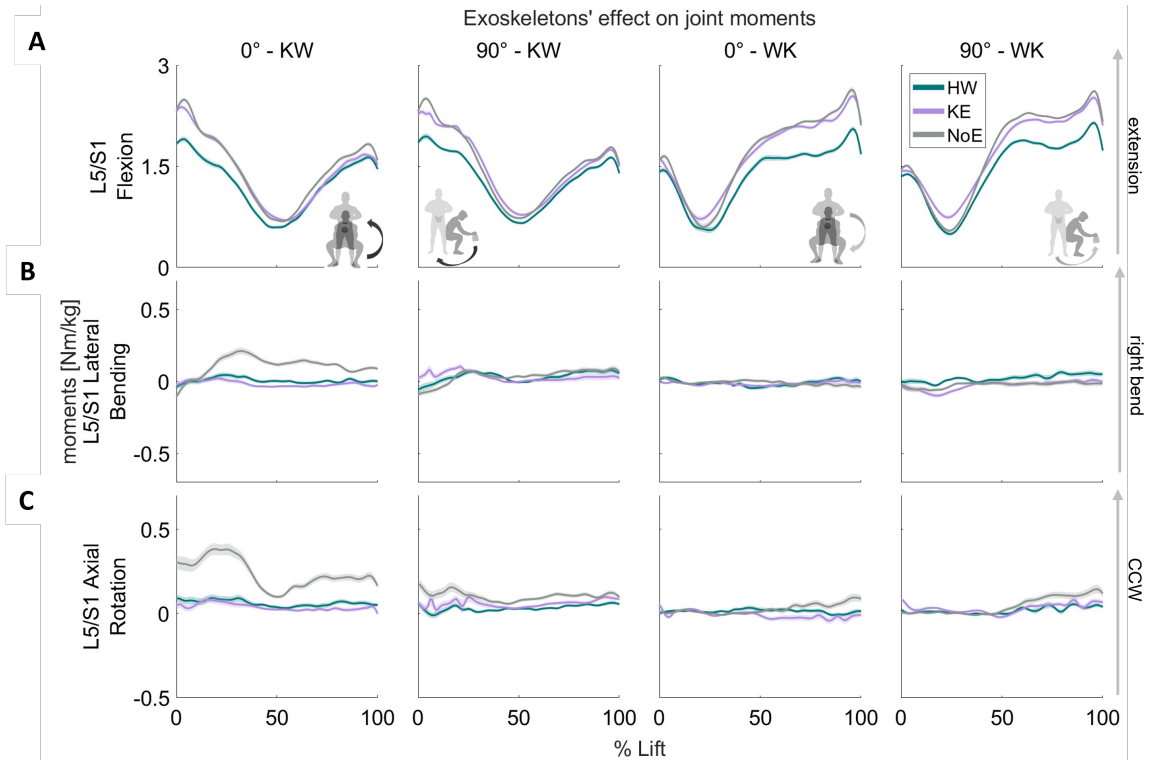

Figure 23 - The group averaged joint moments of L5/S1 flexion (A), L5/S1 lateral bending (B), and L5/S1 axal rotation (C) during symmetric and asymmetric knee-to-waist (KW) and waist-to-knee (WK) lifting conditions. Conditions of exoskeleton usage are illustrated as no exoskeleton (NoE – gray), passive HeroWear exoskeleton (HW – blue), and active knee exoskeleton (KE – purple). Standard error of the mean is represented by haze surrounding about the average. Positive angles indicate extension in L5/S1 flexion, bending toward the right in lateral bending, and counterclockwise (CCW) rotation in axial rotation.

CHAPTER 4. LEVERAGING WEARABLE SENSING TO ESTIMATE JOINT CONTACT FORCES

The third and final work of my dissertation assesses how various permutations of sensor types (IMUs, insoles, and EMG) influence estimation of internal joint loads at the knee using deep learning methodology. The following chapter comprises of a manuscript draft that I intend to submit to IEEE Transactions on Biomedical Engineering or Annals of Biomedical Engineering and is tentatively titled "Looking from the outside in: Estimating Internal Joint Forces Using External Wearable Sensors".

4.1 Abstract

Internal joint contact forces (JCFs) are an important metric to provide insight into how loading from external factors and surrounding tissues resolve within a given joint. This information is difficult to come by in real time without the use of invasive procedures such as force transducer implantation. While neuromusculoskeletal modeling is a useful tool for the computation of joint contact forces, it can be expensive in terms of laboratory equipment to collect motion capture data and computational time to process these data. In this outlined work, we investigated the ability of various wearable sensors to map ground reaction forces, body segment kinematics, and muscle activations to estimates of JCFs. To do this, we utilized permutations of simulated inertial measurement units (IMUs), simulated pressure insoles, and experimentally collected electromyography (EMG) as inputs into a temporal convolutional network model (TCN) to estimate normal and shear

knee JCFs across a diverse set of dynamic tasks. We found that estimating normal knee JCFs with solely EMG ($R^2 = 0.79$, RMSE = 0.48) performs better than input configurations using IMUs and insoles ($R^2 = 0.65$, RMSE = 0.62) ($p < 0.01$) but performs best using all sensors or EMG and IMUs as input ($R^2 = 0.85, 0.85$; RMSE = 0.43, 0.42) ($p < 0.01$). The provided sensor inputs were not able to map as well to shear JCFs, with the best estimations coming from using all sensors as input ($R^2 = 0.55$, RMSE = 0.12). This work showcases the viability of performing estimations of loading inside the joint capsule using external sensors and deep learning methodologies. Thus, supporting the utility of a generalized joint loading estimator to be prescribed to inform about internal JCFs and potential injury risk for a given task.

4.2 Introduction

Joint contact forces (JCFs), the three-dimensional forces experienced within the joint capsule, are a useful metric for monitoring joint loading and health. JCFs are affected by surrounding muscles, ligaments, tendons, and external forces[128] for given joint kinematics. The limited literature on JCFs is due to the inability to extract this metric without the use of highly invasive procedures to implant a force transducer within the joint, or an instrumented prosthetic device. Furthermore, mechanical analyses that attempt to map net external forces and moments to internal joint loads are not straightforward and require estimates of how antagonistic muscle forces are coordinated[63]. Fortunately, modern day musculoskeletal modeling provides the ability to simulate human motion for targeted tasks and conditions[19,20] and also estimation of JCFs[21–24,64]. In further good news, EMG-

informed solvers are useful in capturing the essence of muscle coactivation in hopes of providing a more accurate representation of forces acting upon the joint, or a more realistic calculation of JCFs[65,66]. Muscle forces contribute to the majority of the summed forces in the resulting JCFs, so it is a valuable addition to be able to incorporate this nuance [67,68]. However, the process to take motion capture data through a musculoskeletal modeling pipeline can be computationally costly and requires accessibility to expensive equipment to obtain the biomechanics dataset. This also requires the ability to know how to utilize such tools. There is a need to be able to estimate JCFs without the use of motion capture data.

The field of wearable sensing could potentially hold the solution to JCF estimations without motion capture. Recent advances in applications of wearable sensing have proven effective at estimating and predicting biological metrics such as kinematics and kinetics[129,130] from wearable sensors and/or motion capture imaging. Ground reaction forces have been shown to hold a strong correlation to knee joint contact forces[131] with force plate data. Findings such as these influence the need to develop robust systems for quantifying injury metrics while minimizing the amount of data collected. Among these developments, machine learning has made strides in informing the risk of injury during loading tasks using a wearable system of internal measurement units (IMUs)[47]. A study by Burton et al. (2021)[132] was among the first to assess the abilities of deep learning models (recurrent, convolutional, and fully-connected neural networks) to predict muscle and joint contact forces[132].

Machine learning has shown promising performance in measuring biological parameters that were once complicated and time-intensive to compute. A growing trend to use wearable sensors such as pressure insoles and/or inertial measurement units (IMUs) to estimate joint moments , internal bone forces[45], and even injury risks[46,47] is paving a way to probe the relationship between injury mitigation and internal joint contact forces. However, there still is a considerable amount we do not know regarding the most robust and widely applicable model to achieve such goals.

The purpose of this study was to explore the intersectionality of wearable sensing and machine learning and to facilitate the estimation of JCFs in the knee during dynamic, manual labor tasks. To bridge this gap, we designed an analysis pipeline utilizing a novel dataset[133] comprised of a diverse set of walking, lifting, squatting, lunging, stair climbing, etc. (Figure 31) which replicates the vast assortment of movements encountered every day in the workplace or in every day society. This data was previously experimentally collected and processed to extract JCFs as our subject-dependent ground truth. With the joint kinematics, which were also an output from the musculoskeletal pipeline used to capture JCFs[105], we simulated segment linear accelerations, angular velocities, and Euler angles. We transformed vertical and shear ground reaction forces and center of pressure (mediolateral and anteroposterior) into the foot frame to replicate data streamed from pressure insoles from force plate data. We then applied a deep learning model on 8 permutations of sensor input combinations between EMG, IMUs, and insoles (and a single super insole version) to estimate normal and shear JCFs (total of 16 models). We hypothesized that the combination between IMUs and insoles would be able to provide a

reliable estimation of normal and shear knee JCFs (R2 > 0.7) (H1). Studies already exploring the utility of wearable sensors find them reliable as a form of injury mitigation and musculoskeletal health monitoring[37]. Due to intersubject variability in EMG signals[134], we expect that the EMG will not prove to be a useful feature for the TCN to map to JCFs, despite the relationship between muscle forces and JCFs. This essential mapping of joint kinematics, ground reaction forces, and, potentially, electromyography (EMG) to joint contact forces will serve to help identify the best practices for training machine learning models and the minimum input required for reliable estimation of joint contact forces across different manual task sets. Investigating the effects of different sensor inputs on JCF estimation across a vast array of tasks on multi-joint internal joint loading will enable the field to move forward with reduced sensor sets to estimate JCFs in environments outside of the lab. In doing so, we hope to wearable sensing systems in conjunction with machine learning can provide a greater awareness of the susceptibility to eventual tissue and bone-damaging JCFs, and ultimately injuries, in the workplace.

4.3 Methods

4.3.1 Experimental data collections

To perform this study, we leveraged data from the previous chapters. In chapter 2, nine participants (Table 1) performed symmetric (0°) and asymmetric (90° and 180°) lifting conditions with starting and ending positions alternating between knee-height, waist-

height, and shoulder-height as outlined in sections 2.3.2 – 2.3.3. In chapter 3, ten participants (Table 4) performed symmetric (0°) and asymmetric (90°) lifting conditions with starting and ending positions alternating between knee-height and waist-height with no exo (1), an active knee exo (2), and a passive back exo (3) as outlined in sections 3.3.2.1 – 3.3.2.2. Combined these two datasets provide data on lifting across 19 different participants; however, the magnitude of datapoints for machine learning purposes was still insufficient. We turned to an open-source dataset collected in our lab group[133] which contains informative cyclic and noncyclic daily tasks which we believed would not only add a considerable amount of data, but also would broaden our JCF estimation abilities to a diverse set of movements. Within this study, twelve participants (Tables 5 and 6) performed tasks which include calisthenics, various modes of walking, lifting weight, stair ambulation, agility tasks (e.g., cutting), etc. All 31 participants across the three studies included within this work provided signed consent to the study prior to data collection in experiments approved by the Georgia Institute of Technology Institutional Review Board.

4.3.1.1 Motion capture

Participants in the unassisted lifting study (Chapter 2) and exo lifting study (Chapter 3) wore a full-body reflective marker set to record segment positions (Vicon, Oxford, UK, 100Hz). Participants in the dynamic tasks study wore a lower-limb and torso reflective marker to record segment positions (200Hz).

Table 5 - Dynamic taskset participant weights[133]. . Standard deviation = SD.

Participant	Weight (kg)
1	78.9
2	82.2
3	113.5
4	71.5
5	79.1
6	62.3
7	87.6
8	84.1
9	67.5
10	65.1
11	64.0
12	67.6
Mean ± SD	80.7 ± 15.0

Table 6 - Dynamic taskset group demographics. . Standard deviation = SD.

	Gender	Age (years)	Height (cm)
Mean ± SD	7M / 5F	21.8 ± 3.2	176.7 ± 8.6

4.3.1.2 Ground reaction forces

Across all three studies, we collected ground reaction forces (GRFs) under each foot (Bertec, Columbus, OH, USA, 2000 Hz). Steady-state walking, running, step over, and some calisthenics trials were conducted on a split-belt instrumented treadmill, whereas all other tasks were performed on over ground force plates (2000 Hz – unassisted & exo lifting studies; 1000 Hz dynamic tasks study).

4.3.1.3 Electromyography

In the unassisted lifting study (Chapter 2) and exo lifting study (Chapter 3), we collected surface electromyography (EMG) (Delsys, Natick, Massachusetts, USA, 2000 Hz) from seven muscles in the right leg. These muscles included tibialis anterior (TA), lateral gastrocnemius (LG), rectus femoris (RF), vastus medialis (VM), vastus lateralis (VL), bicep femoris (BF), and semitendinosus (ST) (Figure 24). In the dynamic task study surface EMG was collected bilaterally, on the left and right legs. These muscles included tibialis anterior (TA), rectus femoris (RF), vastus lateralis (VL), and bicep femoris (BF). SENIAM procedures informed sensor placements[76].

We bandpass filtered (20-400 Hz, 2nd order Butterworth), full-wave rectified, lowpass filtered (6 Hz, 5th -order Butterworth), and half-wave rectified raw EMG signals. Across all studies, the task where the most muscles experienced a peak activation was utilized for normalization. The top five maximum activations per muscle within the condition were averaged to provide the normalization factor for each muscle, which was then applied to the respective signals in all trials.

4.3.2 Musculoskeletal analysis

Motion capture data from the unassisted lifting study (Chapter 2), the exo lifting study (Chapter 3), and the dynamic tasks study was modeled with a modified OpenSim model (Full Body Running (FBR) model) (SimTK, Stanford, CA, USA)[22]. We selected this model because it has a high resolution of knee muscles to better represent the effects

of surrounding muscles and tissues on internal joint forces. We modified ranges-of-motion constraints on the model within the arms, torso, pelvis, and legs to better fit the participants' movements. For the lifting tasks performed in Chapters 2 and 3, we distributed half the dumbbell mass (25 lbs., 12.5 lbs.) to each hand using OpenSim *WeldJoint* to incorporate the effects of the mass on the skeleton.

The same pipeline used in the studies outlined in sections 2.3.3 and 2.2.3.2 of performing scaling, Inverse Kinematics, Inverse Dynamics, Muscle Analysis, Joint Reaction Analysis, and the Calibrated EMG-Informed Neuromusculoskeletal Modeling Toolbox (CEINMS)[78] was applied to the dynamic taskset study. OpenSim version 4.0 was used for all relevant analyses. We then divided the resulting knee JCFs into normal and shear components. We calculated shear JCFs using the Euclidean norm of the anterior-posterior and mediolateral shear forces. JCFs were normalized by the product of participant mass and acceleration of gravity (x BW) and were used as our ground truth for machine learning practices outlined in section 4.3.4.2.

4.3.3 Simulating Sensors

IMU and insole simulation provides an opportunity to utilize these diverse datasets and test how comprehensive their information can be for a machine learning model attempting to estimate internal joint forces. To do so, we utilized the joint angle outputs from Inverse Kinematics as inputs to OpenSim's Forward Kinematics tool to compute the simulated kinematics (linear accelerations, angular velocities, and Euler angles) for each desired segment (torso, pelvis, thighs, shanks, and feet). Simulated IMU placements are

shown in Figure (24). GRFs and center of pressures (COPs) were read from force plates and transformed into their respective foot frame to model a pressure insole's reference frame. The Euclidean norm of the mediolateral and anteroposterior shear forces from the force plate was used as a super insole configuration.

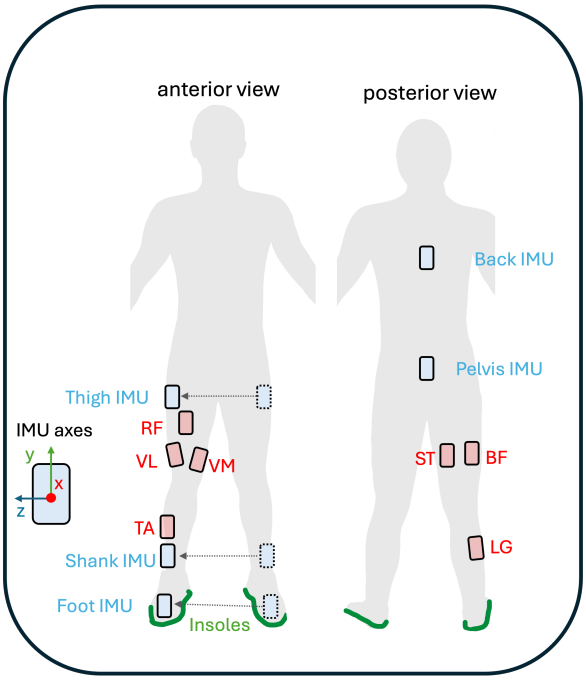

Figure 24 – Placements of wearable sensors both simulated and experimental. Simulated IMUs are shown in blue and are placed anteriorly on the thigh, shank, and foot segments, and posteriorly on the torso and pelvis. EMG are shown in red and measure muscle activations from the rectus femoris (RF), vastus medialis (VM), vastus lateralis (VL), tibialis anterior (TA), semitendinosus (ST), biceps femoris (BF), and lateral gastrocnemius) (LG). Simulated pressure insoles are shown in green and captured vertical and norm shear GRFs, as well as anteroposterior and mediolateral center of pressure (COP).

The lifting studies were conducted with only the right left instrumented with EMG; therefore, to maintain consistency in sensor configurations across all three studies, we

mirrored key IMU and insole signals on the left leg as if they were to be expressed as the right leg in the dynamic task study. This allowed us to double the knee data of this taskset.

4.3.4 TCN Model

4.3.4.1 Structure

Two separate single-headed TCN models were used for JCF estimations, one for normal knee JCFs and the other for shear knee JCFs – both with the same structure. The size of the initial layer of the TCN varied depending on the desired sensor input types, but consisted of 400 channels, and one output variable. The hyperparameters set in this model (Table 7) proved effective for knee joint moment estimations[135]. The effective time history required from the hyperparameters was 250 datapoints.

Table 7 - TCN Hyperparameters used.

Epochs	Kernel size	Channels sizes	Levels	Dropout probability	Patience	Effective history limit	Learning rate	Loss function
250	5	80	5	0.15	20	250	5E-5	MSE

4.3.4.2 Training, validation, and testing data

Data from the unassisted lifting study, exo lifting study, and dynamic tasks study were utilized in the performance of this JCF estimator. Simulated IMUs were upsampled to double their collection frequency, this led to an increase from 100 Hz to 200 Hz. We downsampled EMG and simulated insoles to temporally align with the resampled

simulated IMU data. As outlined in section 4.3.1.3, the dynamic task dataset comprised of 4/7 overlapping EMG from muscles experimentally collected in the lifting studies. Because the experimental EMG are simultaneously optimized in CEINMS with the simulated EMG (from non-experimentally collected muscles) to resolve for muscle forces, we were confident in utilizing the adjusted muscle activations for the remaining muscles (ST, LG, VM) for consistency in sensor inputs across studies.

We designed the input data tables to contain the model's features and labels for the ipsilateral (right) and contralateral (left) leg. The features included 9-axis IMUs (x,y,z for linear acceleration, angular velocity, and Euler angles), insoles (normal force, shear force, mediolateral COP, and anteroposterior COP), and EMG (RF, VM, VL, TA, LG, BF, ST). The labels consisted of normal and shear JCFs from the right and left knee. The model was then configured to read in the relevant ipsilateral features and desired outcome metric to estimate – the other variables were ignored.

The TCN was developed to function with subject independence when training. Leave-one-out cross-validation[136] approach was applied with the participants by excluding one participant for validation, and another for testing. The unassisted and exo lifting studies were limited in their ability to estimate JCFs for tasks outside of lifting, so we constrained the model to only use their data in the training set, but not for validation or testing. This means there were always 29 participants in the training dataset (although 19 of those participants couldn't contribute to most of the task types).

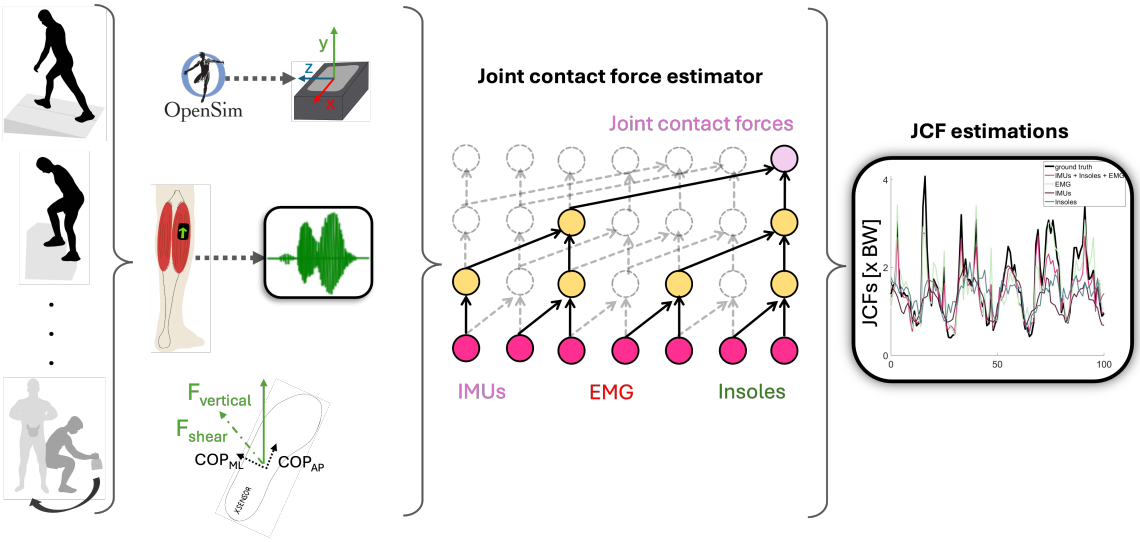

Figure 25 – Pipeline of joint contact force estimations. This process leverages measuring joint and muscle level biomechanical data throughout a diverse taskset and finding the configuration of wearable sensors which leads to the best estimates of internal joint forces.

We trained, validated, and tested two batches of eight different models (16 total) – one batch for normal JCFs and the other for shear JCFs—to evaluate how varying sensor input configurations affect JCF estimation performance and what is the minimal set of sensors which can provide a reliable estimation metric ($R^2 > 0.7$)[137]. The eight versions consisted of the following permutations: IMUs + insoles + EMG, IMUs + insoles, IMUs + EMG, EMG + insoles, IMUs, insoles, super insoles, and EMG. Each model variation could run up to 200 epochs, with early stopping permissible after reaching the preset patience value of 20 (Table 7).

4.3.5 Statistical analysis

A one-way repeated measures Analysis of Variance (ANOVA) and *post hoc* Bonferroni pairwise multivariate comparison test informed on the significance of the wearable sensor permutations on JCF estimation (H1) with the threshold for significance set at $\alpha = 0.05$. In the ANOVA, participants were defined as the random effects with the various sensor permutations as the fixed effect. The correlation coefficient (R^2) and root mean squared error (RMSE) were computed between the estimated JCFs and ground truth for each trial. Individual-participant averages and group averages for the R^2 and RMSE of each task type and overall were computed. Custom Matlab scripts were employed for these statistical analyses (Mathworks, Natick, MA).

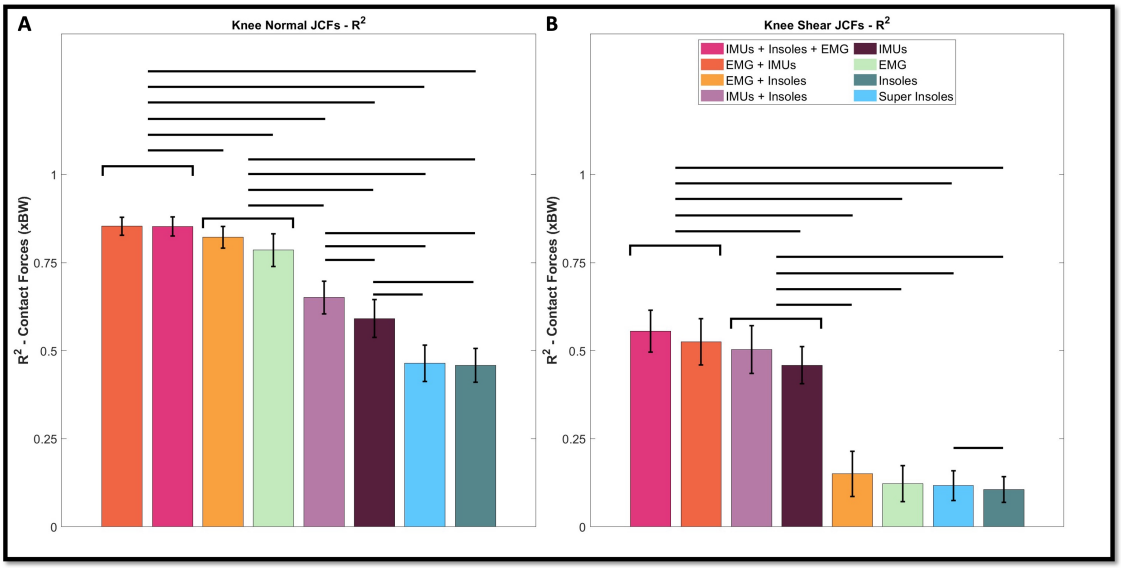

Figure 26 - Group averaged R^2 values in normal (A) and shear (B) knee joint contact forces. The color of each bar relates to the wearable sensor configuration used as inputs for the TCN to estimate knee JCFs. Significant differences between wearable sensor configurations are shown by a hovering bar.

4.4 Results

4.4.1 Joint contact force estimates – generalized tasks

We investigated the effects of wearing IMUs, EMG, and insoles on offline normal and shear JCF estimation. Additionally, we assessed how combinations of these wearable sensors can improve JCF estimations to identify the minimal sensor set required to obtain an $R^2 > 0.7$[137]. We leveraged data from dynamic datasets including movements such as walking, lifting, using stairs, jumping, and more to help us understand the utility and feasibility of JCF estimations in different contexts. We found that the TCN model was in fact able to map wearable sensor data to the ground truth of normal knee JCFs. Across all tasks utilized in our analyses, wearable sensor configurations which included EMG-only achieved at least an R^2 value of 0.79 when estimating normal knee JCFs. Adding insoles ($R^2 = 0.82$), IMUs ($R^2 = 0.85$), or both ($R^2 = 0.88$) to an EMG-only sensor set only slightly augmented the model's normal JCF estimation abilities without significance. The following sensor configurations have significantly greater R^2 values than sensor combinations with IMUs and/or insoles ($p < 0.01$): (1) EMG and IMUs, (2) all, (3) EMG only, and (4) EMG and insoles. Without EMG, the model failed to map IMUs ($R^2 = 0.59$) to JCFs without insoles (IMUs + insoles, $R^2 = 0.65$), but it also poorly estimated normal JCFs with solely the use of GRFs ($R^2 = 0.45$). (Figure 26A).

To gain a better sense of the model's accuracy in estimating JCFs, we also calculated the RMSE. In task agnostic (generalizable) normal knee JCF estimation, the sensor input configuration resulting in the lowest error was all sensors (IMUs, EMG, and

insoles) with an RMSE of 0.42, followed by the combination of IMUs and EMG sensors (RMSE = 0.43). The following sensor configurations have significantly lower RMSE values than sensor combinations with IMUs or insoles (p <0.01): (1) All, (2) EMG and IMUs, (3) EMG and insoles, and (4) EMG only. Like the R^2, the RMSE significantly increases without the inclusion of EMG. (Figure 28A).

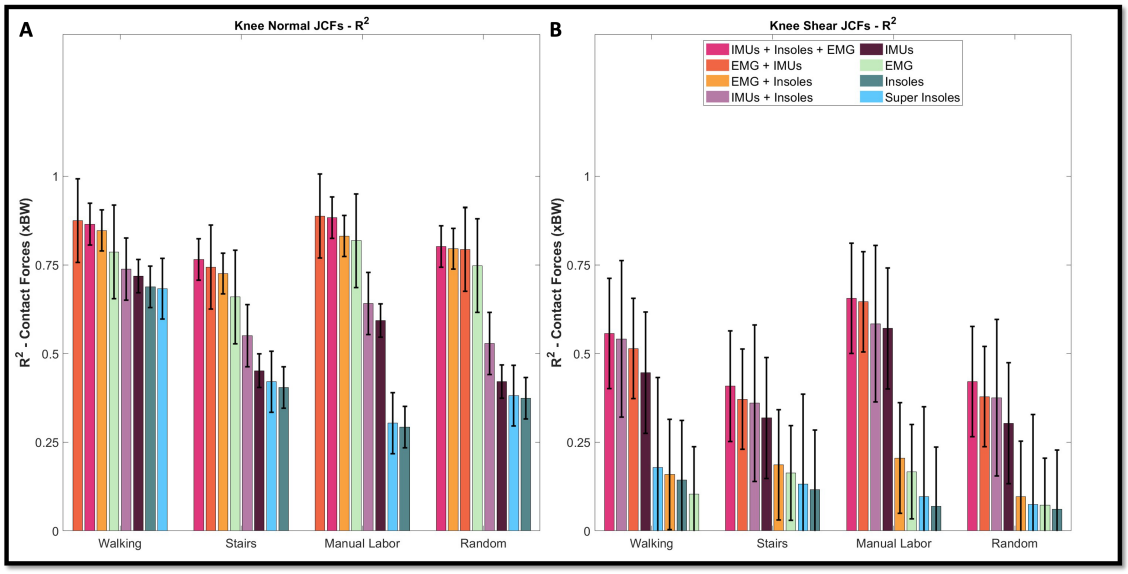

Figure 27 - Group averaged R^2 values in normal (A) and shear (B) knee joint contact forces in walking, stairs, manual labor, and random task groups. The color of each bar relates to the wearable sensor configuration used as inputs for the TCN to estimate knee JCFs.

On the other hand, we found the TCN to be unsuccessful in identifying relevant features and relationships between wearable sensor data and shear knee JCFs as the ground truth. Overall, none of the wearable sensor configurations achieved an $R^2 > 0.7$[137] (Figure 26B). Using the combination of IMUs, insoles, and EMG again performed the best of the configurations (R^2 = 0.56) in estimating shear knee JCFs. However, IMUs appear to be

responsible for this capability as all the top performing configurations include this sensor. An IMU-only sensor set could moderately estimate shear knee JCFs (R^2 = 0.46), but the addition of insoles (R^2 = 0.50) or EMG (R^2 =0.53) show minor, but not significant, improvements in the TCN's ability to map to shear JCFs. Sensor configurations utilizing insoles or a super insole could not converge on a strong solution to connect GRFs to shear knee JCFs and shared $R^2 < 0.12$. The following sensor configurations have significantly higher R^2 values than sensor combinations without IMUs (p <0.01): (1) All, (2) EMG and IMUs, (3) IMUs and insoles, and (4) IMUs only.

The performance in task agnostic (generalizable) shear knee JCF estimation followed a similar trend with the R^2. The following sensor configurations have significantly lower RMSE values than sensor combinations without IMUs (p <0.01): (1) EMG and IMUs, (2) all, (3) IMUs and insoles, and (4) IMUs only.

4.4.2 Joint contact force estimates – industry-relevant tasks

In order to consider deploying this approach as a potential mitigation strategy for joint force and health monitoring, it is important to characterize how task classification may influence the TCN's ability to discern task-specific knee JCFs for reliable estimations. We honed in on locomotion modes commonly experienced during the average daily manual workload of a manual labor employee: walking, climbing stairs, lifting, and random, aimless movement. The group of walking tasks included normal walking at different speeds, loaded carriage, walking backwards, walking on an inclined slope, and walking on a declined slope. The group of stair tasks included stair ascent and descent.

Manual labor tasks comprised of lifting with and without added weight, lunges, squats, sit-to-stand, tug-of-war, step ups, and ball tossing. Lastly, the random task group contains movement which occurs aimlessly throughout the day: meandering, turning, running into something or being bumped (push-pull), stepping over obstacles, standing, awkward stances (twister), and overcoming a curb.

We found that the TCN excelled at estimating normal knee JCFs across each locomotion mode. In all task groups, the sensor configuration of EMG and insoles meets our goal of achieving a performance of $R^2 > 0.70$ in offline joint loading estimations, with stair tasks being the lowest at $R^2 = 0.72$ (Figure 27A). The TCN showed its ability to map an EMG-only sensor set to normal knee JCFs in walking, manual labor, and random movement tasks. The combination of IMUs and insoles are relatable to normal knee JCFs in walking ($R^2 = 0.76$). IMU-only and insole-only sensor sets map poorly to normal knee JCFs, with the except of IMU-only achieving an R2 of 0.73 in walking.

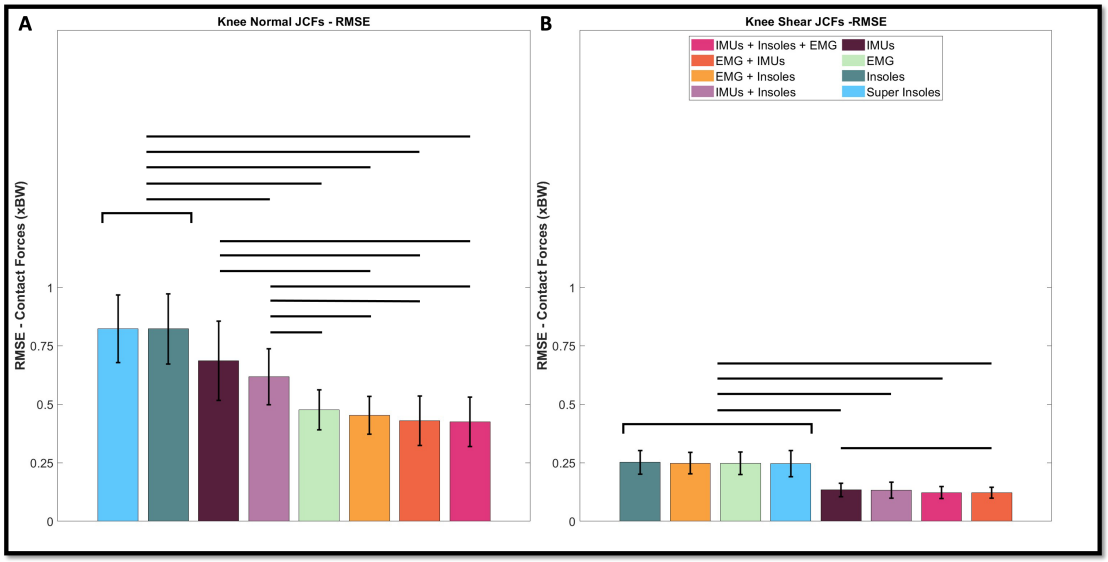

Figure 28 - Group averaged RMSE values in normal (A) and shear (B) knee joint contact forces. The color of each bar relates to the wearable sensor configuration used as inputs for the TCN to estimate knee JCFs. Significant differences between wearable

As shown in 4.4.1, TCN struggles to find the relationship between the sensor configurations as inputs to the shear knee JCFs as its ground truth across each locomotion mode. Similar to results of estimating normal knee JCFs, locomotion modes of walking, manual labor, and random tasks achieve higher R^2 values in shear knee JCF estimates. In each task group, sensor configurations using IMUs (IMUs + insoles + EMG, EMG + IMUs, IMUs + insoles, IMUs-only) are the relatively stronger performing sensor sets of the group. The combination of IMUs and insoles performed as well as having an R^2 of 0.57 in walking showing the usefulness of GRFs in estimating shear knee JCFs, as the average R^2 from using an IMU-only sensor set is 0.37 (Figure 26B). On the other hand, sensor configurations containing insoles, are the weaker performing sensor sets. All combinations of sensor sets obtained an $R^2 < 0.20$ across all locomotion mode groups.

4.5 Discussion

We hypothesized that the combination of IMUs and insoles as inputs to our model would be able to estimate knee JCFs with a performance of $R^2 > 0.7$[137]. We rejected this hypothesis, as we found that EMG are necessary for the accomplishment of this goal.

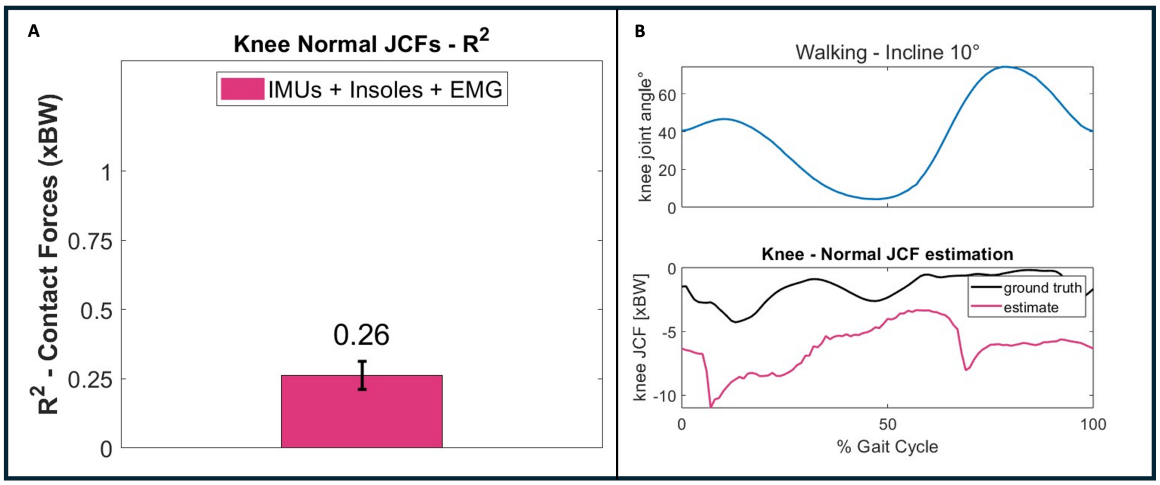

Figure 29 - Normal knee JCF estimation using real sensor inputs. Average R2 value across all tasks using IMUs + Insoles + EMG (A). Knee joint angles during a single gait cycle from a representative participant, temporally aligned with time series tracking of normal knee JCFs compared to the ground truth (B).

Because the knee is a lower-limb joint, we anticipated that the lower-limb and torso segment kinematics and vertical GRFs would provide a sufficient amount of information to map from the simulated inputs to the normal and shear knee JCF ground truths (H1). Work by Stetter et al., (2019)[138] showcased success of IMUs to estimate knee joint forces (joint moments) in a two-sensor setup. Sancho-Bru et al. (2023)[139] showed the ability to capture foot contact forces using pressure insoles. A study by Elstub et al., (2022)[45] demonstrates the success of estimating tibial bone forces with the use of an IMU and pressure insole. Altogether these efforts supported out hypothesis that IMU and insole-

informed machine learning JCF estimates would be a reliable sensing system for normal and shear JCFs. In actuality, we found that models trained with EMG in their combinations all provided reliable normal JCF estimates ($R^2 > 0.7$). Studies have shown the intra and intersubject variability in EMG which we believed would significantly hinder our ability to estimate JCFs. However, we believe the use of subject-dependent ground truth data for model training likely led to its success in drastically improving normal knee JCF estimates. Figure 29 showcases in a time series tracking of normal knee JCFs during lifting tasks, that EMG-only estimate is the only version which maintains satisfactory JCF tracking even through the nuances of the ground truth with changing knee flexion angles, especially knee flexion.

Observing the capability of estimating normal knee JCFs across different task groups solidifies our confidence in recommending the use of an EMG-only wearable sensing system for this purpose. The addition of other sensor types does not significantly improve the model's performance captured as R^2 or RMSE values (Figures 26-28). This leads us to believe that there may be too much data being input to the TCN model and negatively influencing how the TCN identifies patterns. Therefore, to further improve normal knee JCF estimation, the next task would be to investigate which subset of muscle activations as input channels to the TCN are absolutely necessary to obtain similar performance.

We also we reject the hypothesis (H1) that IMUs and insoles could estimate shear knee JCFs with an R^2 of at least 0.7. In fact, none of the sensor configurations provided a strong estimation capability. Giarmatzis et al. (2020)[140] predicted knee JCFs in walking at

varying speeds using an ANN and a support vector regression model, while inputting kinematic and kinetic data[140]. Their predictions performed well with moderate to strong Pearson R values (0.45 – 0.85) with a leave-one-out cross-validation[136] approach, and observed good knee JCF predictions without the use of ground reaction forces[140]. One aspect to consider is their use of motion capture, whereas our system was solely wearable sensor based – but modeled with simulated IMUs and insoles with experimental EMG as inputs. Additionally, the shear forces in the majority of the tasks used (except e.g., cutting) are not very large. Consequently, it is possible that the model was unable to track shear knee JCFs across these different tasks due to the subtle changes or inability to relate the sensor channel inputs to those small magnitudes.

The poor performance of the TCN model in estimating shear knee JCFs proposes a few recommendations for future investigations. First, as outlined in Chapters 2 and 3, our goal is to find and eventually implement mitigation technologies which reduce hazardous peak and cumulative joint loading. Informing employees about the injury risk associated with a certain work tasks would not be contingent upon continuous monitoring of JCFs – we place higher priority on alerting workers about large joint loads and prolonged exposure to these loads. Therefore, there is a need to discover if reducing datapoints to concentrate the model's estimation on peak and/or cumulative loading would lead to significant changes in its performance, especially in its potential transition into a biofeedback paradigm. Second, moving forward with a sensing system comprised of EMGs, IMUs, and insoles may be overkill. Seeing the promising and useful results that EMG alone can provide regarding normal knee JCFs, running additional machine learning-based

estimations and developing various prototypes of wearable sensing suits with a minimized amount of sensors (e.g., not all seven EMG) would be imperative to know how practical and deployable this mitigation strategy could be for the workplace and every day wear.

As an extension of our work, we sought to test the ability of the strongest performing trained model (all sensors, estimating normal knee JCFs) to estimate normal knee JCFs with the use of all real sensors. We see that an estimation ability of $R^2 = 0.86$ plunges to $R^2 = 0.26$ and fails to uphold its ability to track knee JCFs temporally (Figure 29). This highlights the poor ability of the TCN model that was trained on simulated sensor data to map JCFs computed with real sensors as inputs instead. Thus, emphasizing the need for advanced machine learning methodologies such as transfer learning to find the proper transform from simulated to real sensor data and boost this model's overall utility in estimating JCFs.

4.5.1 Limitations

There are a few limitations to note in the conduction of this research. Previous success in estimating joint moments showed a strong performance when including joint angles as an input, often from motor encoders. Because we would prefer to deploy a sensing system which can function without outputs from exos, we prefer a model which does not require additional information to succeed. However, it is possible that knee joint angles could have allowed the model to estimate normal and shear JCFs better. Another limitation is blending datasets which only contain lifting tasks which a larger dataset which contains 25+ diverse task types. Initially we feared that the model would overfit for the lifting

conditions; however we found the two lifting-only datasets did not provide enough datapoints for overfitting. In order to fully leverage the power of having a 31-participant dataset, it would likely allow the model to perform even better if all individuals had data from each task type. In preliminary validation analyses using the dynamic taskset, we saw a decrease in the model's ability to estimate joint moments when including the two lifting-only datasets to the training datasets. It is possible that the addition of data for only one task could be hurting the overall performance of the model in JCFs estimations.

4.6 Conclusion

This study examined the performance of a deep learning model in estimating normal and shear knee JCFs in a dynamic and diverse taskset using different combinations of wearable sensors. We found that the combination of EMG and IMUs allotted the best estimations of normal JCFs ($R^2 = 0.85$) independent of task, whereas no combination of sensors provided an estimate of shear knee JCFs with R^2 values greater than 0.7. Our findings in normal knee JCFs estimations also shed light on the importance of EMG in estimating ground truth JCFs computed using EMG-assisted methods[65,105]. In shear knee JCFs estimations, although not significant, IMUs appeared to provide the strongest mapping to JCFs compared to other inputs. Altogether, the results of this research will enable the field to move forward with reduced sensor sets to more practically estimate JCFs in environments outside of the lab. Thus, further supporting our awareness of internal joint

loading and our overall susceptibility to JCFs injurious to tissues and bones in the workplace.

4.7 Conflict of Interest Statement

There is no conflict of interest reported by the authors.

4.8 Acknowledgements

This work was supported by Sandia National Laboratories, a multi-mission laboratory managed and operated by the National Technology and Engineering Solutions of Sandia LLC, a wholly owned subsidiary of Honeywell International Inc. for the U.S. Department of Energy's National Nuclear Security Administration under contract DE-NA0003525. This paper describes objective technical results and analysis. Any subjective views or opinions that might be expressed in the paper do not necessarily represent the views of the U.S. Department of Energy or the United States Government. We would also like to show our appreciation to all the participants of this study.

4.9 Supplementary Figures for Chapter 4

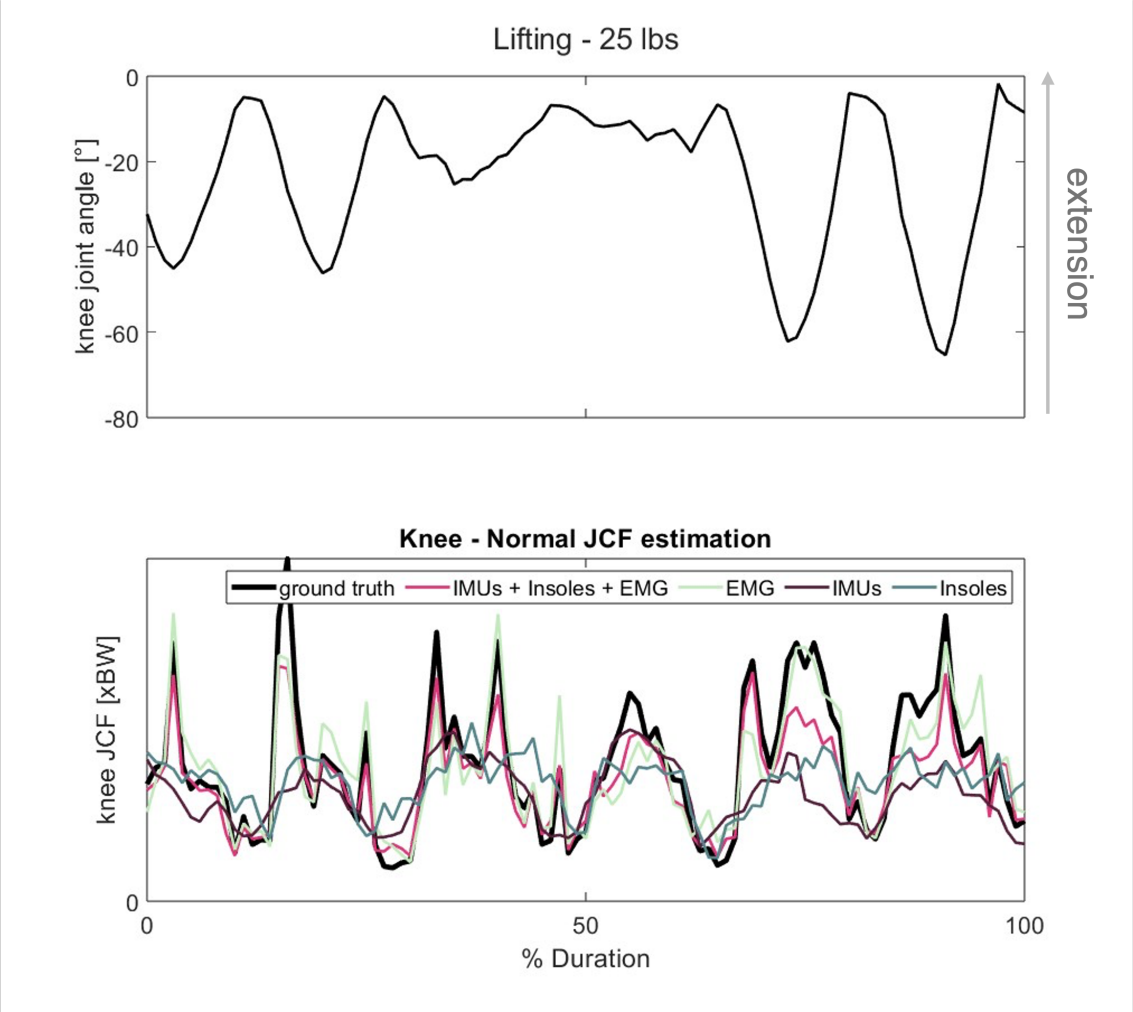

Figure 30 - Time series of knee joint kinematics and tracking of normal knee JCF estimations from various sensor configuration compared to the ground truth. The data shown stems from a representative participant performing different lifting with a 25 lb. weight. TCN estimations using IMUs + insoles + EMG are shown with a pink line, EMG only with a green line, IMU only with a burgundy line, and insoles only with a blue line.

Task list	Lunges
Walking	Squats
Weighted walking	Being pushed and pulled
Walking backwards	Abrupt starting and
Incline walking	stopping
Decline walking	Sit to stand
Running	Twister
Calisthenics	Ball tossing
Curb encounters	Standing
Step over obstacles	Turning
Step ups	Meandering
Lifting weights	Stair ascent
Jumping	Stair descent

Figure 31 - List of tasks included in the dynamic taskset (N = 12).

CHAPTER 5. CONCLUSION

In this dissertation, we explored to accomplish three main objectives: 1) to understand the characterization of lower back and knee JCFs across manual lifting which varied in height and degree of twisting (symmetry), 2) measure the effectiveness of exoskeletons as a mitigation strategy for reducing lower back and knee JCFs in symmetric and asymmetric manual lifting tasks, and 3) determine the minimal sensor set required to reliably estimate normal and shear knee JCFs using deep learning. In doing so, I conducted 3 studies (and adopted a 4th additional dataset) on healthy, able-bodied participants whose outcomes are outlined in 3 chapters.

The first work, Chapter 2, a submitted article to the Journal of Applied Biomechanics (Davenport et al., 2024)[105], proposes a framework that relates JCFs in a lower back joint (L5/S1) and knee joint to an assortment of symmetric and asymmetric manual lifting tasks. This framework allowed us to identify which task(s), symmetric, below-the-waist lifting, expose the joints to higher internal joint loads, potentially indicating work-specific movements that exposes workers to higher risks of injury. We also found that the lower back and knee joints share a directly proportional relationship in JCF load distribution as a two-joint system independent of task. This result supports the possibility of an inherent motor control principle to limit peak loading at any one joint when performing injurious movements. I anticipate that this research will spark further analyses and investigations which probe to understand JCFs throughout the musculoskeletal system in various movements and environments. This could open possibilities to exploring motor control of

joint forces with intact nervous system based on experimentally collected and computed joint kinematics and muscle activity.

Chapter 3, a manuscript undergoing internal review prior to submission, is work I intend to submit to IEEE Transactions on Medical Robotics and Bionics. This chapter provides a quantitative assessment on the effectiveness of exoskeletons in reducing acute and chronic joint loading in the manual lifting conditions that elicited higher JCFs at the lower back joint (L5/S1) and knee joint in Chapter 2 (symmetric, below-the-waist lifts). This chapter contributes a novel method of accounting for exo assistance prior to performing inverse dynamics. By including exo assistive torques (active KE) and forces (passive HW) prior to inverse dynamics, the exos assistance vectors were factored in as external forces, each applied at a certain moment arm distance away from the joint to be calculated into the overall net force (joint moment). This method allowed us to see that the powered assistance we provided at the knee caused an increase in the biological knee moment, which otherwise may not have been captured by subtracting exo torque from the total joint moment. This work also showed that both the HW and KE reduced peak and integrated JCFs at the lower back and knee, respectively, but neither were able to *significantly* reduce (or increase) JCFs at the unprescribed joint. Although, on average the HW did reduce normal and total knee JCFs. I hope this research may inspire This research highlights an important under-the-skin effect of exos, not often focused on throughout literature. I am hopeful that this research inspires the continued exploration of the unseen interaction effects of wearable devices not only on internal joint forces, but also throughout the musculoskeletal system prior to true, mass implementation as a mitigation strategy. Also, this

research can inform the design and implementation of work-specific exos to increase safety in manual labor professions.

I plan to submit to the research proposed in Chapter 4 to the IEEE Transactions on Biomedical Engineering or Annals of Biomedical Engineering. This work probes a different injury prevention strategy: looking to deep learning to support JCF estimations without the use of neuromusculoskeletal modeling. With knowledge of the utility of wearable sensors such as IMUs, EMG, and pressure insoles to inform us of other biomechanical metrics, our goal was to find out the most minimalistic combination of sensor types needed to support the TCN's capability to reliably estimate normal and shear JCFs. The structure of the model utilized in this aim's analyses supports the generalizability of JCF estimations across a broad array of dynamic, and manual labor-inspired tasks. This work shows promise to a trajectory of JCF estimative research to provide users with instructional feedback on mechanical modifications to influence and, hopefully, lower JCFs. This approach also serves as a cost-effective tool that can inform rehabilitative strategies.

At the conclusion of this combined work as a full project, still some unanswered questions remain. Because the focus of my work did not include the pathophysiological mechanisms responsible for injury development and all data was collected using healthy individuals, I still am curious about how the JCFs characterized in this work scale to those elicited during actual joint injury and which component(s) in the responsible biomechanical injury mechanisms are we actually capturing? If a certain aspect or metric from JCFs can

be extracted that is directly correlated some portion of an injury mechanism, we can solidify this metric as a biomarker to injury. I believe a long-term study leveraging the use of wearable sensing-based JCF estimates would permit the monitoring of injurious forces as they occur and a better way of mapping these inputs to the occurrence of injuries. Having pre- and post- JCFs information as context to an injury occurrence would provide an opportunity address this gap and further support the field in addressing injury mitigation strategies. My second looming question is how would this data look in a population which is more representative of those working manual labor jobs – or even those with a history of recurring or continuous (neuro)musculoskeletal injuries? I appreciate that this project provides a baseline understanding, a framework, to gauge JCFs in a best-case scenario. However, to be a practical and effective solution to reducing injurious joint forces, and injuries, this would need to be based on a diverse population. Age-related changes to tendons[141] and other tissues surrounding the joints, as well as osteoarthritis, could have a significant effect on JCFs and should be evaluated. Using the wearable technology interventions outlined in this research as a monitoring or instructional tool could pose an ability to inform of predisposition to injury reoccurrence for those with existing injuries.

Altogether, this body of work explored under-the-skin, bone-on-bone, JCFs as a metric to infer joint injury risks during dynamic, manual labor tasks and assessed how wearable technology (exos and sensors) can be viable solutions to alleviating these internal joint forces. I anticipate future work delving into JCF-controller exoskeletons, real-time biofeedback paradigms with wearable sensors, and in the wild experimentation with portable wearable assistance systems.

REFERENCES

1. Wellsandt E, Gardinier ES, Manal K, Axe MJ, Buchanan TS, Snyder-Mackler L. Decreased Knee Joint Loading Associated With Early Knee Osteoarthritis After Anterior Cruciate Ligament Injury. *Am J Sports Med*. 2016;44(1):143-151. doi:10.1177/0363546515608475

2. *Work Injury Costs*. National Safety Council; 2022. Accessed February 22, 2022. https://injuryfacts.nsc.org/work/costs/work-injury-costs/

3. Jabbour R, Turner S, Hussey L, Page F, Agius R. Workplace injury data reported by occupational physicians and general practitioners. *OCCMED*. 2015;65(4):296-302. doi:10.1093/occmed/kqv014

4. Wurzelbacher SJ, Meyers AR, Lampl MP, et al. Workers' compensation claim counts and rates by injury event/exposure among state-insured private employers in Ohio, 2007–2017. *Journal of Safety Research*. 2021;79:148-167. doi:10.1016/j.jsr.2021.08.015

5. Glover W, McGregor A, Sullivan C, Hague J. Work-related musculoskeletal disorders affecting members of the Chartered Society of Physiotherapy. *Physiotherapy*. 2005;91(3):138-147. doi:10.1016/j.physio.2005.06.001

6. Milhem M, Kalichman L, Ezra D, Alperovitch-Najenson D. Work-related musculoskeletaldisorders among physical therapists:A comprehensive narrative review. *Int J Occup Med Environ Health*. 2016;29(5):735-747. doi:10.13075/ijomeh.1896.00620

7. Schneider SP. Musculoskeletal Injuries in Construction: A Review of the Literature. *Applied Occupational and Environmental Hygiene*. 2001;16(11):1056-1064. doi:10.1080/104732201753214161

8. Klein BP, Jensen RC, Sanderson LM. Assessment of Workers' Compensation Claims for Back Strains/Sprains: *Journal of Occupational and Environmental Medicine*. 1984;26(6):443-448. doi:10.1097/00043764-198406000-00017

9. McGill SM. The biomechanics of low back injury: Implications on current practice in industry and the clinic. *Journal of Biomechanics*. 1997;30(5):465-475. doi:10.1016/S0021-9290(96)00172-8

10. Kumar S. Theories of musculoskeletal injury causation. *Ergonomics*. 2001;44(1):17-47. doi:10.1080/00140130120716

11. Hartvigsen J, Hancock MJ, Kongsted A, et al. What low back pain is and why we need to pay attention. *The Lancet*. 2018;391(10137):2356-2367. doi:10.1016/S0140-6736(18)30480-X

12. Silverstein B, Evanoff B. Musculoskeletal disorders. *Occupational and environmental health: Recognizing and preventing disease and injury*. Published online 2011:335-365.

13. Bureau of Labor Statistics. *U.S. Department of Labor, MSD by Nature of Injury or Illness by Days Away from Work (Number, Rate, Median)*. U.S. Department of Labor Accessed February 22, 2022. https://www.bls.gov/iif/nonfatal-injuries-and-illnesses-tables/soii-case-and-demographic-characteristics-historical-data/msd-case-and-demographic-nature-2020-national.xlsx

14. Chen TLW, Wang Y, Wong DWC, Lam WK, Zhang M. Joint contact force and movement deceleration among badminton forward lunges: a musculoskeletal modelling study. *Sports Biomechanics*. 2022;21(10):1249-1261. doi:10.1080/14763141.2020.1749720

15. Shirazi-Adl A. Analysis of large compression loads on lumbar spine in flexion and in torsion using a novel wrapping element. *Journal of Biomechanics*. 2006;39(2):267-275. doi:10.1016/j.jbiomech.2004.11.022

16. Adams M. Mechanical influences in disc degeneration and prolapse: medico-legal relevance. *Bone & Joint 360*. 2014;3(2):32-65.

17. Zhou X, Liu G, Han B, Li H, Zhang L, Liu X. Different Prevention and Treatment Strategies for Knee Osteoarthritis (KOA) with Various Lower Limb Exoskeletons – A Comprehensive Review. *Robotica*. 2021;39(8):1345-1367. doi:10.1017/S0263574720001216

18. Westerhoff P, Graichen F, Bender A, et al. In vivo measurement of shoulder joint loads during activities of daily living. *Journal of biomechanics*. 2009;42(12):1840-1849.

19. Bernard TM, Ayoub MM, Lin CJ. Evaluation of a biomechanical simulation model for sagittal plane lifting. *International Journal of Industrial Ergonomics*. 1999;24(2):157-171. doi:10.1016/S0169-8141(98)00011-0

20. Lin CJ, Ayoub MM, Bernard TM. Computer motion simulation for sagittal plane lifting activities. *International Journal of Industrial Ergonomics*. 1999;24(2):141-155. doi:10.1016/S0169-8141(98)00010-9

21. Beaucage-Gauvreau E, Robertson WSP, Brandon SCE, et al. Validation of an OpenSim full-body model with detailed lumbar spine for estimating lower lumbar spine loads during symmetric and asymmetric lifting tasks. *Computer Methods in Biomechanics and Biomedical Engineering*. 2019;22(5):451-464. doi:10.1080/10255842.2018.1564819

22. Delp SL, Anderson FC, Arnold AS, et al. OpenSim: Open-Source Software to Create and Analyze Dynamic Simulations of Movement. *IEEE Trans Biomed Eng*. 2007;54(11):1940-1950. doi:10.1109/TBME.2007.901024

23. Bedo BLS, Catelli DS, Lamontagne M, Santiago PRP. A custom musculoskeletal model for estimation of medial and lateral tibiofemoral contact forces during tasks with high knee and hip flexions. *Computer Methods in Biomechanics and Biomedical Engineering*. 2020;23(10):658-663. doi:10.1080/10255842.2020.1757662

24. Garg A, Chaffin DB, Freivalds A. Biomechanical Stresses From Manual Load Lifting: A Static vs Dynamic Evaluation. *A I I E Transactions*. 1982;14(4):272-281. doi:10.1080/05695558208975240

25. Vigotsky AD, Zelik KE, Lake J, Hinrichs RN. Mechanical misconceptions: Have we lost the "mechanics" in "sports biomechanics"? *Journal of Biomechanics*. 2019;93:1-5. doi:10.1016/j.jbiomech.2019.07.005

26. Young People With Old Knees Research Team, Saxby DJ, Bryant AL, et al. Relationships Between Tibiofemoral Contact Forces and Cartilage Morphology at 2 to 3 Years After Single-Bundle Hamstring Anterior Cruciate Ligament Reconstruction and in Healthy Knees. *Orthopaedic Journal of Sports Medicine*. 2017;5(8):232596711772250. doi:10.1177/2325967117722506

27. Gardinier ES, Manal K, Buchanan TS, Snyder-Mackler L. Clinically-relevant measures associated with altered contact forces in patients with anterior cruciate ligament deficiency. *Clinical Biomechanics*. 2014;29(5):531-536. doi:10.1016/j.clinbiomech.2014.03.011

28. Molinaro DD, King AS, Young AJ. Biomechanical analysis of common solid waste collection throwing techniques using OpenSim and an EMG-assisted solver. *Journal of Biomechanics*. 2020;104:109704. doi:10.1016/j.jbiomech.2020.109704

29. Wrigley AT, Albert WJ, Deluzio KJ, Stevenson JM. Differentiating lifting technique between those who develop low back pain and those who do not. *Clinical Biomechanics*. 2005;20(3):254-263.

30. Bernard BP, Putz-Anderson V. Musculoskeletal disorders and workplace factors; a critical review of epidemiologic evidence for work-related musculoskeletal disorders of the neck, upper extremity, and low back. Published online 1997.

31. Chen W, Wu S, Zhou T, Xiong C. On the biological mechanics and energetics of the hip joint muscle–tendon system assisted by passive hip exoskeleton. *Bioinspir Biomim*. 2018;14(1):016012. doi:10.1088/1748-3190/aaeefd

32. Kermavnar T, De Vries AW, De Looze MP, O'Sullivan LW. Effects of industrial back-support exoskeletons on body loading and user experience: an updated systematic review. *Ergonomics*. 2021;64(6):685-711. doi:10.1080/00140139.2020.1870162

33. Baltrusch SJ, Van Dieën JH, Koopman AS, et al. SPEXOR passive spinal exoskeleton decreases metabolic cost during symmetric repetitive lifting. *Eur J Appl Physiol*. 2020;120(2):401-412. doi:10.1007/s00421-019-04284-6

34. Matijevich ES, Volgyesi P, Zelik KE. A promising wearable solution for the practical and accurate monitoring of low back loading in manual material handling. *Sensors*. 2021;21(2):340.

35. Medrano RL, Rouse EJ, Thomas GC. Biological Joint Loading and Exoskeleton Design. *IEEE Trans Med Robot Bionics*. 2021;3(3):847-851. doi:10.1109/TMRB.2021.3098920

36. De Looze MP, Bosch T, Krause F, Stadler KS, O'Sullivan LW. Exoskeletons for industrial application and their potential effects on physical work load. *Ergonomics*. 2016;59(5):671-681. doi:10.1080/00140139.2015.1081988

37. McDevitt S, Hernandez H, Hicks J, et al. Wearables for biomechanical performance optimization and risk assessment in industrial and sports applications. *Bioengineering*. 2022;9(1):33.

38. Anderson MT. The reduction/prevention of muscle and tendon sprains, strains, and overexertion injuries thru pre-work stretching and flexibility training at Polaris Industries, Inc. Osceola facility. Published online 2002.

39. Li RT, Salata MJ, Rambhia S, Sheehan J, Voos JE. Does Overexertion Correlate With Increased Injury? The Relationship Between Player Workload and Soft Tissue Injury in Professional American Football Players Using Wearable Technology. *Sports Health*. 2020;12(1):66-73. doi:10.1177/1941738119868477

40. Brown KA. Workplace safety: A call for research. *Journal of operations management*. 1996;14(2):157-171.

41. Lavender SA, Andersson GB, Schipplein OD, Fuentes HJ. The effects of initial lifting height, load magnitude, and lifting speed on the peak dynamic L5/S1 moments. *International Journal of Industrial Ergonomics*. 2003;31(1):51-59.

42. Reese CD. *Occupational Health and Safety Management: A Practical Approach*. CRC press; 2018.

43. Chaffin DB. The evolving role of biomechanics in prevention of overexertion injuries. *Ergonomics*. 2009;52(1):3-14. doi:10.1080/00140130802479812

44. Yin W, Chen Y, Reddy C, Zhang* X. Towards Real-Time Minimum-Input Prediction of Lumbar Moment Based on Flexible Sensors and Machine Learning. In: Vol 66. SAGE Publications Sage CA: Los Angeles, CA; 2022:656-660.

45. Elstub L, Nurse C, Grohowski L, Volgyesi P, Wolf D, Zelik K. Tibial bone forces can be monitored using shoe-worn wearable sensors during running. *Journal of sports sciences*. 2022;40(15):1741-1749.

46. Nurse CA, Elstub LJ, Volgyesi P, Zelik KE. How accurately can wearable sensors assess low back disorder risks during material handling? Exploring the fundamental capabilities and limitations of different sensor signals. *Sensors*. 2023;23(4):2064.

47. Conforti I, Mileti I, Del Prete Z, Palermo E. Measuring biomechanical risk in lifting load tasks through wearable system and machine-learning approach. *Sensors*. 2020;20(6):1557.

48. Saxby DJ, Killen BA, Pizzolato C, et al. Machine learning methods to support personalized neuromusculoskeletal modelling. *Biomechanics and Modeling in Mechanobiology*. 2020;19:1169-1185.

49. Pizzolato C, Reggiani M, Saxby DJ, Ceseracciu E, Modenese L, Lloyd DG. Biofeedback for gait retraining based on real-time estimation of tibiofemoral joint contact forces. *IEEE Transactions on Neural Systems and Rehabilitation Engineering*. 2017;25(9):1612-1621.

50. McGill SM. Distribution of tissue loads in the low back during a variety of daily and rehabilitation tasks. *Journal of rehabilitation research and development*. 1997;34:448-458.

51. Schipplein OD, Trafimow JH, Andersson GBJ, Andriacchi TP. Relationship between moments at the L5/S1 level, hip and knee joint when lifting. *Journal of Biomechanics*. 1990;23(9):907-912. doi:10.1016/0021-9290(90)90355-7

52. Vahdat I, Rostami M, Tabatabai Ghomsheh F, Khorramymehr S, Tanbakoosaz A. Effects of external loading on lumbar extension moment during squat lifting. *Int J Occup Med Environ Health*. Published online May 29, 2017. doi:10.13075/ijomeh.1896.00896

53. Jäger M, Luttmann A. The load on the lumbar spine during asymmetrical bi-manual materials handling. *Ergonomics*. 1992;35(7-8):783-805. doi:10.1080/00140139208967363

54. Kitagawa K, Nodagashira H, Kurosawa T, Maeyama H, Wada C. Compressive and Shear Forces of L5/S1 during Patient Transfer in Different Loads on Hands. *Int J Pharma Med Biol Sci*. 2023;12(2):21-25.

55. Kingma I, Bosch T, Bruins L, Van Dieën JH. Foot positioning instruction, initial vertical load position and lifting technique: effects on low back loading. *Ergonomics*. 2004;47(13):1365-1385.

56. Anderson CK, Chaffin DB. A biomechanical evaluation of five lifting techniques. *Applied Ergonomics*. 1986;17(1):2-8. doi:10.1016/0003-6870(86)90186-9

57. Escamilla RF, Fleisig GS, Lowry TM, Barrentine SW, Andrews JR. A three-dimensional biomechanical analysis of the squat during varying stance widths: *Medicine and Science in Sports and Exercise*. 2001;33(6):984-998. doi:10.1097/00005768-200106000-00019

58. De Looze MP, Toussaint HM, Van Dieën JH, Kemper HCG. Joint moments and muscle activity in the lower extremities and lower back in lifting and lowering tasks. *Journal of Biomechanics*. 1993;26(9):1067-1076. doi:10.1016/S0021-9290(05)80006-5

59. Davis KG, Marras WS, Waters TR. Evaluation of spinal loading during lowering and lifting. *Clinical Biomechanics*. 1998;13(3):141-152. doi:10.1016/S0268-0033(97)00037-5

60. Budihardjo I. *Studies of Compressive Forces on L5/S1 during Dynamic Manual Lifting*. Doctor of Philosophy. Iowa State University, Digital Repository; 2002. doi:10.31274/rtd-180813-12063

61. NACHEMSON A, MORRIS JM. In Vivo Measurements of Intradiscal Pressure: discometry, a method for the determination of pressure in the lower lumbar discs. *JBJS*. 1964;46(5). https://journals.lww.com/jbjsjournal/fulltext/1964/46050/in_vivo_measurements_of_intradiscal_pressure_.12.aspx

62. Wilke HJ, Neef P, Hinz B, Seidel H, Claes L. Intradiscal pressure together with anthropometric data – a data set for the validation of models. *Clinical Biomechanics*. 2001;16:S111-S126. doi:10.1016/S0268-0033(00)00103-0

63. Fregly BJ, Besier TF, Lloyd DG, et al. Grand challenge competition to predict in vivo knee loads. *Journal Orthopaedic Research*. 2012;30(4):503-513. doi:10.1002/jor.22023

64. Cholewicki J, McGill SM, Norman RW. Comparison of muscle forces and joint load from an optimization and EMG assisted lumbar spine model: Towards development of a hybrid approach. *Journal of Biomechanics*. 1995;28(3):321-331. doi:10.1016/0021-9290(94)00065-C

65. Pizzolato C, Lloyd DG, Sartori M, et al. CEINMS: A toolbox to investigate the influence of different neural control solutions on the prediction of muscle excitation and joint moments during dynamic motor tasks. *Journal of Biomechanics*. 2015;48(14):3929-3936. doi:10.1016/j.jbiomech.2015.09.021

66. Hoang HX, Diamond LE, Lloyd DG, Pizzolato C. A calibrated EMG-informed neuromusculoskeletal model can appropriately account for muscle co-contraction in the estimation of hip joint contact forces in people with hip osteoarthritis. *Journal of Biomechanics*. 2019;83:134-142. doi:10.1016/j.jbiomech.2018.11.042

67. Uhlrich SD, Jackson RW, Seth A, Kolesar JA, Delp SL. Muscle coordination retraining inspired by musculoskeletal simulations reduces knee contact force. *Sci Rep*. 2022;12(1):9842. doi:10.1038/s41598-022-13386-9

68. McCain EM, Dalman MJ, Berno ME, et al. The influence of induced gait asymmetry on joint reaction forces. *Journal of Biomechanics*. 2023;153:111581. doi:10.1016/j.jbiomech.2023.111581

69. Gagnon M, Plamondon A, Gravel D. Pivoting with the Load: An Alternative for Protecting the Back in Asymmetrical Lifting. *Spine*. 1993;18(11). https://journals.lww.com/spinejournal/fulltext/1993/09010/pivoting_with_the_load__an_alternative_for.17.aspx

70. Skals S, Bláfoss R, De Zee M, Andersen LL, Andersen MS. Effects of load mass and position on the dynamic loading of the knees, shoulders and lumbar spine during lifting: a musculoskeletal modelling approach. *Applied Ergonomics*. 2021;96:103491. doi:10.1016/j.apergo.2021.103491

71. Splittstoesser R, Davis K, Marras W. Trade-Offs between trunk flexion, hip flexion, and knee angle in lifting below waist level. In: Vol 44. SAGE Publications Sage CA: Los Angeles, CA; 2000:5-9.

72. Davis KG, Splittstoesser RE, Marras WS. Kinematic contribution and synchronization of the trunk, hip, and knee during free-dynamic lifting. *OER*. 2003;3(2):99-108. doi:10.3233/OER-2003-3202

73. Bejjani FJ, Gross CM, Pugh JW. Model for static lifting: Relationship of loads on the spine and the knee. *Journal of Biomechanics*. 1984;17(4):281-286. doi:10.1016/0021-9290(84)90138-6

74. Ng JKF, Kippers V, Parnianpour M, Richardson CA. EMG activity normalization for trunk muscles in subjects with and without back pain: *Medicine & Science in Sports & Exercise*. 2002;34(7):1082-1086. doi:10.1097/00005768-200207000-00005

75. Vera-Garcia FJ, Moreside JM, McGill SM. MVC techniques to normalize trunk muscle EMG in healthy women. *Journal of Electromyography and Kinesiology*. 2010;20(1):10-16. doi:10.1016/j.jelekin.2009.03.010

76. Stegeman D, Hermens H. Standards for surface electromyography: The European project Surface EMG for non-invasive assessment of muscles (SENIAM). *Enschede: Roessingh Research and Development*. 2007;10:8-12.

77. Hamner SR, Seth A, Delp SL. Muscle contributions to propulsion and support during running. *Journal of Biomechanics*. 2010;43(14):2709-2716. doi:10.1016/j.jbiomech.2010.06.025

78. Pizzolato C, Lloyd DG, Sartori M, et al. CEINMS: A toolbox to investigate the influence of different neural control solutions on the prediction of muscle excitation and joint moments during dynamic motor tasks. *Journal of biomechanics*. 2015;48(14):3929-3936.

79. Skals S, Bláfoss R, Andersen LL, Andersen MS, De Zee M. Manual material handling in the supermarket sector. Part 2: Knee, spine and shoulder joint reaction forces. *Applied Ergonomics*. 2021;92:103345. doi:10.1016/j.apergo.2020.103345

80. Anderson CK. *A Biomechanical Model of the Lumbosacral Joint for Lifting Activities*. Ph.D. Dissertation. The University of Michigan; 1983. https://www.proquest.com/docview/303179337?pq-origsite=gscholar&fromopenview=true&sourcetype=Dissertations%20&%20Theses

81. Waters TR, Putz-Anderson V, Garg A, Fine LJ. Revised NIOSH equation for the design and evaluation of manual lifting tasks. *Ergonomics*. 1993;36(7):749-776. doi:10.1080/00140139308967940

82. McGill SM, Norman RW, Yingling VR, Wells RP, Neumann P. Shear Happens! Suggested guidelines for ergonomists to reduce the risk of low back injury from shear loading. In: *The 30th Annual Conference of the Human Factors Association of Canada (HFAC)*. ; 1998:157-161. https://www.researchgate.net/profile/W-Neumann/publication/268298574_Shear_Happens_Suggested_guidelines_for_ergonomists_to_reduce_the_risk_of_low_back_injury_from_shear_loading/links/54d4f76d0cf246475806b125/Shear-Happens-Suggested-guidelines-for-ergonomists-to-reduce-the-risk-of-low-back-injury-from-shear-loading.pdf

83. Gallagher S, Marras WS. Tolerance of the lumbar spine to shear: A review and recommended exposure limits. *Clinical Biomechanics*. 2012;27(10):973-978. doi:10.1016/j.clinbiomech.2012.08.009

84. Skals S, Bláfoss R, De Zee M, Andersen LL, Andersen MS. Effects of load mass and position on the dynamic loading of the knees, shoulders and lumbar spine during lifting: a musculoskeletal modelling approach. *Applied Ergonomics*. 2021;96:103491. doi:10.1016/j.apergo.2021.103491

85. D'Lima DD, Fregly BJ, Patil S, Steklov N, Colwell CW. Knee joint forces: prediction, measurement, and significance. *Proc Inst Mech Eng H*. 2012;226(2):95-102. doi:10.1177/0954411911433372

86. Atkinson PJ, Haut RC. Injuries produced by blunt trauma to the human patellofemoral joint vary with flexion angle of the knee. *Journal Orthopaedic Research*. 2001;19(5):827-833. doi:10.1016/S0736-0266(00)00073-5

87. Haut RC. Contact pressures in the patellofemoral joint during impact loading on the human flexed knee. *Journal Orthopaedic Research*. 1989;7(2):272-280. doi:10.1002/jor.1100070216

88. Janusz Kajzer, Matsui Y, Ishikawa H, Schroeder G, Bosch U. Shearing and Bending Effects at the Knee Joint at Low Speed Lateral Loading. *SAE Transactions*. 1999;108:1159-1170.

89. Kumar S. Spinal compression at peak isometric and isokinetic exertions in simulated lifting in symmetric and asymmetric planes. *Clinical Biomechanics*. 1996;11(5):281-289. doi:10.1016/0268-0033(96)00015-0

90. Nuesslein C, Bhakta K, Fernandez J, et al. Comparing Metabolic Cost and Muscle Activation for Knee and Back Exoskeletons in Lifting. *IEEE Trans Med Robot Bionics*. 2024;6(1):224-234. doi:10.1109/TMRB.2023.3329567

91. Gagnon M, Plamondon A, Gravel D, Lortie M. Knee movement strategies differentiate expert from novice workers in asymmetrical manual materials handling. *Journal of Biomechanics*. 1996;29(11):1445-1453. doi:10.1016/0021-9290(96)84540-4

92. Nisell R, Ekholm J. Patellar forces during knee extension. *Scand J Rehabil Med*. 1985;17(2):63-74.

93. Hartmann H, Wirth K, Klusemann M. Analysis of the load on the knee joint and vertebral column with changes in squatting depth and weight load. *Sports medicine*. 2013;43:993-1008.

94. Wilk KE, Escamilla RF, Fleisig GS, Barrentine SW, Andrews JR, Boyd ML. A Comparison of Tibiofemoral Joint Forces and Electromyographic Activit During Open and Closed Kinetic Chain Exercises. *Am J Sports Med*. 1996;24(4):518-527. doi:10.1177/036354659602400418

95. Huberti HH, Hayes WC. Patellofemoral contact pressures. The influence of q-angle and tendofemoral contact. *JBJS*. 1984;66(5).

https://journals.lww.com/jbjsjournal/fulltext/1984/66050/patellofemoral_contact_pressures__the_influence_of.10.aspx

96. Dahlkvist NJ, Mayo P, Seedhom BB. Forces during Squatting and Rising from a Deep Squat. *Engineering in Medicine*. 1982;11(2):69-76. doi:10.1243/EMED_JOUR_1982_011_019_02

97. Van Rossom S, Smith CR, Thelen DG, Vanwanseele B, Van Assche D, Jonkers I. Knee Joint Loading in Healthy Adults During Functional Exercises: Implications for Rehabilitation Guidelines. *J Orthop Sports Phys Ther*. 2018;48(3):162-173. doi:10.2519/jospt.2018.7459

98. Delisle A, Gagnon M, Desjardins P. Knee flexion and base of support in asymmetrical handling: effects on the worker's dynamic stability and the moments of the L5/S1 and knee joints. *Clinical Biomechanics*. 1998;13(7):506-514. doi:10.1016/S0268-0033(98)00014-X

99. Hwang S, Kim Y, Kim Y. Lower extremity joint kinetics and lumbar curvature during squat and stoop lifting. *BMC Musculoskelet Disord*. 2009;10(1):15. doi:10.1186/1471-2474-10-15

100. Burgess-Limerick R, Abernethy B. Qualitatively different modes of manual lifting. *International Journal of Industrial Ergonomics*. 1997;19(5):413-417. doi:10.1016/S0169-8141(96)00065-0

101. Meyers JM, Fathallah FA, Janowitz I. Stooped and squatting postures in the workplace. *Natl Ag Saf Database*. Published online 2015:2-7.

102. Splittstoesser RE, Yang G, Knapik GG, et al. Spinal loading during manual materials handling in a kneeling posture. *Journal of Electromyography and Kinesiology*. 2007;17(1):25-34. doi:10.1016/j.jelekin.2005.12.003

103. Lu ML, Waters TR, Krieg E, Werren D. Efficacy of the Revised NIOSH Lifting Equation to Predict Risk of Low-Back Pain Associated With Manual Lifting: A One-Year Prospective Study. *Hum Factors*. 2014;56(1):73-85. doi:10.1177/0018720813513608

104. Hung IYJ, Shih TTF, Chen BB, Liou SH, Ho IK, Guo YL. The roles of lumbar load thresholds in cumulative lifting exposure to predict disk protrusion in an Asian population. *BMC Musculoskelet Disord*. 2020;21(1):169. doi:10.1186/s12891-020-3167-y

105. Davenport FR, Leestma JK, Staten A, et al. EMG-informed estimates of joint contact forces within the lower-back and knee joints during a diverse set of industry-relevant manual lifting tasks. *Journal of Applied Biomechanics*. Published online In Review.

106. Singerman R, Berilla J, Kotzar G, Daly J, Davy DT. A six-degree-of-freedom transducer for in vitro measurement of patellofemoral contact forces. *Journal of Biomechanics*. 1994;27(2):233-238. doi:10.1016/0021-9290(94)90213-5

107. Collins SH, Wiggin MB, Sawicki GS. Reducing the energy cost of human walking using an unpowered exoskeleton. *Nature*. 2015;522(7555):212-215. doi:10.1038/nature14288

108. Nuckols RW, Dick TJM, Beck ON, Sawicki GS. Ultrasound imaging links soleus muscle neuromechanics and energetics during human walking with elastic ankle exoskeletons. *Sci Rep*. 2020;10(1):3604. doi:10.1038/s41598-020-60360-4

109. Lamers EP, Yang AJ, Zelik KE. Feasibility of a Biomechanically-Assistive Garment to Reduce Low Back Loading During Leaning and Lifting. *IEEE Trans Biomed Eng*. 2018;65(8):1674-1680. doi:10.1109/TBME.2017.2761455

110. Lamers EP, Soltys JC, Scherpereel KL, Yang AJ, Zelik KE. Low-profile elastic exosuit reduces back muscle fatigue. *Sci Rep*. 2020;10(1):15958. doi:10.1038/s41598-020-72531-4

111. Van Der Have A, Rossini M, Rodriguez-Guerrero C, Van Rossom S, Jonkers I. The Exo4Work shoulder exoskeleton effectively reduces muscle and joint loading during simulated occupational tasks above shoulder height. *Applied Ergonomics*. 2022;103:103800. doi:10.1016/j.apergo.2022.103800

112. Theurel J, Desbrosses K. Occupational Exoskeletons: Overview of Their Benefits and Limitations in Preventing Work-Related Musculoskeletal Disorders. *IISE Transactions on Occupational Ergonomics and Human Factors*. 2019;7(3-4):264-280. doi:10.1080/24725838.2019.1638331

113. Lanotte F, Baldoni A, Dell' Agnello F, et al. Design and characterization of a multi-joint underactuated low-back exoskeleton for lifting tasks. In: *2020 8th IEEE RAS/EMBS International Conference for Biomedical Robotics and Biomechatronics (BioRob)*. IEEE; 2020:1146-1151. doi:10.1109/BioRob49111.2020.9224370

114. Hondzinski JM, Ikuma L, De Queiroz M, Wang C. Effects of exoskeleton use on movement kinematics during performance of common work tasks: A case study. *WOR*. 2019;61(4):575-588. doi:10.3233/WOR-162827

115. Yandell MB, Wolfe AE, Marino MC, Harris MP, Zelik KE. Effect of a Back-Assist Exosuit on Logistics Worker Perceptions, Acceptance, and Muscle Activity. In: Moreno JC, Masood J, Schneider U, Maufroy C, Pons JL, eds. *Wearable Robotics: Challenges and Trends*. Vol 27. Biosystems & Biorobotics. Springer International Publishing; 2022:7-11. doi:10.1007/978-3-030-69547-7_2

116. Lee D, McLain B, Kang I, Young A. Biomechanical Comparison of Assistance Strategies Using a Bilateral Robotic Knee Exoskeleton. *IEEE Trans Biomed Eng*. 2021;68(9):2870-2879. doi:10.1109/TBME.2021.3083580

117. Hondzinski JM, Ikuma L, De Queiroz M, Wang C. Effects of exoskeleton use on movement kinematics during performance of common work tasks: A case study. *WOR*. 2019;61(4):575-588. doi:10.3233/WOR-162827

118. Koch MA, Font-Llagunes JM. Lower-Limb Exosuits for Rehabilitation or Assistance of Human Movement: A Systematic Review. *Applied Sciences*. 2021;11(18):8743. doi:10.3390/app11188743

119. Goršič M, Song Y, Dai B, Novak D. Evaluation of the HeroWear Apex back-assist exosuit during multiple brief tasks. *Journal of Biomechanics*. 2021;126:110620.

120. Arauz PG, Chavez G, Reinoso V, Ruiz P, Cevallos C, Garcia G. Influence of a passive exoskeleton on kinematics, joint moments, and self-reported ratings during a lifting task. *Journal of Biomechanics*. 2024;162.

121. Bhardwaj S, Shinde AB, Singh R, Vashista V. Manipulating device-to-body forces in passive exosuit: An experimental investigation on the effect of moment arm orientation using passive back-assist exosuit emulator. *Wearable Technol*. 2023;4:e17. doi:10.1017/wtc.2023.12

122. Kang SH, Mirka GA. Effect of trunk flexion angle and time on lumbar and abdominal muscle activity while wearing a passive back-support exosuit device during simple posture-maintenance tasks. *Ergonomics*. 2023;66(12):2182-2192. doi:10.1080/00140139.2023.2191908

123. Bär M, Steinhilber B, Rieger MA, Luger T. The influence of using exoskeletons during occupational tasks on acute physical stress and strain compared to no exoskeleton–A systematic review and meta-analysis. *Applied Ergonomics*. 2021;94:103385.

124. Poggensee KL, Collins SH. How adaptation, training, and customization contribute to benefits from exoskeleton assistance. *Science Robotics*. 2021;6(58):eabf1078.

125. Crea S, Beckerle P, De Looze M, et al. Occupational exoskeletons: A roadmap toward large-scale adoption. Methodology and challenges of bringing exoskeletons to workplaces. *Wearable Technologies*. 2021;2:e11.

126. McLain BJ, Lee D, Mulrine SC, Young AJ. Effect of assistance using a bilateral robotic knee exoskeleton on tibiofemoral force using a neuromuscular model. *Annals of Biomedical Engineering*. 2022;50(6):716-727.

127. Choi G, Lee D, Kang I, Young AJ. Effect of assistance timing in knee extensor muscle activation during sit-to-stand using a bilateral robotic knee exoskeleton. In: IEEE; 2021:4879-4882.

128. De Brabandere A, Emmerzaal J, Timmermans A, Jonkers I, Vanwanseele B, Davis J. A machine learning approach to estimate hip and knee joint loading using a mobile phone-embedded IMU. *Frontiers in bioengineering and biotechnology*. 2020;8:320.

129. Ostaszewski M, Pauk J. Estimation of ground reaction forces and joint moments on the basis on plantar pressure insoles and wearable sensors for joint angle measurement. *Technology and Health Care*. 2018;26(S2):605-612.

130. Mehrizi R, Peng X, Metaxas DN, Xu X, Zhang S, Li K. Predicting 3-D lower back joint load in lifting: A deep pose estimation approach. *IEEE Transactions on Human-Machine Systems*. 2019;49(1):85-94.

131. Jensen RL. Relationship of ground reaction and knee joint reaction forces in plyometric exercises. Published online 2010.

132. Burton II WS, Myers CA, Rullkoetter PJ. Machine learning for rapid estimation of lower extremity muscle and joint loading during activities of daily living. *Journal of Biomechanics*. 2021;123:110439.

133. Scherpereel K, Molinaro D, Inan O, Shepherd M, Young A. A human lower-limb biomechanics and wearable sensors dataset during cyclic and non-cyclic activities. *Scientific Data*. 2023;10(1):924.

134. Winter DA, Yack H. EMG profiles during normal human walking: stride-to-stride and inter-subject variability. *Electroencephalography and clinical neurophysiology*. 1987;67(5):402-411.

135. Scherpereel KL, Molinaro DD, Shepherd MK, Inan OT, Young AJ. Improving Biological Joint Moment Estimation During Real-World Tasks with EMG and Instrumented Insoles. *IEEE Transactions on Biomedical Engineering*. Published online 2024.

136. Halilaj E, Rajagopal A, Fiterau M, Hicks JL, Hastie TJ, Delp SL. Machine learning in human movement biomechanics: Best practices, common pitfalls, and new opportunities. *Journal of biomechanics*. 2018;81:1-11.

137. Moore DS. *The Basic Practice of Statistics*. 5th ed. W. H. Freeman and Company; 2010.

138. Stetter BJ, Ringhof S, Krafft FC, Sell S, Stein T. Estimation of knee joint forces in sport movements using wearable sensors and machine learning. *Sensors*. 2019;19(17):3690.

139. Sancho-Bru JL, Sanchis-Sales E, Rodríguez-Cervantes PJ, Vergés-Salas C. Foot Sole Contact Forces vs. Ground Contact Forces to Obtain Foot Joint Moments for In-Shoe Gait—A Preliminary Study. *Sensors*. 2023;23(15):6744.

140. Giarmatzis G, Zacharaki EI, Moustakas K. Real-Time Prediction of Joint Forces by Motion Capture and Machine Learning. *Sensors*. 2020;20(23):6933. doi:10.3390/s20236933

141. Stenroth L, Peltonen J, Cronin NJ, Sipilä S, Finni T. Age-related differences in Achilles tendon properties and triceps surae muscle architecture in vivo. *Journal of applied physiology*. 2012;113(10):1537-1544.